

# An Investigation of Energy Efficiency in Heterogeneous Wireless Networks



Siyi Wang

Department of Electronic and Electrical Engineering  
University of Sheffield

A thesis submitted for the degree of

*Doctor of Philosophy*

12<sup>th</sup> December 2013

I would especially like to dedicate this thesis to my loving parents for whom there are no sufficient words to express my infinite gratitude and love, and my girl friend Qin Chen for her continuous support and irreplaceable care during these years.

## Acknowledgements

I would like to thank all those who have offered me help in my pursuit of the Doctor's Degree and in my thesis writing. Without their dedication and steady support, I could not have produced this dissertation.

First of all, my special thanks are due to my supervisor, Professor Timothy O'Farrell, for the opportunity he gave me to become a member of Virtual Centre of Excellence in Mobile and Personal Communications (MVCE) and for his confidence and support in my investigations during these 3.5 years. I will always be grateful to him for it.

I would also like to thank the other members in the group, Dr. Weisi Guo, Mr. Charles Turyagyenda and Mr. Hassan Hamdoun, for their valuable suggestions and constructive criticisms, which have benefited me greatly and made this thesis possible.

Too many to mention individually are the various people who have contributed in one way or another to this thesis. They include my other family members except parents whose encouragement has helped to reduce my anxiety in the past years, Dr. Xiaoli Chu and Professor Jie Zhang who have been willing to give me advice, and those who have helped me on other occasions. All of them have my full and warm appreciation.

Finally yet importantly, my Ph.D candidature was jointly supported by MVCE and UK Engineering and Physical Sciences Research Council (EPSRC).

# List of Publications

## Scholarly Book Chapter

1. Siyi Wang, Weisi Guo. *Handbook of Research on Progressive Trends in Wireless Communications and Networking*. chapter Sustainable Growth for Cellular Wireless Networks. IGI Global, February, 2014.

## Referred Journal Articles

1. Siyi Wang, Yuan Hu, Weisi Guo. Interference Aware Band and Route Selection for D2D and Cellular Co-Existence. *submitted to IEEE Transactions on Wireless Communications*.. September, 2013.
2. Siyi Wang, Amir Jafari, Weisi Guo. Cascade Decode-and-Forward: Spatial Diversity Reuse in Sensor Networks. *submitted to Transactions on Emerging Telecommunications Technologies*. September, 2013.
3. Weisi Guo, Conor Devine, Siyi Wang, Shijun Guo. Performance Analysis of Micro Unmanned Airborne Communication Relays for Cellular Networks. *submitted to IEEE Communications Magazine. Special issue on Enabling Next Generation Airborne Communications*. September, 2013.
4. Weisi Guo, Siyi Wang. Dynamic Data Traffic Mapping for 5G Heterogeneous Network Deployment. *submitted to IEEE Communications Magazine. Special issue on 5G Wireless Communication Systems: Prospects and Challenges*. August, 2013.

- 
5. Yuan Hu, Yue Wu, Weisi Guo, Siyi Wang, Xiaoli Chu, Jie Zhang. D2D Routing and Resource Allocation in Co-Existence with Cellular Communications. *submitted to IEEE Communications Magazine. Special issue on Smart Device-to-Smart Device Communications*. August, 2013.
  6. Siyi Wang, Weisi Guo, Chadi Khirallah, Dejan Vukobratović, John Thompson. Interference Allocation Scheduler for Green Multi-Media Delivery. *submitted to IEEE Transactions on Vehicular Technology. Special Section on Green Mobile Multimedia Communications*. August, 2013.
  7. Siyi Wang, Weisi Guo, Tim O'Farrell. Spectral and Energy Efficiency Performance for Two-tier Cellular Network with Frequency Selective Surface. *submitted to IEEE Transactions on Vehicular Technology*. January, 2013.
  8. Siyi Wang, Weisi Guo. [Energy and Cost Implications of a Traffic Aware and QoS Constrained Sleep Mode Mechanism](#). *IET Communications*. 7(18):2092-2101, December, 2013.
  9. Weisi Guo, Siyi Wang, Andrew Eckford, Jianguan Wu. [Reliable Communication Envelopes of Molecular Diffusion Channels](#). *IET Electronics Letters*. August, 2013. 49(19):1248–1249, September, 2013
  10. Weisi Guo, Siyi Wang. [Radio-Frequency Energy Harvesting Potential: a Stochastic Analysis](#). *Transactions on Emerging Telecommunications Technologies* (formerly known as European Transactions on Telecommunications). 24(5):453–457, August, 2013.
  11. Weisi Guo, Siyi Wang. [Mobile Crowd-Sensing Wireless Activity with Measured Interference Power](#). *IEEE Wireless Communications Letters*. PP(99):1–4, July, 2013.
  12. Weisi Guo, Siyi Wang, Xiaoli Chu, Jiming Chen, Hui Song, Jie Zhang. [Automated Small-Cell Deployment for Heterogeneous Cellular Networks](#). *IEEE Communications Magazine*. 51(5):46–53, May, 2013.

- 
13. Weisi Guo, Siyi Wang. [Interference-Aware Self-Deploying Femto-Cell](#). *IEEE Wireless Communications Letters*. 1(6):609–612, December, 2012.
  14. Weisi Guo, Siyi Wang, Tim O’Farrell. [Economically and Environmentally Sustainable Cellular Networks](#). *River Publisher Journal on Green Engineering*. 2(3):273–283, May, 2012.
  15. Siyi Wang, Weisi Guo, Tim O’Farrell. [Low Energy Indoor Network: Deployment Optimisation](#). *EURASIP Journal on Wireless Communication Networks (JWCN)*. *Special issue on Green Radio, nominated as Best Readings in Green Communications*. 2012(1):193, June, 2012.

#### Referred Conference Articles

1. Siyi Wang, Weisi Guo, Song Qiu, Mark D. McDonnell. Performance of Macro-Scale Molecular Communications with Sensor Cleanse Time *submitted to IEEE International Conference on Communications (ICC)*. Sydney, Australia, 10–14 June, 2014.
2. Siyi Wang, Weisi Guo, Mark D. McDonnell. Downlink Interference Estimation without Feedback for Heterogeneous Network Interference Avoidance *submitted to IEEE International Conference on Communications (ICC)*. Sydney, Australia, 10–14 June, 2014.
3. Yue Wu, Siyi Wang, Weisi Guo, Xiaoli Chu and Jie Zhang. Optimal Resource Sharing for Device-to-Device Communications Underlying SC-FDMA Systems *submitted to IEEE International Conference on Communications (ICC)*. Sydney, Australia, 10–14 June, 2014.
4. Weisi Guo, Siyi Wang, Tim O’Farrell, Simon Fletcher. Energy Consumption of 4G Cellular Networks: A London Case Study. In *IEEE 77<sup>th</sup> Vehicular Technology Conference (VTC2013-Spring)*. Dresden, Germany, 2–5 June 2013.
5. Weisi Guo, Siyi Wang, Yue Wu, Jonathan Rigelsford, Xiaoli Chu, Tim O’Farrell. [Spectral- and Energy-Efficient Antenna Tilting in a HetNet](#)

- 
- using Reinforcement Learning. In *IEEE Wireless Communications and Networking Conference (WCNC)*. Shanghai, China, 7–10 April, 2013.
6. Weisi Guo, Siyi Wang, Xiaoli Chu. [Capacity Expression and Power Allocation for Arbitrary Modulation and Coding Rates](#). In *IEEE Wireless Communications and Networking Conference (WCNC)*. Shanghai, China, 7–10 April, 2013.
  7. Qin Chen, Siyi Wang, Angela Lin. [The Joint Beta Distribution with Refund Rate in Online C2C Trust Building: A Theoretical Study on Taobao](#). In *IEEE The International Conference on E-Learning and E-Technologies in Education (ICEEE)*. Lodz, Poland, 24–26 September, 2012.
  8. Weisi Guo, Siyi Wang, Charles Turyagyenda, Tim O’Farrell. [Integrated Cross-Layer Energy Savings in a Smart and Flexible Cellular Network](#). In *IEEE 1<sup>st</sup> International Conference on Communications in China (ICCC)*. Beijing, China, 15–17 August, 2012.
  9. Siyi Wang, Weisi Guo, Tim O’Farrell. [Two-tier Cellular Networks with Frequency Selective Surface](#). In *IEEE International Conference on High Performance Computing and Communications (HPCC)*. Liverpool, UK, 25–27 June, 2012.
  10. Siyi Wang, Weisi Guo, Tim O’Farrell. [Optimising Indoor Femtocell Placement: Theory and Simulation](#). In *IEEE 76<sup>th</sup> Vehicular Technology Conference (VTC2013-Fall)*. Québec City, Canada, 3–6 September, 2012.
  11. Siyi Wang, Charles Turyagyenda, Tim O’Farrell. [Energy Efficiency and Spectral Efficiency Trade-off of a Novel Interference Avoidance Approach for LTE-Femtocell Networks](#). In *IEEE 75<sup>th</sup> Vehicular Technology Conference (VTC2013-Spring)*. Yokohama, Japan, 6–9 May, 2012.
  12. Siyi Wang, Weisi Guo, Tim O’Farrell. [Energy Efficiency Evaluation of SISO and MIMO between LTE-femtocells and 802.11n Network](#). In *IEEE 75<sup>th</sup> Vehicular Technology Conference (VTC2013-Spring)*. Yokohama, Japan, 6–9 May, 2012.

- 
13. Weisi Guo, Charles Turyagyenda, Hassan Hamdoun, Siyi Wang, Pavel Loskot, Tim O'Farrell. [Towards a Low Energy LTE Cellular Network: Architectures](#). In *EURASIP European Signal Processing Conference (EUSIPCO)*. Barcelona, Spain, 29 August–2 September, 2011.
  14. Siyi Wang, Weisi Guo, Tim O'Farrell. Energy Efficiency Comparison of LTE-Femtocell and 802.11n Networks. In *IEEE International Workshop on Femtocells*. London, UK, 22 June, 2011.



## Abstract

Energy efficiency is an important issue as the amount of high rate multimedia wireless communication grows substantially in order to accommodate more users. Over the past 10 years, there has been an unprecedented growth in the wireless information transfer volume and the associated wireless node density. This is especially true in urban areas in which over 50% of the world's population reside. Currently, there are over 7 billion active handsets and 4 million cell-sites globally. Additional infrastructure, in particular Wi-Fi hotspots in urban areas, has reached over 350 nodes per square kilometre.

On the other hand, telecommunications operators and vendors are also facing a serious challenge as the total energy consumed by network infrastructure as well as the CO<sub>2</sub> emissions resulting from their manufacturing and operation increase significantly. Recently, it has been reported that energy costs can account for as much as half of a mobile carrier's annual operating expenses. Moreover, the environmental and financial consequences would also be disastrous if the aggregate energy consumption of Information and Communication Technologies (ICT) were to follow the predicted growth trajectory. The current combination of the energy consumption of service centres and wireless communication networks accounts for 2–4% of global CO<sub>2</sub> emissions and is expected to reach up to 10% in less than 10 years. Therefore it is essential for the research community to investigate state-of-the-art technologies, such as energy-efficient network architecture and protocols, energy-efficient wireless transmission techniques, energy-efficient home networking, and opportunistic spectrum sharing without causing tremendous harmful interference pollution to meet the challenges to improve energy efficiency in communications.

As there are many ways to improve energy efficiency in wireless communications illustrated above, this thesis mainly focuses on improving the energy efficiency through the enhancement of network capacity. It starts to examine the relative merits of Long Term Evolution (LTE) femtocell access points (FAP) and 802.11n Wi-Fi radio access technologies (RATs) so as to establish a baseline system-level performance. The results from Monte-Carlo simulations reveal that LTE-femtocells best suit small home networks, providing a high level of spectral- and energy-efficiency. With this result in mind, attention is paid to the next generation of heterogeneous cellular networks, in more detail, in the DownLink (DL) of Orthogonal Frequency Division Multiple Access (OFDMA) based LTE networks.

The thesis furthers the study of interference avoidance for a heterogeneous network and applies a novel Radio Resource Management (RRM) algorithm for indoor femtocells. After this, the thesis examines how to create an algorithm that optimises the location of home FAP(s) with respect to the dominant interference. This investigation covers the scenarios of single room single FAP, single room multiple FAPs and multi-room multi-floor multi-FAPs. Finally, special attention is paid to evaluate the system-level performance using a stochastic-geometry theoretical framework which acts as a fundamental basis in the analysis of heterogeneous networks and paves the way for the study of mitigating interference using a frequency-selective-surface (FSS) and the work of the trade-off between interference mitigation via FSS for indoor home network and outdoor-indoor resource sharing by turning on and off the FSS.

# Glossary of Abbreviations

|                |  |
|----------------|--|
| <b>3GPP</b>    | 3 <sup>rd</sup> Generation Partnership Project         |
| <b>4G</b>      | 4 <sup>th</sup> Generation                             |
| <b>AMC</b>     | Adaptive Modulation and Coding                         |
| <b>AP</b>      | Access Point   |
| <b>ARPU</b>    | Average Revenue Per User                               |
| <b>BER</b>     | Bit Error Rate   |
| <b>BLER</b>    | Block Error Rate                                       |
| <b>BS</b>      | Base Station   |
| <b>CCDF</b>    | Complementary Cumulative Distribution Function         |
| <b>CDF</b>     | Cumulative Distribution Function                       |
| <b>CSMA/CA</b> | Carrier Sense Multiple Access with Collision Avoidance |
| <b>CSI</b>     | Channel State Information                              |
| <b>CSG</b>     | Closed Subscriber Group                                |
| <b>DCF</b>     | Distributed Coordination Function                      |
| <b>ECG</b>     | Energy Consumption Gain                                |
| <b>ECR</b>     | Energy Consumption Ratio                               |

---

|                |  |
|----------------|--|
| <b>EPS</b>     | Evolved Packet System                      |
| <b>ERG</b>     | Energy Reduction Gain                      |
| <b>E-UTRAN</b> | Evolved Universal Terrestrial Radio Access |
| <b>FAP</b>     | Femtocell Access Point                     |
| <b>FFR</b>     | Fractional Frequency Reuse                 |
| <b>FoM</b>     | Figure of Merit                            |
| <b>FSS</b>     | Frequency Selective Surfaces               |
| <b>ICT</b>     | Information and Communication Technologies |
| <b>IP</b>      | Internet Protocol                          |
| <b>i.i.d</b>   | Independent and Identically Distributed    |
| <b>LTE</b>     | Long Term Evolution                        |
| <b>MAC</b>     | Medium Access Control                      |
| <b>MBS</b>     | Macro-cell Base Station                    |
| <b>MBWA</b>    | Mobile Broadband Wireless Access           |
| <b>MCS</b>     | Modulation and Coding Scheme               |
| <b>MGF</b>     | Moment Generating Function                 |
| <b>MIMO</b>    | Multiple Input, Multiple Output            |
| <b>OFDM</b>    | Orthogonal Frequency-division Multiplexing |
| <b>OPEX</b>    | Operational Expenditure                    |
| <b>pdf</b>     | Probability Density Function               |
| <b>PHY</b>     | Physical                                   |
| <b>PRB</b>     | Physical Resource Blocks                   |

---

|              |   |
|--------------|---|
| <b>QoS</b>   | Quality of Service                              |
| <b>RAN</b>   | Radio Access Network                            |
| <b>RH</b>    | Radio Head                                      |
| <b>RRM</b>   | Radio Resource Management                       |
| <b>SON</b>   | Self-organising Network                         |
| <b>SINR</b>  | Signal to Interference-plus-Noise Ratio         |
| <b>SNR</b>   | Signal to Noise Ratio                           |
| <b>SISO</b>  | Single Input, Single Output                     |
| <b>SPPP</b>  | Spatial Poisson Point Process                   |
| <b>TD</b>    | Time Division                                   |
| <b>TTI</b>   | Transmission Time Interval                      |
| <b>WLAN</b>  | Wireless Local Area Network                     |
| <b>Wi-Fi</b> | Wireless Fidelity                               |
| <b>WiMAX</b> | Worldwide Interoperability for Microwave Access |

# List of Notations

|                                  |   |
|----------------------------------|---|
| $\alpha$                         | Path loss exponent  |
| $\alpha_i$                       | Path loss exponent in the $i^{\text{th}}$ -tier network               |
| $\alpha_F$                       | Path loss exponent for indoor scenario                                |
| $\beta$                          | Equals to 0.05  |
| $\beta_{\mathbf{t}}$             | Binary values from 0 or 1   |
| $\beta_i$                        | $\frac{1}{P_{\text{tiPLC}}}$  |
| $\Delta$                         | Extra wall loss factor on SNR efficiency                              |
| exp                              | Exponential distribution  |
| $\gamma$                         | Received Signal to Interference-plus-Noise Ratio (SINR)               |
| $\gamma_{\text{eff}}$            | Factor of SNR efficiency  |
| $\gamma_{\text{MIMO}2 \times 2}$ | SINR of the estimated signal of Alamouti $2 \times 2$ channels        |
| $\gamma_{\text{SISO}}$           | SINR of the estimated signal in SISO configuration                    |
| $\gamma_s$                       | Saturation SNR threshold  |
| $\gamma_{x,y}$                   | User's received SINR from the FAP located at $(a, b)$                 |
| $\gamma_{x,y}^F$                 | Received SINR of the scenario where dominant interference is from FAP |
| $\hat{y}_0[t]$                   | Estimated received signal of the desired BS at time $t$               |

---

|                                |   |
|--------------------------------|---|
| $\lambda$                      | Cell Density  |
| $\lambda_{\text{FAP}}$         | Indoor femtocell density  |
| $\lambda_{\text{MBS}}$         | MBS density   |
| $\lambda_i$                    | Cell intensity in the $i^{\text{th}}$ -tier network   |
| $\lambda_u$                    | User intensity  |
| $\mathbb{E}(l_p)$              | Average packet payload bits successfully transmitted in a virtual time slot   |
| $\mathbb{E}(t)$                | Expected length of a time slot  |
| $\hat{\mathbf{y}}_{0.22}[t]$   | Estimated received signal of Alamouti $2 \times 2$ channels at time $t$   |
| $\mathbf{H}^{-1}$              | Pseudo inverse of the equivalent channel matrix   |
| $\mathbf{H}_{1i.22}$           | Equivalent Alamouti matrix of received antenna 1  |
| $\mathbf{H}_{2i.22}$           | Equivalent Alamouti matrix of received antenna 2  |
| $\mathbf{H}_{i.22}$            | Equivalent channel matrix   |
| $\mathbf{I}$                   | Identity matrix   |
| $\mathbf{w}_{0.22}[t]$         | Noise vector at time $t$  |
| $\mathbf{x}_{0.22}[t]$         | Transmitted vector of the desired BS at time $t$  |
| $\mathbf{x}_{k.22}[t]$         | Transmitted vector the $k^{\text{th}}$ interfering BS at time $t$   |
| $\mathbf{y}_{0.22}[t]$         | Downlink received signal of Alamouti $2 \times 2$ channels at time $t$  |
| $\mathcal{A}(\zeta, \alpha_k)$ | $\int_{[\gamma_{\text{eff}}(2^\zeta - 1)]^{-\frac{2}{\alpha_k}}}^{+\infty} \frac{[\gamma_{\text{eff}}(2^\zeta - 1)]^{\frac{2}{\alpha_k}}}{1 + u^{\frac{\alpha_k}{2}}} du$ |
| $\mathcal{B}(\zeta, \alpha_k)$ | $\frac{2\pi[\gamma_{\text{eff}}(2^\zeta - 1)]^{\frac{2}{\alpha_k}}}{\alpha_k \sin\left(\frac{2\pi}{\alpha_k}\right)}$   |

---

|  |  |
|--|--|
| $\mathcal{CN}$                                   | Complex normal distribution  |
| $\mathcal{F}$                                    | Number of interfering frequency bands in MHz   |
| $\mathcal{J}$                                    | Test or reference network  |
| $\mathcal{L}$                                    | Traffic load   |
| $\mathcal{L}_{\mathfrak{k}}$                     | Offered load of FAP $\mathfrak{k}$ in Mbit/s   |
| $\mathcal{S}$                                    | Log-normal shadowing   |
| $\mathcal{W}$                                    | Indoor room width  |
| $\mathfrak{A}(\xi, \alpha_{\mathfrak{k}})$       | $\xi^{\frac{2}{\alpha_{\mathfrak{k}}}} \int_{\xi^{-\frac{2}{\alpha_{\mathfrak{k}}}}^{+\infty} (1 + u^{\frac{\alpha_{\mathfrak{k}}}{2}})^{-1} du$ |
| $\mathfrak{D}$                                   | $\pi r^2$  |
| $\mathfrak{I}_{\mathfrak{k}\mathfrak{j}}$        | Random variable of aggregate interference  |
| $\mathfrak{k}$                                   | FAP index  |
| $\mathfrak{L}$                                   | Indoor room length   |
| $\mathfrak{r}$                                   | Coverage radius of a cell in Hexagonal layout  |
| $\mathfrak{W}$                                   | Minimum contention window size   |
| $\text{ECR}_{\mathcal{J}}$                       | Energy Consumption Ratio of type $\mathcal{J}$ network   |
| $\text{ERG}_{\text{RANupper-bound}}^{\text{OP}}$ | Upper-bound of over-head energy reduction gain   |
| $\text{ERG}_{\text{RAN}}^{\text{OP}}$            | Over-head energy reduction gain of the RAN   |
| $\text{ERG}_{\text{RAN}}^{\text{RH}}$            | Radio-head energy reduction gain of the RAN  |
| $\text{PL}$                                      | Path loss in dBs   |
| $\text{PL}_{\text{C}}$                           | Path loss constant   |
| $\text{PL}_{\text{in}}^{\text{LOS}}$             | Indoor line-of-sight path loss in dBs (between FAP and indoor users)   |



---

|                                   |  |
|-----------------------------------|--|
| $PL_{\text{in}}^{\text{NLOS}}$    | Indoor Non-line-of-sight path loss in dBs (between FAP and indoor users)   |
| $PL_{\text{out-to-in}}$           | Outdoor-to-indoor path loss in dBs (between micro-cell BS and indoor users)  |
| $PL_{\text{wall}}$                | Wall loss penetration factor in dBs  |
| $\mathcal{L}$                     | Laplace transform  |
| $C$                               | Average typical user's data rate of the overall network is taken over both the SPPP $\Phi_i$ for all tiers and the exponential fading distribution |
| $C_{\text{FAP}}^{\text{NoFSS}}$   | Theoretical FAP user's spectral efficiency in a two-tier closed access network without FSS   |
| $C_{\text{Macro}}^{\text{NoFSS}}$ | Theoretical macro-cell user's spectral efficiency in a two-tier closed access network without FSS  |
| $C_i$                             | Mean achievable user data rate in the $i^{\text{th}}$ -tier open access network  |
| $C_i^{\text{CA}}$                 | Mean achievable user data rate in the $i^{\text{th}}$ -tier with closed access   |
| $d_{\text{Cell}}$                 | Cell height  |
| $d_{i1}$                          | Distance between the typical user and the $1^{\text{th}}$ BSs in the $i^{\text{th}}$ -tier network   |
| $D_i$                             | Statistical distance between the typical user and the serving BS   |
| $d_{kj}$                          | Distance between the typical user and the $j^{\text{th}}$ interfering BSs in the $k^{\text{th}}$ -tier network                                     |
| $G_i$                             | $P_{ti}PL_C H_i$   |
| $H_i$                             | Random variable of Rayleigh fading   |

---

|                                     |   |
|-------------------------------------|---|
| $K$                                 | Number of tiers   |
| $l$                                 | Index of serving BS   |
| $m$                                 | Number of occurrences in a SPPP   |
| $P_{\text{cov}}$                    | Probability of coverage in open access network                                    |
| $R_i$                               | Distance between the typical user and the nearest BS in the $i^{\text{th}}$ -tier |
| $r_i$                               | Distance separating the typical mobile user and its associated closest home BS    |
| $u$                                 | Dummy variable  |
| $v$                                 | Dummy variable  |
| $z$                                 | $P_{\text{tk}} \mathbf{d}_{\text{Cell}}^{-\alpha_k}$                              |
| $\mu_{\Sigma}$                      | Radio-head efficiency   |
| $\bar{P}_{\text{icov}}^{\text{CA}}$ | Probability of coverage averaging the whole plane in an closed access network     |
| $\bar{P}_{\text{iout}}^{\text{CA}}$ | Probability of outage averaging the whole plane in an closed access network       |
| $\bar{P}_{\text{cov}}$              | Probability of coverage averaging the whole plane in an open access network       |
| $\bar{P}_{\text{out}}$              | Probability of outage averaging the whole plane in an open access network         |
| $\bar{C}^b$                         | Mean throughput of a user attached to the FAP along the length of the room        |
| $\bar{C}^F$                         | Mean throughput of the scenario where dominant interference is from FAP           |

---

|                          |   |
|--------------------------|---|
| $\bar{C}_{a,b}$          | Mean throughput of a user attached to the FAP across all positions                                    |
| $\bar{G}_{\text{micro}}$ | Expected value of the antenna gain from the micro-BS  |
| $\Phi_i$                 | Spatial Poisson Point Process of cells  |
| $\Phi_u$                 | Spatial Poisson Point Process of users  |
| $\sigma^2$               | Variance of $h$   |
| $\tau$                   | Transmission probability in a virtual time slot   |
| $\ \cdot\ $              | Operation of the Frobenius norm for a vector or matrix  |
| $ h_0 $                  | Absolute value of $h_0$   |
| $\xi$                    | SINR threshold  |
| $\zeta$                  | User's data rate threshold  |
| $A$                      | A certain area  |
| $a$                      | x coordinate of FAP   |
| $B$                      | $10^{\frac{b}{20\alpha}} \left( \frac{K_\gamma}{10^{\frac{\gamma_s}{10}}} \right)^{\frac{1}{\alpha}}$ |
| $b$                      | y coordinate of FAP   |
| $b_1$                    | Before this point the throughput is saturated   |
| $b_1^F$                  | $\frac{K_F D_F}{\alpha \sqrt{10^{\frac{\gamma_s}{10}}}}$  |
| $b_2$                    | After this point the throughput is saturated  |
| $b_2^F$                  | $Y - \frac{K_F(D_F - Y)}{\alpha \sqrt{10^{\frac{\gamma_s}{10}}}}$                                     |
| $B_{\text{eff}}$         | Factor of bandwidth efficiency  |
| $b_{\text{opt}}$         | Optimal coordinate of the scenario where dominant interference is from micro-BS                       |

---

|                         |   |
|-------------------------|---|
| $b_{\text{opt}}^F$      | Optimal coordinate of the scenario where dominant interference is from FAP                                    |
| $C_s$                   | Saturated throughput  |
| $D$                     | Distance between micro-cell BS and the nearest building wall  |
| $d$                     | Distance between UE and cell in metres  |
| $d_{\text{FAP}}$        | Distance between FAP and indoor users   |
| $d_{\text{micro}}$      | Distance between micro-cell BS and indoor users   |
| $d_{bp1F}$              | $\frac{K_F D_F}{K_F + \alpha_F \sqrt{10^{\frac{\gamma_s}{10}}}}$  |
| $d_{bp1}$               | Breaking point 1  |
| $d_{bp2F}$              | $\frac{K_F D_F + \alpha_F \sqrt{10^{\frac{\gamma_s}{10}}} b}{K_F + \alpha_F \sqrt{10^{\frac{\gamma_s}{10}}}}$ |
| $d_{bp2}$               | Breaking point 2  |
| $D_F$                   | Distance between interfering FAP and the nearest room wall  |
| $d_{x,y,\text{FAPint}}$ | Distance between the interfering FAP and the serving user   |
| $d_{x,y,\text{FAP}}$    | FAP-to-grid distance  |
| $d_{x,y,\text{in}}$     | Wall-to-grid distance   |
| $d_{x,y,\text{micro}}$  | Micro-BS-to-grid distance   |
| $F$                     | $\frac{\ln 10}{20\alpha} B$   |
| $f$                     | Frequency of transmission in MHz  |
| $f_{\text{FSS}}$        | FSS band-stop frequency   |
| $F_X(x)$                | Cumulative distribution function of the random variable $X$   |
| $f_X(x)$                | Probability density function of the random variable $X$   |
| $G$                     | Antenna gain  |

---

|  |   |
|--|---|
| $h_{\text{micro}}$                         | Channel coefficient of the micro-cell BS  |
| $h_0$                                      | Channel coefficient of the desired BS at time $t$   |
| $h_0^*$                                    | Complex conjugate of $h_0$  |
| $H_{22}$                                   | $( h_{101} ^2 +  h_{102} ^2)( h_{1k1} ^2 +  h_{1k2} ^2) + ( h_{201} ^2 +  h_{202} ^2)( h_{2k1} ^2 +  h_{2k2} ^2)$   |
| $h_i$                                      | Channel coefficient of the observed FAP   |
| $h_k$                                      | Channel coefficient of interfering FAPs   |
| $h_k[t]$                                   | Channel coefficient of the $k^{\text{th}}$ interfering BS at time $t$   |
| $K$  | Total number of interfering BSs   |
| $k$  | $k^{\text{th}}$ interfering BS  |
| $K_\gamma$                                 | $\frac{P_{\text{FAP}} D^{3.67} \times 10^{(22.7 + \text{PL}_{\text{wall}})/10} \times (\frac{f}{5})^{2.6}}{P_{\text{micro}} \bar{G}_{\text{micro}} \times 10^{46.8/10} \times (\frac{f}{5})^2}$ |
| $K_F$                                      | $10^{-0.25}$  |
| $L$  | Packet size in bits   |
| $L_{\text{FSS}}$                           | FSS in-band attenuation   |
| $L_{\text{wall}}$                          | External wall loss in dB  |
| $M$  | Number of traffic in bits   |
| $m$  | Maximum backoff stage   |
| $M_{\mathfrak{J}_{\text{kj}}}(\mathbf{s})$ | Moment generating function of the random variable $\mathfrak{J}_{\text{kj}}$ evaluated at $\mathbf{s}$  |
| $N_0$                                      | AWGN power spectral density   |
| $N_J$                                      | Number of APs in the type $J$ network   |
| $N_s$                                      | Total number of contending station  |

---

|                    |  |
|--------------------|--|
| $p$                | Unsuccessful transmission probability conditioned on that there is a transmission in a time slot |
| $P_{\text{FAP}}$   | Transmit power of FAP  |
| $P_{\text{micro}}$ | Received power of the same sub-carrier as the observed FAP from the micro-cell BS                |
| $P_{\text{micro}}$ | Transmit power of micro-BS   |
| $P_0$              | Received power of a certain sub-carrier from the desired BS                                      |
| $P_1$              | $\frac{(b+d_{bp2})C_s}{Y}$   |
| $P_1^F$            | $\frac{(b+d_{bp2F})C_s}{Y}$  |
| $P_2$              | $\frac{(d_{bp1}+d_{bp2})C_s}{Y}$   |
| $P_2^F$            | $\frac{(d_{bp1F}+d_{bp2F})C_s}{Y}$   |
| $P_3$              | $\frac{(Y-b+d_{bp1})C_s}{Y}$   |
| $P_3^F$            | $\frac{(Y-b+d_{bp1F})C_s}{Y}$  |
| $P_j^{\text{RH}}$  | Radio-head power of type $\mathcal{J}$ network   |
| $P_{\text{FAP}}$   | Femtocell transmit power   |
| $P_{\text{MBS}}$   | Macro-cell transmit power  |
| $P_{\text{ti}}$    | Transmit power of BSs in the $i^{\text{th}}$ -tier   |
| $p_{\text{Ti}}$    | Probability that the typical user is tagged to the $i^{\text{th}}$ -tier                         |
| $P_{\text{tk}}$    | Transmit power of interfering BSs in the $k^{\text{th}}$ -tier                                   |
| $p_\sigma$         | Probability of an idle slot  |
| $P_b$              | Wireless channel Bit Error Rate  |
| $p_c$              | Packet conditional collision probability   |

---

|                      |  |
|----------------------|--|
| $p_e$                | Packet error probability on condition that there is a successful transmission in the time slot                                     |
| $P_i$                | Received power of a certain sub-carrier from the observed FAP  |
| $P_k$                | Received power of of the same sub-carrier as the desired BS from the $k^{\text{th}}$ interfering BS                                |
| $P_k$                | Received power of the same sub-carrier as the observed FAP from the interfering FAPs   |
| $p_{s.nc}$           | Probability of a non-collided transmission   |
| $p_{tr}$             | Probability for a transmission in a time slot  |
| $Q_1$                | $\frac{(Y-b-d_{bp2}) \log_2 K_\gamma}{Y}$  |
| $Q_1^F$              | $\frac{(Y-b-d_{bp2F}) \log_2 K_F}{Y}$  |
| $Q_2$                | $\frac{(Y-d_{bp1}-d_{bp2}) \log_2 K_\gamma}{Y}$  |
| $Q_2^F$              | $\frac{(Y-d_{bp1F}-d_{bp2F}) \log_2 K_F}{Y}$   |
| $Q_3$                | $\frac{(b-d_{bp1}) \log_2 K_\gamma}{Y}$  |
| $R_1$                | $\frac{\beta \log_2 10}{2Y} [Y^2 - (b + d_{bp2})^2]$   |
| $R_1^F$              | $\frac{\alpha_F \left[ (Y-D_F) \log_2 (D_F-Y) + (D_F-b-d_{bp2F}) \log_2 (D_F-b-d_{bp2F}) - \frac{Y-b-d_{bp2F}}{\ln 2} \right]}{Y}$ |
| $R_2$                | $\frac{\beta \log_2 10}{2Y} (b - d_{bp1})^2$   |
| $R_2^F$              | $\frac{\alpha_F \left[ D_F \log_2 D_F - (D_F-b+d_{bp1F}) \log_2 (D_F-b+d_{bp1F}) - \frac{b-d_{bp1F}}{\ln 2} \right]}{Y}$           |
| $R_J$                | Traffic demanded under type J network  |
| $R_{\ddagger}$       | FAP interference rank measurement  |
| $R_{\text{traffic}}$ | Traffic demanded   |

---

|               |   |
|---------------|---|
| $S$           | Network saturation throughput   |
| $S_1$         | $T_1 - U_1$   |
| $S_t$         | Set of {Idle, VLow, Low, MediumL, MediumH, High, VHigh}                             |
| $s_t^A$       | Agent Player  |
| $s_t^P$       | Principal Player  |
| $T_1$         | $Y \log_2(Y - b) - (b + d_{bp2}) \log_2 d_{bp2}$                                    |
| $T_2$         | $(b - d_{bp1}) \log_2 d_{bp1}$  |
| $T_{AP}^{OH}$ | Observation time in seconds   |
| $T_\sigma$    | System's empty slot time  |
| $T_c$         | Collision virtual time slot's length  |
| $T_e$         | Error virtual time slot's length  |
| $T_s$         | Successful virtual time slot's length   |
| $U_1$         | $\frac{Y-b-d_{bp2}}{\ln 2} + b \log_2 \frac{Y-b}{d_{bp2}}$                          |
| $U_2$         | $\frac{b-d_{bp1}}{\ln 2} + b \log_2 \frac{d_{bp1}}{b}$                              |
| $W$           | Lambert W function  |
| $w_0$         | Noise signal at time $t$  |
| $x$           | User's x coordinate   |
| $x_0[t]$      | Baseband downlink transmit signal of the desired BS at time $t$                     |
| $x_k[t]$      | Baseband downlink transmit signal of the $k^{\text{th}}$ interfering BS at time $t$ |
| $Y$           | Length of room  |



---

|                 |   |
|-----------------|---|
| $y$             | User's $y$ coordinate   |
| $Y_{\text{ns}}$ | Non-saturated capacity region                                   |
| $Y_{\text{s}}$  | Saturated capacity region                                       |
| $y_0[t]$        | Baseband downlink received signal of the desired BS at time $t$ |

# Contents

|   |              |
|---|--------------|
| <b>Abstract</b>   | <b>xix</b>   |
| <b>Glossary of Abbreviations</b>  | <b>xiv</b>   |
| <b>List of Notations</b>  | <b>xxv</b>   |
| <b>Contents</b>   | <b>xxvi</b>  |
| <b>List of Figures</b>  | <b>xxxix</b> |
| <b>1 Introduction</b>   | <b>1</b>     |
| 1.1 Background . . . . .  | 1            |
| 1.2 Structure of This Thesis . . . . .                                  | 3            |
| <b>2 Radio Access Technology Comparison</b>                             | <b>6</b>     |
| 2.1 Introduction . . . . .  | 6            |
| 2.2 Investigation Framework . . . . .                                   | 8            |
| 2.3 LTE-femtocell Simulator Model . . . . .                             | 10           |
| 2.3.1 Simulation Flow . . . . .   | 11           |
| 2.3.2 Initialisation . . . . .  | 12           |
| 2.3.3 Propagation Model . . . . .                                       | 13           |
| 2.3.4 Signal Model and SINR Calculation . . . . .                       | 14           |
| 2.3.5 Link Adaptation . . . . .   | 18           |
| 2.3.6 Scheduling . . . . .  | 24           |
| 2.3.7 QoS . . . . .   | 24           |
| 2.4 802.11n Analytical Model for Energy Efficiency Evaluation . . . . . | 25           |

|          |  |           |
|----------|--|-----------|
| 2.5      | Energy Metrics . . . . .   | 27        |
| 2.6      | Network Simulations and Results . . . . .  | 30        |
| 2.6.1    | Baseline Results . . . . .   | 30        |
| 2.6.1.1  | 1 Access Point . . . . .   | 32        |
| 2.6.1.2  | 2 or More Access Points . . . . .  | 32        |
| 2.6.1.3  | SISO vs. MIMO . . . . .  | 33        |
| 2.6.2    | Results with Outdoor Interference . . . . .  | 33        |
| 2.6.3    | Shannon Capacity Equation vs. Adaptive MCS table . . . . .                             | 35        |
| 2.6.4    | Alternative (Frequency Reuse) Scenario . . . . .                                       | 37        |
| 2.6.5    | Remarks . . . . .  | 38        |
| 2.7      | Conclusions . . . . .  | 40        |
| <b>3</b> | <b>Femtocell Interference Avoidance</b>  | <b>41</b> |
| 3.1      | Review of Existing Work . . . . .  | 42        |
| 3.2      | Research Contribution . . . . .  | 43        |
| 3.3      | System Model . . . . .   | 44        |
| 3.3.1    | Introduction . . . . .   | 44        |
| 3.3.2    | Sequential Game Coordinated Radio Resource Management<br>(SGC/RRM) Algorithm . . . . . | 46        |
| 3.3.2.1  | Player Status Assignment (PSA) . . . . .   | 46        |
| 3.3.2.2  | Game Strategy Definition . . . . .   | 47        |
| 3.3.2.3  | Player Interference Rank Measurement . . . . .   | 47        |
| 3.3.3    | Player Strategy Selection . . . . .  | 49        |
| 3.4      | Simulation Results . . . . .   | 50        |
| 3.5      | Conclusions . . . . .  | 53        |
| <b>4</b> | <b>Deployment Location Optimisation of Indoor Femtocells</b>                           | <b>54</b> |
| 4.1      | Review of Existing Work . . . . .  | 55        |
| 4.2      | Research Contribution . . . . .  | 56        |
| 4.3      | Single Room Single FAP Placement . . . . .   | 56        |
| 4.3.1    | System Model . . . . .   | 56        |
| 4.3.2    | Simulation Framework . . . . .   | 58        |
| 4.4      | Theoretical Framework . . . . .  | 58        |

|          |   |            |
|----------|---|------------|
| 4.4.1    | Dominant Micro-BS Interference . . . . .                          | 59         |
| 4.4.1.1  | Formulation Scenario 1 . . . . .                                  | 62         |
| 4.4.1.2  | Formulation Scenario 2 . . . . .                                  | 63         |
| 4.4.1.3  | Formulation Scenario 3 . . . . .                                  | 65         |
| 4.4.2    | Formulation Summary and Convex Optimisation . . . . .             | 65         |
| 4.4.3    | Dominant FAP Interference . . . . .                               | 66         |
| 4.5      | Simulation and Theoretical Results . . . . .                      | 68         |
| 4.5.1    | Dominant Micro-BS Interference . . . . .                          | 69         |
| 4.5.1.1  | Throughput Results . . . . .                                      | 69         |
| 4.5.1.2  | Energy Results . . . . .  | 71         |
| 4.5.2    | Dominant FAP Interference . . . . .                               | 71         |
| 4.5.2.1  | Throughput Results . . . . .                                      | 72         |
| 4.5.2.2  | Energy Results . . . . .  | 72         |
| 4.5.2.3  | Comparison with 3GPP Simulator . . . . .                          | 72         |
| 4.6      | Single Room Multiple FAPs Placement . . . . .                     | 73         |
| 4.7      | Multi-Room Multi-Floor FAP Placement . . . . .                    | 75         |
| 4.8      | Practical Implementation . . . . .                                | 77         |
| 4.9      | Conclusions . . . . .   | 78         |
| <b>5</b> | <b>Heterogeneous Network: Capacity, Coverage and Interference</b> |            |
|          | <b>Performance Characterisation</b>                               | <b>80</b>  |
| 5.1      | Existing Common Analytical Models . . . . .                       | 81         |
| 5.2      | System Model . . . . .  | 84         |
| 5.2.1    | Open Access . . . . .   | 85         |
| 5.2.2    | Closed Access . . . . .   | 93         |
| 5.2.3    | Non-co-channel Deployment . . . . .                               | 97         |
| 5.3      | Statistical Interference Model . . . . .                          | 98         |
| 5.4      | Conclusions . . . . .   | 101        |
| <b>6</b> | <b>Energy Efficiency in Heterogeneous Network: Outdoor-Indoor</b> |            |
|          | <b>Coordination</b>   | <b>103</b> |
| 6.1      | Introduction . . . . .  | 104        |
| 6.1.1    | Related Work . . . . .  | 104        |

|          |  |            |
|----------|--|------------|
| 6.1.2    | Contributions . . . . .  | 105        |
| 6.2      | System Setup . . . . .   | 106        |
| 6.2.1    | Network Topology . . . . .   | 106        |
| 6.2.2    | Frequency-Selective-Surfaces . . . . .   | 108        |
| 6.3      | Baseline Performance of the Two-tier Closed-access Heterogeneous Network . . . . .   | 110        |
| 6.3.1    | Performance of Mean Data Rate per User in the One-Tier Network . . . . .             | 111        |
| 6.3.2    | Performance of Mean Data Rate per User in the Two-Tier Network without FSS . . . . . | 112        |
| 6.4      | Integrated Performance with FSS . . . . .  | 113        |
| 6.4.1    | Throughput Performance . . . . .   | 114        |
| 6.4.2    | Energy Reduction Results . . . . .   | 115        |
| 6.5      | Offloading Indoor Users to Outdoor Macro-cell Base Station . . . . .                 | 116        |
| 6.5.1    | Hexagonal Model . . . . .  | 117        |
| 6.5.2    | SPPP Model . . . . .   | 117        |
| 6.6      | Conclusions . . . . .  | 118        |
| <b>7</b> | <b>Conclusions and Future Work</b>   | <b>120</b> |
| 7.1      | Conclusions . . . . .  | 120        |
| 7.1.1    | Wi-Fi or Femtocells . . . . .  | 121        |
| 7.1.2    | Interference Avoidance . . . . .   | 121        |
| 7.1.3    | Optimal Indoor FAPs Deployment . . . . .   | 122        |
| 7.1.4    | Extending Analytical Heterogeneous Network Model with Stochastic Geometry . . . . .  | 123        |
| 7.1.5    | Interference Mitigation via FSS and Indoor-outdoor Interactions Evaluation . . . . . | 123        |
| 7.2      | Future Works . . . . .   | 124        |
| 7.2.1    | Traffic Aware and QoS Constrained Sleep Mode Mechanisms                              | 124        |
| 7.2.2    | Migration to Extremely High Frequencies . . . . .                                    | 125        |
| 7.2.3    | D2D Communications . . . . .   | 125        |

|                                     |            |
|-------------------------------------|------------|
| <b>A Appendix</b>                   | <b>127</b> |
| A.1 Copyright permissions . . . . . | 127        |
| <b>References</b>                   | <b>136</b> |

# List of Figures

|      |  |    |
|------|--|----|
| 1.1  | Energy Consumption of a) ICT and b) Wireless Communications as of 2008–2010. A single UK cellular network typically consumes 40 MW. c) Operational Expenditure (OPEX) of typical 3G Cellular Network [1] . . . . . | 2  |
| 2.1  | Non-overlapping channels for 2.4 GHz 802.11n network . . . . .   | 8  |
| 2.2  | System comparison between LTE-femtocell and 802.11 networks . . . . .  | 9  |
| 2.3  | E-UTRAN architecture as part of an LTE network . . . . .   | 10 |
| 2.4  | LTE-femtocell Simulation flow . . . . .  | 12 |
| 2.5  | Femtocell access point placement for 1,2,3 and 4 . . . . .   | 14 |
| 2.6  | BLER and throughput versus SNR plots for the 27 MCSs with SISO and MIMO Alamouti $2 \times 2$ antenna configurations . . . . .   | 22 |
| 2.6  | BLER and throughput versus SNR plots for the 27 MCSs with SISO and MIMO Alamouti $2 \times 2$ antenna configurations . . . . .   | 23 |
| 2.7  | User QoS and average user data rate vs. the number of indoor base stations for LTE-femtocells and 802.11n with SISO and MIMO deployment without outdoor interference . . . . .                                     | 31 |
| 2.8  | Maximum downlink user QoS and average user data rate comparison between LTE-femtocells and 802.11n with SISO and MIMO deployment without outdoor interference . . . . .  | 34 |
| 2.9  | ERG comparison for LTE-femtocells and 802.11n with SISO and MIMO deployment without outdoor interference . . . . .   | 35 |
| 2.10 | QoS and average user data rate comparison between LTE-femtocells and 802.11n with SISO and MIMO deployment with outdoor interference . . . . .   | 36 |

|      |  |    |
|------|--|----|
| 2.11 | QoS and average user data rate comparison between Shannon capacity equation and MCS tables with SISO deployment without outdoor interference . . . . .   | 37 |
| 2.12 | ERG comparison between Shannon and look-up table with SISO and MIMO deployment without outdoor interference . . . . .  | 37 |
| 2.13 | User data rate and ERG comparison vs. 3 FAPs and 3 APs SISO deployment between conventional and alternative scenarios . . . . .  | 38 |
| 3.1  | Simulation model . . . . .   | 45 |
| 3.2  | SGC/RRM algorithm player strategy definition . . . . .   | 48 |
| 3.3  | Trade-off of spectral efficiency and energy efficiency . . . . .   | 52 |
| 4.1  | Simulation and theoretical model . . . . .   | 57 |
| 4.2  | Throughput vs. SNR from WINNER_II A1 SISO configuration and Shannon bound . . . . .  | 59 |
| 4.3  | SINR grid map . . . . .  | 61 |
| 4.4  | Illustration of the analytical scenarios in terms of the saturated throughput region with respect to different FAP positions inside the room. . . . .  | 62 |
| 4.5  | Mean throughput difference (between optimal scenario and the baseline) and operational energy reduction gain (ERG): Theoretical (line) and simulation (symbols) results for optimal FAP placement. . . . . | 70 |
| 4.6  | Mean capacity gain and ERG comparison: Theoretical (line) and simulation (symbols) results of optimal FAP placement with a dominant FAP interference from adjacent room. . . . .                           | 71 |
| 4.7  | Optimal FAP deployment for maximum uniform coverage in: a) investigation setup in iBuildNet; b) a single room; c) multiple rooms. . . . .  | 73 |
| 4.8  | 2 to 6 FAPs optimal location with respect to mutual interference . . . . .   | 74 |
| 4.9  | Average RAN throughput and ERG performance for 2 to 6 FAPs between optimal and conventional deployment . . . . .   | 74 |
| 4.10 | Simulation model of 3D multi-floors-multi-rooms (each grid on every floor represents a room) . . . . .   | 76 |



|      |   |     |
|------|---|-----|
| 4.11 | Optimising indoor femtocell deployment and the capacity and energy consumption improvements . . . . .   | 79  |
| 5.1  | Average LTE spectral efficiency versus the ratio of FAP density to the macro-cell BS density comparison between open access and closed access policy in a two-tier interference-limited heterogeneous network . . . . .   | 96  |
| 5.2  | Probability of outage vs. SNR threshold comparison between open access and closed access policy in a two-tier interference-limited heterogeneous network, with FAP to MBS ratio 10, 30 and 50 . . .   | 97  |
| 5.3  | Interference power comparison between the strongest outdoor BS and all the remaining cells vs. different transmit power of BS . . .   | 102 |
| 6.1  | Network topology uniform hexagonal outdoor and indoor cell-site model . . . . .   | 106 |
| 6.2  | Network topology of non-uniform SPPP two-tier network model in an 20 km × 20 km area . . . . .  | 107 |
| 6.3  | Typical frequency response and deployment of Frequency-Selective-Surface (FSS) . . . . .  | 109 |
| 6.4  | Mean data rate per user and fairness index results for: 6.4(a) one-tier outdoor network, 6.4(b) one-tier indoor network. . . . .  | 111 |
| 6.5  | Mean data rate per user and fairness index results for: 6.5(a) two-tier outdoor network, 6.5(b) two-tier indoor network. . . . .  | 113 |
| 6.6  | Mean data rate per user and fairness index results for: 6.6(a) outdoor network with FSS, 6.6(b) indoor network with FSS in a two-tier heterogeneous network . . . . .   | 114 |
| 6.7  | ERG <sup>RH</sup> comparison between the baseline without FSS and the test network with FSS: 6.7(a) Outdoor two-tier ERG <sup>RH</sup> results with indoor interference] and 6.7(b) Indoor two-tier ERG <sup>RH</sup> results with outdoor interference . . . . . | 116 |
| 6.8  | Required percentage of resource blocks from MBS versus the distance from the MBS to the FAP and ERG <sup>OP</sup> results versus targeted number of indoor users in hexagonal model . . . . .   | 118 |

6.9 Required percentage of resource blocks from MBS versus the ratio of FAP intensity to MBS intensity and  $ERG^{OP}$  results versus targeted number of indoor users in SPPP model . . . . . 119

# Chapter 1

## Introduction

### 1.1 Background

The fourth generation (4G) of mobile communications technology has started around 2005 which enables a wide range of services including computing and multimedia applications ranging from navigation to mobile video streaming [2]. The emergence of new technologies and the increasing growth of subscriber demand have triggered the researcher and industries to move on to the 4G network. Cellular networks are evolving from their telecommunications roots to become more Internet protocol (IP)-based network as in 4G systems, and are expected to further converge into the future mobile Internet protocols over the next decade. With the rapid growth of mobile telephony and networks, end users have witnessed that cellular radio link speed has increased from about 2 Mbit/s with early 3G systems in the year 2000 to 100 Mbit/s with 4G (Long Term Evolution (LTE) and Worldwide Interoperability for Microwave Access (WiMax)) systems using Multiple Input, Multiple Output (MIMO) radio technology. Similarly, short-range Wireless Fidelity (Wi-Fi) radio speeds have also increased from 11 Mbit/s 802.11b in the year 2000 to 300 Mbit/s with 802.11n [3].

In the 4G cellular network context, one of the fastest emerging growing areas of information transfer is the mobile data sector. In 2012, the global traffic for mobile data alone grew by 70%, most of which is video based. In terms of digital connectivity, approximately 70% of the developed world and less than 20% of

## 1. INTRODUCTION

---

the developing world is digitally connected [4]. However, the volume of data communication has increased by more than a factor of 10 over the past 5 years and the associated energy consumption by 20% [5]. Therefore, there is an urgent need to improve the wireless capacity of cellular networks in order to match this tendency of growth in data demand. Moreover, to foster economic growth and reduce the wealth and knowledge gap: a low energy solution that can increase connectivity and meet the growing data demand must be found.

One of the key issues faced by mobile operators is the fall in average revenue per user (ARPU) and the growing operational expenditure (OPEX) due to capacity growth and rising energy prices. The challenge is therefore how to grow the wireless capacity in a way that minimises the OPEX, and thus improves the ARPU. Furthermore, there is growing focus on the environmental impact of information and communication technologies (ICT) sectors. There are tangible financial and environmental motivations for reducing the energy expenditure of wireless networks whilst growing its capacity [6].

Currently, the energy story as shown in Fig. 1.1 is as follows:

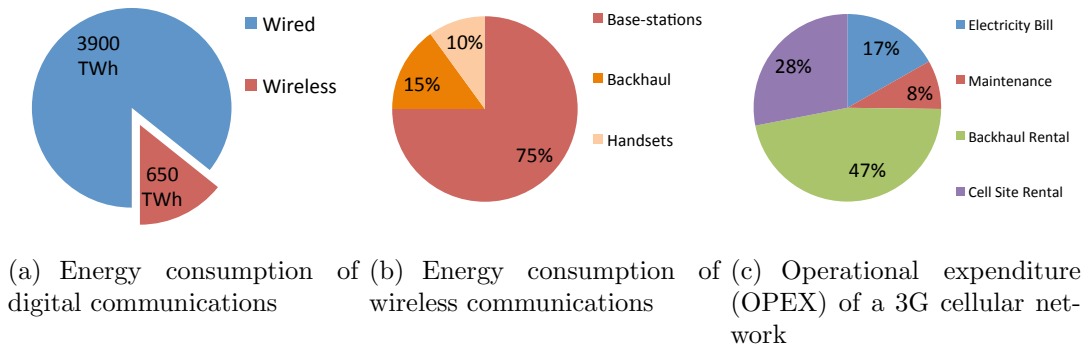


Figure 1.1: Energy Consumption of a) ICT and b) Wireless Communications as of 2008–2010. A single UK cellular network typically consumes 40 MW. c) Operational Expenditure (OPEX) of typical 3G Cellular Network [1]

- 0.5% of the world's total energy (14% of the ICT energy) is consumed by wireless communications, equivalent to 650 TWh.
- Over 90% of this energy is consumed in the outdoor cellular network, of which 75% is consumed by base-stations, which includes 60 TWh of elec-

tricity (20 million households).

- The utility bill is over \$10 billion and 40 MT of CO<sub>2</sub> is directly attributed, with a further 500 MT indirectly attributed.

Thus, many operators are also pledging to reduce carbon emissions [7].

Femtocell is one of the solutions to offload outdoor cellular traffic drastically so as to tackle the ever increasing energy and cost demand. Along with Wi-Fi, femtocells is expected to carry 60% of all global data traffic by femtocells by 2015 [8]. Note that the Wi-Fi counterpart based on 802.11n standards differ from LTE-femtocells in the sense that they continue to use Carrier Sense Multiple Access with Collision Avoidance (CSMA/CA) at the Medium Access Control (MAC) layer in order to maintain compatibility with previous versions of the standard and to limit implementation complexity. Whether to use femtocells or Wi-Fi access points remains unclear in terms of the energy consumption. Moreover, with the introduction of the new small cells to the current macro-cell dominated cellular network, what are the best radio access techniques to reduce the required radiated power and overall power to achieve the required network throughput needs extensively exploring.

## 1.2 Structure of This Thesis

The thesis is structured as follows:

- In Chapter 2, the body of investigation first examines the relative merits of LTE and 802.11n Wi-Fi radio access technologies (RATs), in order to establish a baseline system-level performance. A simulated novel trade-off between capacity and energy consumption is presented for indoor networks, which serves as a useful guidance for deployment [9].

**Contribution:** This chapter addresses the question on the energy comparison of femtocell technology versus 802.11n technology. The comparison investigations have been undertaken in two scenarios. In the baseline conventional scenario, 802.11n APs are deployed on three non-overlapping channels using a total bandwidth of 60 MHz while FAPs are assumed to operate on the same frequency with a total bandwidth of 20 MHz. In the alternative scenario, both 802.11n APs and FAPs have a total bandwidth

of 20 MHz with a frequency reuse pattern 1 and 3, respectively. A full portfolio comparison between these two techniques in terms of different number of nodes and using both adaptive modulation and coding scheme as well as the Shannon Equation has been characterised.

- Chapter 3 exploits the balance between spectral efficiency and energy efficiency by employing a new radio resource management (RRM) and hard frequency reuse approach [10].

**Contribution:** This chapter furthers the study of interference avoidance for a network where both the micro-cell and the LTE-femtocells use OFDMA signalling. A novel interference management approach based on game theory is proposed and the channel quality improvements derived from there are shown to improve the energy efficiency of the E-UTRAN.

- Chapter 4 examines how to create an algorithm that optimises the location of FAP with respect to the dominant interference. This distributed self-deployment solution includes a novel theoretical throughput framework which considers the effects of capacity saturation of realistic modulation and coding schemes and a statistical indoor propagation model [11–14]

**Contribution:** This chapter provides a best practice in optimising FAP deployment with very little SINR degradation for micro-cell users. In the first part of this investigation, this thesis optimises one indoor FAP position with the aim of achieving the highest mean network throughput in the presence of co-channel interference from a dominant source (either a micro-cell or a FAP in an adjacent room). The novel contribution is the simulation results and the proposed theoretical framework that reinforces the key deployment solutions. Moreover, for a given building size, the trade-off between increased user QoS and power consumption, as well as the capacity saturation points are demonstrated in the second part of the study. Finally, it is shown by simulation that the key results hold for a generic building with multiple rooms on multiple floors with an outdoor interference source. The combined results of the three scenarios lead to a general low energy indoor deployment rule.

- In Chapter 5, existing commonly used analytical models of heterogeneous cellular networks are reviewed. It then incorporates all the modelling de-

tails available in the literature for studying the downlink performance of heterogeneous cellular network and proposed a tractable characterisation for both open- and closed-access multi-tier co-channel/non-co-channel heterogeneous networks [15].

**Contribution:** In the proposed extended Spatial Poisson Point Process (SPPP), the statistical interference abstraction is introduced for the first time as of when the study was conducted apart from the the downlink SINR, and the outage probability (i.e., difference between 1 and coverage probability) and the ergodic spectral efficiency.

- Chapter 6 utilises the tractable analytical model derived in the previous chapter to quantify the overall network capacity and the outage probability in closed-access two-tier heterogeneous networks. A frequency-selective-surface (FSS) is proposed to act as a barrier between the two networks to reduce the interference to either side of the users. The effect of the FSS is characterised with the proposed SPPP model as well.

**Contribution:** The body of investigation is conducted by extending a mathematically tractable SPPP framework of a two-tier network for closed access to include wall and FSS loss and the theoretical energy reduction gain. The throughput benefit of FSS on the outdoor-indoor cellular network, the potential transmission energy saving compared to the reference network without FSS deployment and the total energy efficiency compared to the reference network of deploying more non-co-channel indoor FAPs to improve the mean user throughput have been intensively examined by a multi-cell-multi-user simulator reinforced by the extended analytical and tractable framework provided by SPPP. Lastly, the trade-off between outdoor interference to the indoor users and off-loading indoor traffic to outdoor MBS with the resulting total energy saving has been well balanced and captured [15].

- In Chapter 7, the conclusions are drawn, and possible future works are described.

All the reference items mentioned in the above section “structure of the thesis” are mainly my first-authored publications. The permissions for reusing the papers have been acquired from the publishers and attached at the end of the thesis.

# Chapter 2

## Radio Access Technology Comparison

The body of investigation first examines the relative merits of LTE and 802.11n Wi-Fi radio access technologies (RATs), in order to establish a baseline system-level performance. It was found that LTE-femtocells best suit small home networks, providing a high level of spectral- and energy-efficiency. However, the bandwidth availability of 802.11n allows greater system-level throughput to be achieved for multi-AP networks, suitable for enterprises. A simulated novel trade-off between capacity and energy consumption is presented for indoor networks, which serves as a useful guidance for deployment.

### 2.1 Introduction

In recent years, mobile data traffic has experienced a tremendous growth due to the increased popularity of smartphones. Demand for high data rate has left cellular operators struggling to cope. This is especially the case for indoor mobile users. Femtocells and 802.11n Wi-Fi networks have been deployed for providing service to indoor locations where there is no or poor outdoor cellular coverage. Femtocells have attracted significant attention as a solution to increase the system capacity of wireless networks, which exploit spectrum reuse widely [16]. Femto-cell Access Points (FAPs) like Wi-Fi APs are likely to be randomly deployed



## 2. RADIO ACCESS TECHNOLOGY COMPARISON

---

and to be moved by users easily. Contrast to existing Wi-Fi APs, carriers are in favour of FAPs due to their capability of offloading both real-time voice and data traffic from outdoor 3G base stations (BSs). Both FAPs and Wi-Fi-capable handsets work seamlessly with all mobile phones. With the introduction of femtocell technology, serving indoor users with large service demand are becoming cheaper compared with those served by outdoor macrocells and is also very similar to Wi-Fi technology in terms of architecture, operating frequency, offered services and data rates [17].

Femtocells still face many technical as well as business challenges compared with Wi-Fi technology despite their huge potential. The co-channel deployment of such a large femtocell layer will impact the existing macrocell networks, affecting their capacity and performance [18]. Another serious problem for femtocell deployment is the incidence of handover due to movement of the user. These handovers cause the reduction of user's Quality of Service (QoS) level and system capacity [19]. From the service provider point of view a major concern is the energy efficiency of femtocell technology, which is vital for the practical deployment of femtocell base stations and competition with widely deployed 802.11 networks. This chapter aims to investigate the energy efficiency of femtocell and 802.11 networks in both conventional and alternative scenarios by designing a fair and scalable performance comparison framework and performing extensive comparisons based on the framework. A system level simulator to evaluate a multi-cell multi-user with Single Input, Single Output (SISO) and Multiple Input, Multiple Output (MIMO) antenna configurations LTE-femtocells network is implemented, and an analytical model to evaluate 802.11n network performance for simplicity and scalability is also developed. As the downlink traffic may constitute a major part of an LTE network traffic, the performance comparison has been focused on the downlink with both SISO and MIMO antenna configurations. The results have been obtained for a typical large office, various traffic loads and target QoS requirements.

## 2.2 Investigation Framework

LTE-femtocells support scalable carrier bandwidths, from 1.4 MHz to 20 MHz based on the standards developed by the 3<sup>rd</sup> Generation Partnership Project (3GPP) [20], while the 802.11n currently uses two distinct frequency ranges, 2.4 GHz and 5.0 GHz bands. Each range is divided into a multitude of channels [21]. There are 14 channels designated in the 2.4 GHz range spaced 5 MHz apart (with the exception of a 12 MHz spacing before Channel 14). As the 802.11n protocol requires 25 MHz of channel separation, adjacent channels overlap and will interfere with each other. Consequently, using only channels 1, 5, 9 and 13 is recommended to avoid interference for 802.11n as shown in Fig. 2.1. In the USA, 802.11 operation in the channels 12 and 13 is actually only allowed under low powered conditions.

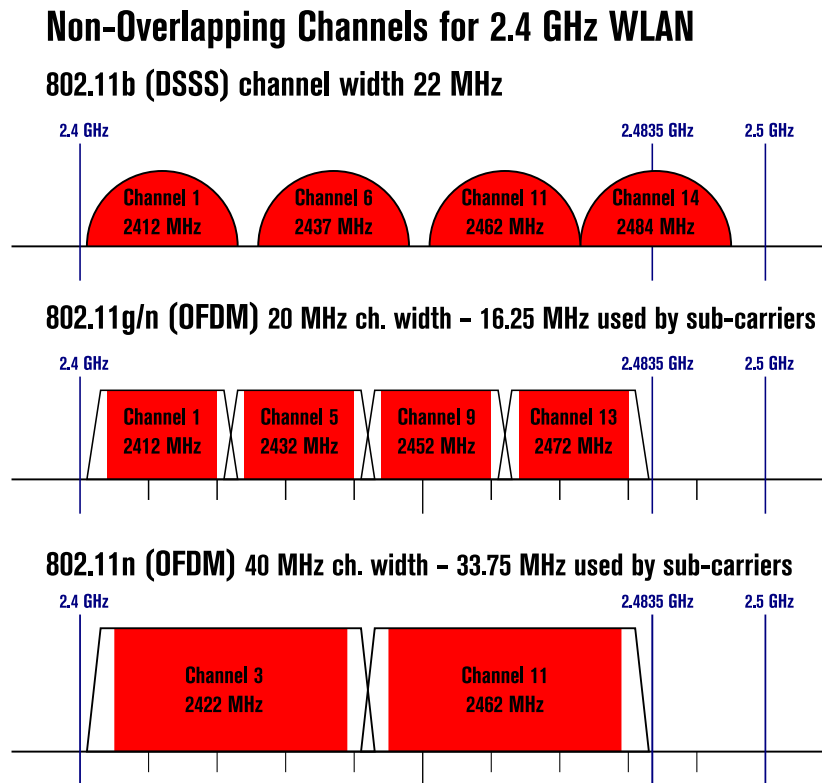


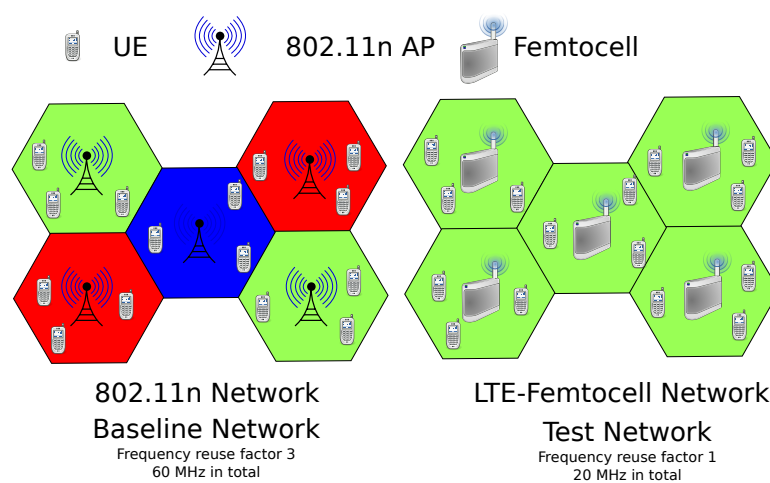
Figure 2.1: Non-overlapping channels for 2.4 GHz 802.11n network

Source: [Wikipedia](#), [IEEE.802.11](#)

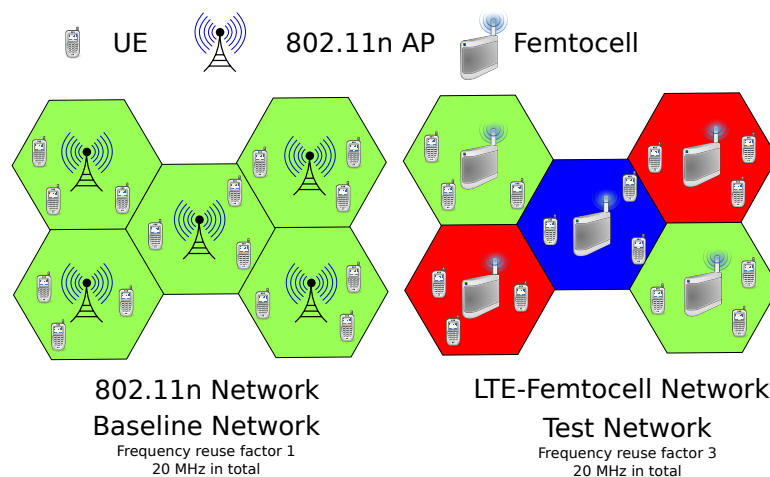
## 2. RADIO ACCESS TECHNOLOGY COMPARISON

---

According to the above specifications, the comparison investigations have been undertaken in two scenarios illustrated in Fig. 2.2. In the baseline conventional scenario 2.2(a), 802.11n APs are deployed on three non-overlapping channels using a total bandwidth of 60 MHz while FAPs are assumed to operate on the same frequency with a total bandwidth of 20 MHz. In the alternative scenario 2.2(b), both 802.11n APs and FAPs have a total bandwidth of 20 MHz with a frequency reuse pattern 1 and 3, respectively.



(a) Conventional scenario



(b) Alternative scenario

Figure 2.2: System comparison between LTE-femtocell and 802.11 networks

## 2.3 LTE-femtocell Simulator Model

In this section, details of the LTE-femtocell simulator are provided. This simulator has been conceived to simulate downlink scheduling strategies in multi-cell multi-users environments taking into account BS planning, user mobility, radio resource optimisation, interference and Quality of Service (QoS) management, frequency reuse techniques, Adaptive Modulation and Coding (AMC) module, Single Input Single Output (SISO) and Multiple Input Multiple Output (MIMO) antenna configurations, and other aspects which are very relevant for industrial and scientific research. It encompasses both the Evolved Universal Terrestrial Radio Access (E-UTRAN), the air interface of 3GPP's LTE upgrade path for mobile networks, and the Evolved Packet System (EPS), the Internet Protocol (IP)-based network architecture as shown in Fig. 2.3.

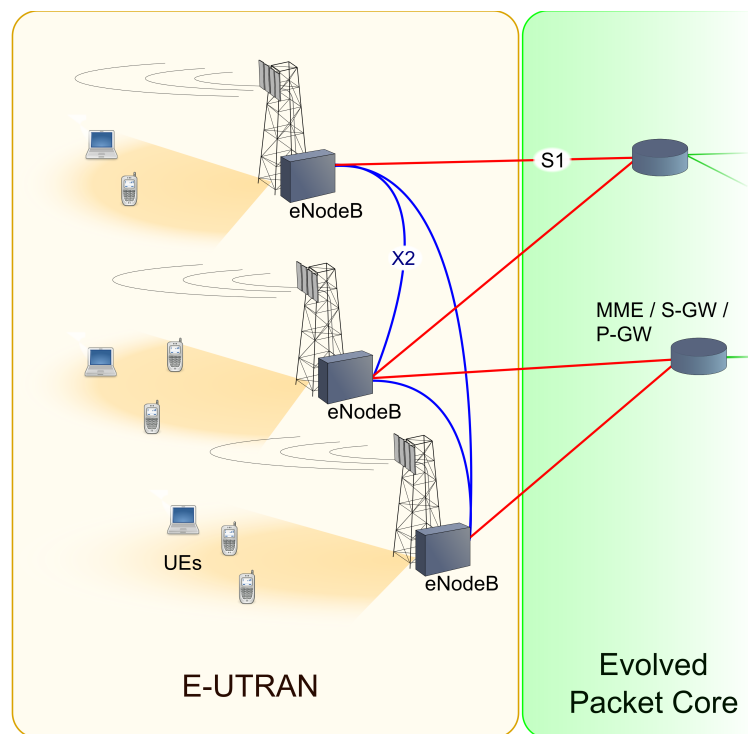


Figure 2.3: E-UTRAN architecture as part of an LTE network

Source: [Wikipedia, E-UTRAN](#)

Three kinds of network nodes are modelled: User Equipment (UE), evolved Node B (eNB)(Macro Radio Access Network (RAN)) and Home Node B (HNB)(3G femtocell). This simulator provides a support for radio resource allocation in a time-frequency domain. LTE allows different timing granularities [22]. Radio resource allocation is performed every Transmission Time Interval (TTI), each one lasting 1 ms. Each TTI consists of two slots of 0.5 ms corresponding to 14 Orthogonal Frequency-division Multiplexing (OFDM) symbols in the default configuration with short cyclic prefix (CP) [23]. In the frequency domain, the whole bandwidth is divided into 180 kHz sub-channels, each of which contains 12 consecutive 15 kHz sub-carriers. A Physical Resource Block (PRB) is defined as a time/frequency radio resource spanning over 7 OFDM symbols in the time domain and 12 sub-carriers in the frequency domain. This is also the smallest resource element which can be assigned to a UE for data transmission. Therefore, one TTI for 20 MHz bandwidth contains 100 PRBs with 14 OFDM symbols. The first three OFDM symbols of every TTI are reserved for transmission of related downlink control channels. The number of PRBs depends on the system bandwidth since the sub-channel dimension is fixed. A system bandwidth of 20 MHz with 100 resource blocks is considered in this thesis unless otherwise specified.

Physical layer (PHY) aspects are managed for all UEs, eNBs and HNBs. This is to say, physical parameters and radio channel models proposed in [22] are connected to each device. Information such as channel quality, perceived interference level, available bandwidth, list of available PRBs and frequency reuse pattern are stored and in matrix form for future reference.

### 2.3.1 Simulation Flow

Fig. 2.4 shows the simulation flow chart for this comparison study. The position of each user and the traffic conditions are updated within each TTI. Next, the propagation channel between each UE and its FAP, and the received Signal to Interference-plus-Noise Ratio (SINR) are properly calculated before scheduling is performed for each snapshot. The network throughput is then computed by combining all UEs' data rates and the QoS data rates are obtained as well.

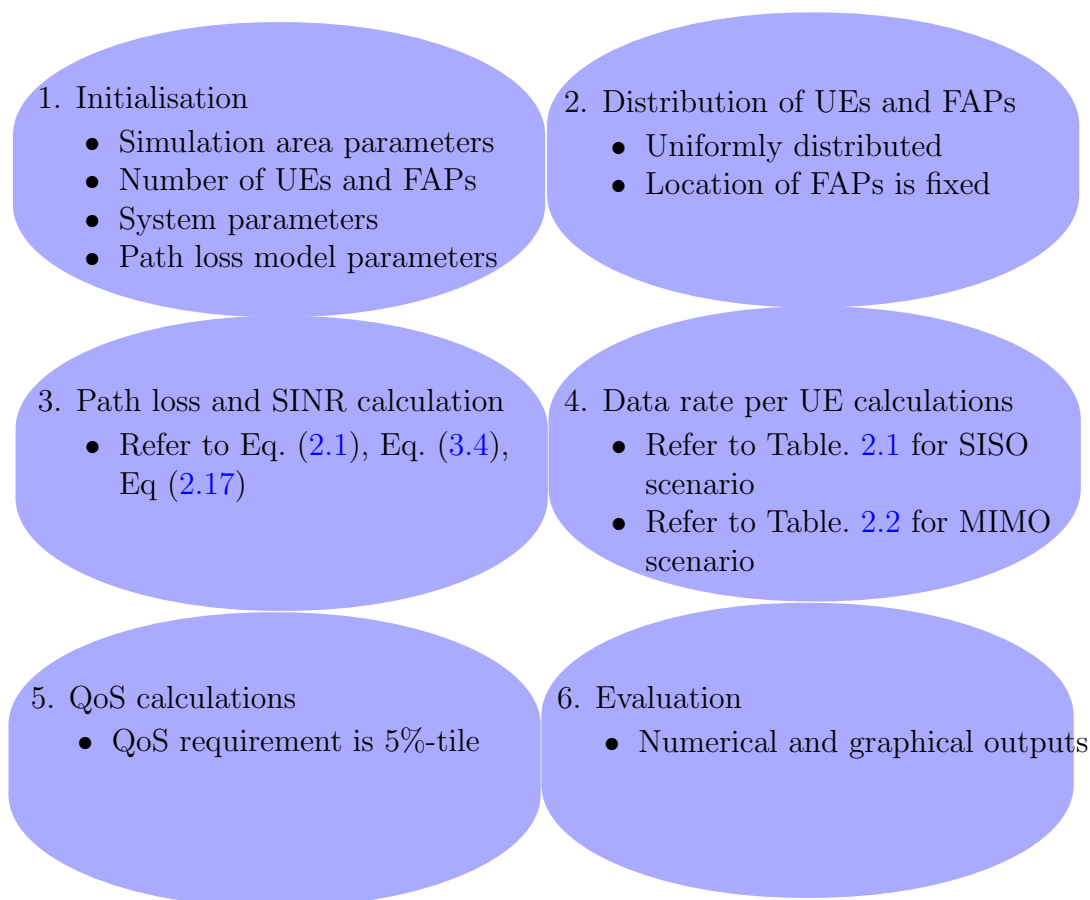


Figure 2.4: LTE-femtocell Simulation flow

### 2.3.2 Initialisation

In the first part of the initialisation procedure for this comparison study, all the parameters that remain constant during the whole simulation lifecycle are set. The following parameters can be adjusted as needed:

- number of users,
- number of FAPs,
- size of the office,
- FAP transmit power
- bandwidth,
- carrier frequency,
- frequency reuse pattern,

- target QoS.

A total number of 50 users are distributed randomly and uniformly across the whole enterprise office whose area is 20 m × 16 m. It is worth mentioning that the number of users and the office size can be configured as required. Only one single floor building with light internal walls (e.g. plaster board) is considered. The number of FAPs varies from 1 to 6. However the number of FAPs can be configured to any integer. The simulation results are less meaningful after the number of FAPs is greater than 6. Due to the omni-directional radiation pattern of the FAP, its deployment was conducted to minimise the mean distance from users to FAP. Therefore, there is always one FAP deployed in the middle of the room except for the case of 2 FAPs, in which case they are placed at the foci of the ellipse layout. For the remaining deployments, all other APs excluding the middle one are placed evenly around the circumference of the ellipse as shown in Fig. 2.5. Investigation of optimal AP placement and interference management are covered in Chapter. 4.

### 2.3.3 Propagation Model

The path loss model implemented in the simulator is adopted from Chapter 4 in the book [24]. The path loss between a FAP and a mobile user can be calculated as follows:

$$PL = 18.7 \log_{10}(d) + 46.8 + 20 \log_{10}\left(\frac{f}{5}\right), \quad (2.1)$$

where, PL is the total path loss in dBs.  $f$  is frequency of transmission in MHz.  $d$  is distance in metres. The model assumes an aggregate loss through furniture, internal walls and doors. Unlike other models, which are site-specific, this method does not require a knowledge of the number of walls between the two terminals. Therefore it enables a simpler implementation and can be generalised across a wide range of buildings.

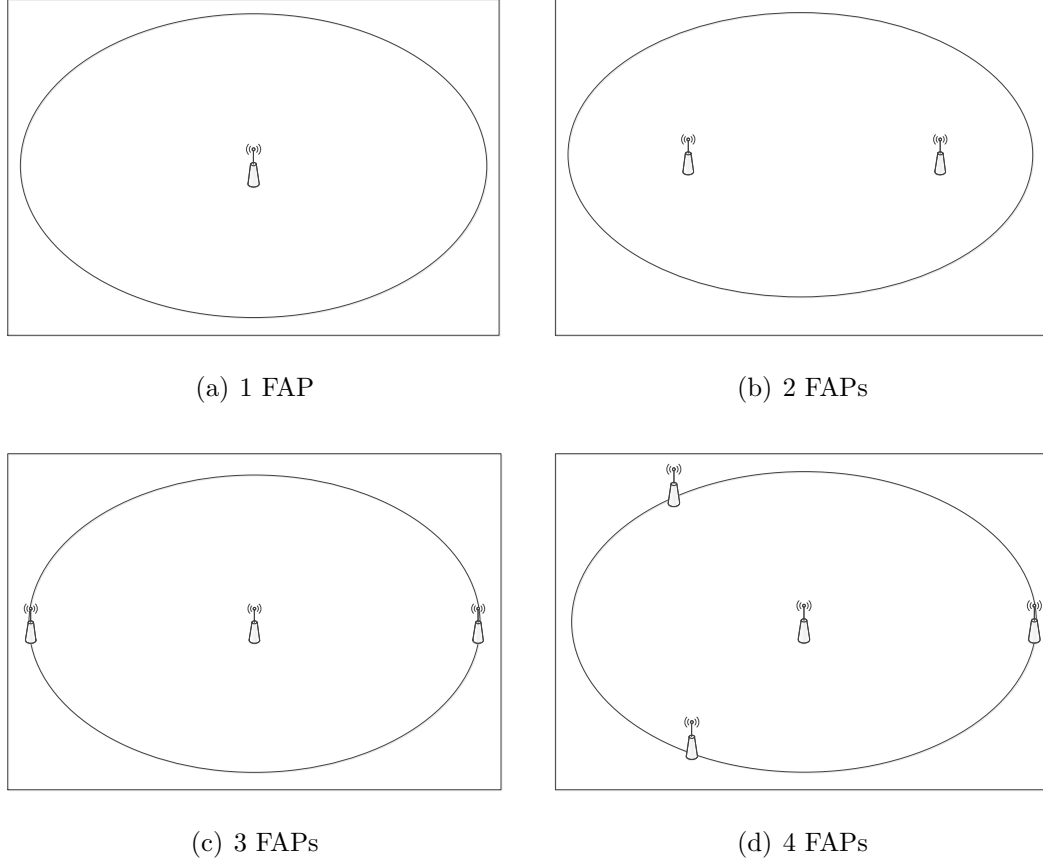


Figure 2.5: Femtocell access point placement for 1,2,3 and 4

### 2.3.4 Signal Model and SINR Calculation

The baseband downlink received signal in the presence of the interference can be expressed as follows:

$$y_0[t] = h_0 x_0[t] + \sum_{k=1}^K h_k x_k[t] + w_0[t], \quad (2.2)$$

where  $h_0, h_k \sim \mathcal{CN}(0, 1)$  and  $w_0 \sim \mathcal{CN}(0, \sigma^2)$  are the channel coefficient of the desired BS,  $k^{\text{th}}$  interfering BS and the noise at time  $t$  for flat fading channels, respectively. They are modelled as independent and identically distributed (i.i.d.) circularly symmetric complex Gaussian random variables with zero mean and a variance of one and  $\sigma^2$  at time  $t$ , respectively. The output estimated signal



from the matched filter is given by Eq. (2.3) (projecting the received signal in the direction of the channel):

$$\begin{aligned}\hat{y}_0[t] &= \frac{h_0^*}{|h_0|^2} y_0[t], \\ &= x_0[t] + \frac{h_0^*}{|h_0|^2} \sum_{k=1}^K h_k x_k[t] + \frac{h_0^*}{|h_0|^2} w_0[t].\end{aligned}\tag{2.3}$$

The SINR of the estimated signal  $\gamma_{\text{SISO}}$  can be calculated as below:

$$\begin{aligned}\gamma_{\text{SISO}} &= \frac{\mathbb{E}(|x_0[t]|^2)}{\mathbb{E}(|\frac{h_0^*}{|h_0|^2} \sum_{k=1}^K h_k x_k[t]|^2) + \mathbb{E}(|\frac{h_0^*}{|h_0|^2} w_0[t]|^2)}, \\ &= \frac{P_0}{\mathbb{E}(|\frac{h_0^*}{|h_0|^2}|^2) \mathbb{E}(\sum_{k=1}^K |h_k x_k[t]|^2) + \mathbb{E}(|\frac{h_0^*}{|h_0|^2}|^2) \mathbb{E}(|w_0[t]|^2)}, \\ &= \frac{1}{\frac{1}{|h_0|^2} \sum_{k=1}^K |h_k|^2 P_k + \frac{1}{|h_0|^2} \sigma^2}, \\ &= \frac{|h_0|^2 P_0}{\sum_{k=1}^K |h_k|^2 P_k + \sigma^2},\end{aligned}\tag{2.4}$$

where  $P_0$  is the received power of a certain sub-carrier from the desired BS,  $P_k$  is the received power of the same sub-carrier from the  $k^{\text{th}}$  interfering BS and  $\sigma^2$  is the noise power. Here, perfect channel synchronisation has been assumed in this thesis unless otherwise specified.

The downlink channel with Alamouti  $2 \times 2$  received signal model can be expressed as:

$$\mathbf{y}_{0.22}[t] = \mathbf{H}_{0.22} \mathbf{x}_{0.22}[t] + \sum_{k=1}^K \mathbf{H}_{k.22} \mathbf{x}_{k.22}[t] + \mathbf{w}_{0.22}[t],\tag{2.5}$$

where  $\mathbf{x}_{0.22}$  and  $\mathbf{x}_{k.22}$  are the transmit vectors ( $2 \times 1$ ),  $\mathbf{w}_{0.22}$  is a noise vector ( $2 \times 1$ ) and its samples are circularly symmetric complex Gaussian distributed variables  $\sim \mathcal{CN}(0, \sigma^2)$  with zero mean and variance of  $\sigma^2$ .  $\mathbf{H}_{i.22}(i = 0, k)$  is an

equivalent channel matrix given by:

$$\mathbf{H}_{i.22} = (\mathbf{H}_{1i.22}, \mathbf{H}_{2i.22})^T, (i = 0, k), \quad (2.6)$$

where

$$\mathbf{H}_{1i.22} = \begin{pmatrix} h_{1i1} & h_{1i2} \\ h_{1i2}^* & -h_{1i1}^* \end{pmatrix}, \quad (2.7)$$

and

$$\mathbf{H}_{2i.22} = \begin{pmatrix} h_{2i1} & h_{2i2} \\ h_{2i2}^* & -h_{2i1}^* \end{pmatrix}, \quad (2.8)$$

are the equivalent Alamouti channel matrices of received antenna 1 and antenna 2, respectively.  $h_{1i1}$ ,  $h_{1i2}$ ,  $h_{2i1}$  and  $h_{2i2}$  are the channel coefficients modelled as i.i.d circularly symmetric complex normal random variables  $\sim \mathcal{CN}(0, 1)$  with zero mean and a variance of one. The first two channel coefficients are from transmitting antenna 1 and 2 to receiving antenna 1, the remaining two are from transmitting antenna 1 and 2 to receiving antenna 2 of the  $i^{th}$  BS. Therefore, Eq. (2.6) can employ Eq. (2.7) and (2.8) to be:

$$\begin{aligned} \mathbf{H}_{i.22} &= \begin{pmatrix} \mathbf{H}_{1i.22} \\ \mathbf{H}_{2i.22} \end{pmatrix}, (i = 0, k), \\ &= \begin{pmatrix} h_{1i1} & h_{1i2} \\ h_{1i2}^* & -h_{1i1}^* \\ h_{2i1} & h_{2i2} \\ h_{2i2}^* & -h_{2i1}^* \end{pmatrix}. \end{aligned} \quad (2.9)$$

The estimated signal from the Alamouti receiver can be obtained by multiplying  $\mathbf{y}_{0.22}[t]$  with the pseudo inverse of the equivalent channel matrix of the corresponding BS. For a general (non-square) matrix, the pseudo inverse is defined as  $\mathbf{H}^{-1} = (\mathbf{H}^H \mathbf{H})^{-1} \mathbf{H}^H$ , where  $\mathbf{H}^H$  is the transpose conjugate, also known as

Hermitian, of the matrix  $\mathbf{H}$ . Hence the estimated signal  $\hat{\mathbf{y}}_{\mathbf{0},\mathbf{21}}[t]$  is given by:

$$\begin{aligned}\hat{\mathbf{y}}_{\mathbf{0},\mathbf{22}}[t] &= (\mathbf{H}_{\mathbf{0},\mathbf{22}}^H \mathbf{H}_{\mathbf{0},\mathbf{22}})^{-1} \mathbf{H}_{\mathbf{0},\mathbf{22}}^H \mathbf{y}_{\mathbf{0},\mathbf{22}}[t], \\ &= (\mathbf{H}_{\mathbf{0},\mathbf{22}}^H \mathbf{H}_{\mathbf{0},\mathbf{22}})^{-1} \mathbf{H}_{\mathbf{0},\mathbf{22}}^H \mathbf{H}_{\mathbf{0},\mathbf{22}} \mathbf{x}_{\mathbf{0},\mathbf{22}}[t] + \sum_{k=1}^K (\mathbf{H}_{\mathbf{0},\mathbf{22}}^H \mathbf{H}_{\mathbf{0},\mathbf{22}})^{-1} \mathbf{H}_{\mathbf{0},\mathbf{22}}^H \mathbf{H}_{k,\mathbf{22}} \mathbf{x}_{k,\mathbf{22}}[t] \\ &\quad + (\mathbf{H}_{\mathbf{0},\mathbf{22}}^H \mathbf{H}_{\mathbf{0},\mathbf{22}})^{-1} \mathbf{H}_{\mathbf{0},\mathbf{22}}^H \mathbf{w}_{\mathbf{0},\mathbf{22}}[t],\end{aligned}\tag{2.10}$$

where  $\mathbf{H}_{i,\mathbf{22}}^H \mathbf{H}_{i,\mathbf{22}}$  and  $(\mathbf{H}_{i,\mathbf{22}}^H \mathbf{H}_{i,\mathbf{22}})^{-1} \mathbf{H}_{i,\mathbf{22}}^H \mathbf{H}_{i,\mathbf{22}}$  can be calculated by the following Eq. (2.11) and Eq. (2.12):

$$\begin{aligned}\mathbf{H}_{i,\mathbf{22}}^H \mathbf{H}_{i,\mathbf{22}} &= \begin{pmatrix} h_{1i1}^* & h_{1i2} & h_{2i1}^* & h_{2i2} \\ h_{1i2}^* & -h_{1i1} & h_{2i2}^* & -h_{2i1} \end{pmatrix} \begin{pmatrix} h_{1i1} & h_{1i2} \\ h_{1i2}^* & -h_{1i1}^* \\ h_{2i1} & h_{2i2} \\ h_{2i2}^* & -h_{2i1}^* \end{pmatrix}, \\ &= \begin{pmatrix} |h_{1i1}|^2 + |h_{1i2}|^2 + |h_{2i1}|^2 + |h_{2i2}|^2 & 0 \\ 0 & |h_{1i1}|^2 + |h_{1i2}|^2 + |h_{2i1}|^2 + |h_{2i2}|^2 \end{pmatrix}, \\ &= \frac{\|\mathbf{H}_{i,\mathbf{22}}\|^2}{2} \mathbf{I}_2, \quad (i = 0, k),\end{aligned}\tag{2.11}$$

$$(\mathbf{H}_{i,\mathbf{22}}^H \mathbf{H}_{i,\mathbf{22}})^{-1} \mathbf{H}_{i,\mathbf{22}}^H \mathbf{H}_{i,\mathbf{22}} = \frac{2}{\|\mathbf{H}_{i,\mathbf{22}}\|^2} \mathbf{I}_2 \frac{\|\mathbf{H}_{i,\mathbf{22}}\|^2}{2} \mathbf{I}_2 = \mathbf{I}_2.\tag{2.12}$$

where  $\mathbf{I}_2$  is a  $2 \times 2$  identity matrix and  $\|\cdot\|$  is an operation of the Frobenius norm for a vector or matrix (e.g.  $\|\mathbf{H}_{i,\mathbf{22}}\| = \sqrt{2(|h_{1i1}|^2 + |h_{1i2}|^2 + |h_{2i1}|^2 + |h_{2i2}|^2)}$ ).

Eq. (2.10) can be simplified as:

$$\hat{\mathbf{y}}_{\mathbf{0},\mathbf{22}}[t] = \mathbf{I}_2 \mathbf{x}_{\mathbf{0},\mathbf{22}}[t] + \frac{2}{\|\mathbf{H}_{\mathbf{0},\mathbf{22}}\|^2} \left( \sum_{k=1}^K \mathbf{H}_{\mathbf{0},\mathbf{22}}^H \mathbf{H}_{k,\mathbf{22}} \mathbf{x}_{k,\mathbf{22}}[t] + \mathbf{H}_{\mathbf{0},\mathbf{22}}^H \mathbf{w}_{\mathbf{0},\mathbf{22}}[t] \right),\tag{2.13}$$

The SINR of the estimated signal  $\gamma_{\text{MIMO}_{2 \times 2}}$  can be calculated as below (Note that the transmit power is shared between two antennas in order to have the same total radiated power from two transmitting antennas and hence the received power is

also halved):

$$\begin{aligned}
 \gamma_{\text{MIMO}2 \times 2} &= \frac{\frac{1}{2}P_0\mathbf{I}_2}{\frac{4}{\|\mathbf{H}_{0.22}\|^4} [\sum_{k=1}^K \mathbb{E}(\mathbf{H}_{0.22}^H \mathbf{H}_{k.22} \mathbf{H}_{k.22}^H \mathbf{H}_{0.22}) \frac{1}{2}P_k + \mathbb{E}(\mathbf{H}_{0.22}^H \mathbf{H}_{0.22})\sigma^2]}, \\
 &= \frac{\|\mathbf{H}_{0.22}\|^4 P_0 \mathbf{I}_2}{4 \sum_{k=1}^K \mathbb{E}(\mathbf{H}_{0.22}^H \mathbf{H}_{k.22} \mathbf{H}_{k.22}^H \mathbf{H}_{0.22}) P_k + 2 \frac{\|\mathbf{H}_{0.22}\|^2}{2} \mathbf{I}_2 \sigma^2}, \\
 &= \frac{\|\mathbf{H}_{0.22}\|^4 P_0 \mathbf{I}_2}{4 \sum_{k=1}^K H_{22} P_k \mathbf{I}_2 + \|\mathbf{H}_{0.22}\|^2 \sigma^2 \mathbf{I}_2}.
 \end{aligned} \tag{2.14}$$

where

$$\mathbb{E}(\mathbf{H}_{0.22}^H \mathbf{H}_{k.22} \mathbf{H}_{k.22}^H \mathbf{H}_{0.22}) = H_{22} \mathbf{I}_2, \tag{2.15}$$

and

$$H_{22} = (|h_{101}|^2 + |h_{102}|^2)(|h_{1k1}|^2 + |h_{1k2}|^2) + (|h_{201}|^2 + |h_{202}|^2)(|h_{2k1}|^2 + |h_{2k2}|^2). \tag{2.16}$$

Eq. (2.14) implies that the SINR values on both antenna streams are identical and the symbols can be decoupled at the receiver easily owing to the characteristic of Alamouti scheme. Hence, the SINR value for the single stream Alamouti  $2 \times 2$  is equal to:

$$\gamma_{\text{MIMO}2 \times 2} = \frac{\|\mathbf{H}_{0.22}\|^4 P_0}{4 \sum_{k=1}^K H_{22} P_k + \|\mathbf{H}_{0.22}\|^2 \sigma^2}. \tag{2.17}$$

The corresponding system capacity will be determined after using the detailed SINR derivation and its associated link adaptation value discussed in the following section.

### 2.3.5 Link Adaptation

Link adaptation, or Adaptive Coding and Modulation (ACM), is a term used in wireless communications to denote the matching of the modulation, coding and other signal and protocol parameters to the conditions on the radio link (e.g. the pathloss, the interference due to signals coming from other transmitters, the sensitivity of the receiver, the available transmitter power margin, etc.). The process of link adaptation is a dynamic one and the signal and protocol param-

## 2. RADIO ACCESS TECHNOLOGY COMPARISON

---

eters change as the radio link conditions change. The simulator supports link adaptation by changing the Modulation and Coding Scheme (MCS) based on the channel quality (i.e., SINR). Table 2.1 and Table 2.2 present the SISO and MIMO link adaptation look-up tables for an indoor scenario. For instance in Table 2.1, if the channel quality (SINR) is greater than 3.54 dB but less than 6.28 dB, link adaptation selects MCS QPSK with code rate 1/3 that translates to 0.57 bits per resource element. The number of bits per resource element is calculated by multiplying the rate by the duration of one TTI (1 ms) and then dividing by the product of the number of OFDM symbols (14) and the total number of resource elements (1200). These look-up tables were generated from the Vienna link level LTE simulator [25] under WINNER II A1 multipath model [26]. The corresponding Block Error Rate (BLER) and throughput versus Signal to Noise Ratio (SNR) curves of the look-up tables are illustrated in Fig. 2.6.

## 2. RADIO ACCESS TECHNOLOGY COMPARISON

---

Table 2.1: Downlink SINR requirement for SISO LTE-femtocell indoor scenario with 20 MHz bandwidth ( $N_{\text{bits/subcarrier}}$  stands for number of bits per subcarrier)

| SINR (dB)                   | Rate (Mbps) | Modulation | Code rate | $N_{\text{bits/subcarrier}}$ |
|-----------------------------|-------------|------------|-----------|------------------------------|
| $-2.00 \leq \gamma < 1.89$  | 3.47        | QPSK       | 1/9       | 0.21                         |
| $1.89 \leq \gamma < 3.54$   | 7.17        | QPSK       | 1/4       | 0.43                         |
| $3.54 \leq \gamma < 6.28$   | 9.54        | QPSK       | 1/3       | 0.57                         |
| $6.28 \leq \gamma < 9.36$   | 12.04       | QPSK       | 0.42      | 0.72                         |
| $9.36 \leq \gamma < 11.34$  | 14.29       | QPSK       | 1/2       | 0.85                         |
| $11.34 \leq \gamma < 11.75$ | 15.64       | QPSK       | 2/3       | 0.93                         |
| $11.75 \leq \gamma < 14.36$ | 17.19       | QPSK       | 0.73      | 1.02                         |
| $14.36 \leq \gamma < 17.48$ | 26.14       | 16QAM      | 0.46      | 1.56                         |
| $17.48 \leq \gamma < 19.42$ | 28.64       | 16QAM      | 1/2       | 1.70                         |
| $19.42 \leq \gamma < 19.72$ | 33.34       | 16QAM      | 0.58      | 1.98                         |
| $19.72 \leq \gamma < 21.47$ | 38.19       | 16QAM      | 2/3       | 2.27                         |
| $21.47 \leq \gamma < 22.72$ | 45.96       | 16QAM      | 4/5       | 2.74                         |
| $22.72 \leq \gamma < 23.26$ | 60.12       | 64QAM      | 2/3       | 3.58                         |
| $23.26 \leq \gamma < 25.15$ | 64.17       | 64QAM      | 0.90      | 3.82                         |
| $25.15 \leq \gamma < 26.38$ | 67.06       | 64QAM      | 0.90      | 3.99                         |
| $26.38 \leq \gamma < 27.65$ | 68.32       | 64QAM      | 0.90      | 4.07                         |
| $27.65 \leq \gamma < 28.82$ | 69.23       | 64QAM      | 0.90      | 4.12                         |
| $28.82 \leq \gamma < 29.92$ | 69.79       | 64QAM      | 0.90      | 4.15                         |
| $29.92 \leq \gamma < 31.97$ | 70.20       | 64QAM      | 0.90      | 4.18                         |
| $31.97 \leq \gamma < 33.67$ | 70.63       | 64QAM      | 0.90      | 4.20                         |
| $33.67 \leq \gamma < 35.94$ | 70.86       | 64QAM      | 0.90      | 4.22                         |
| $\gamma \geq 35.94$         | 71.01       | 64QAM      | 0.90      | 4.23                         |

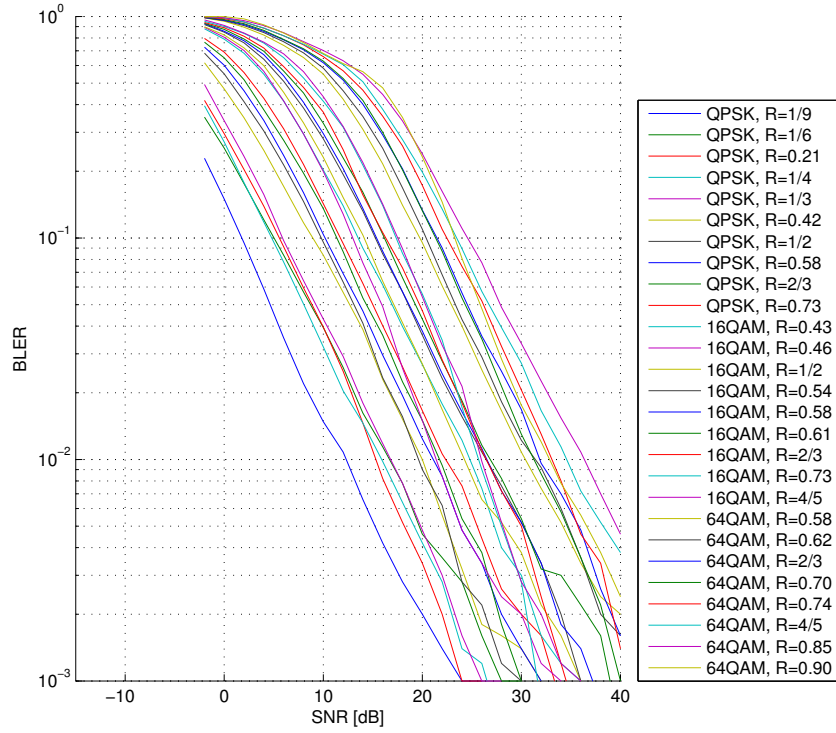
## 2. RADIO ACCESS TECHNOLOGY COMPARISON

---

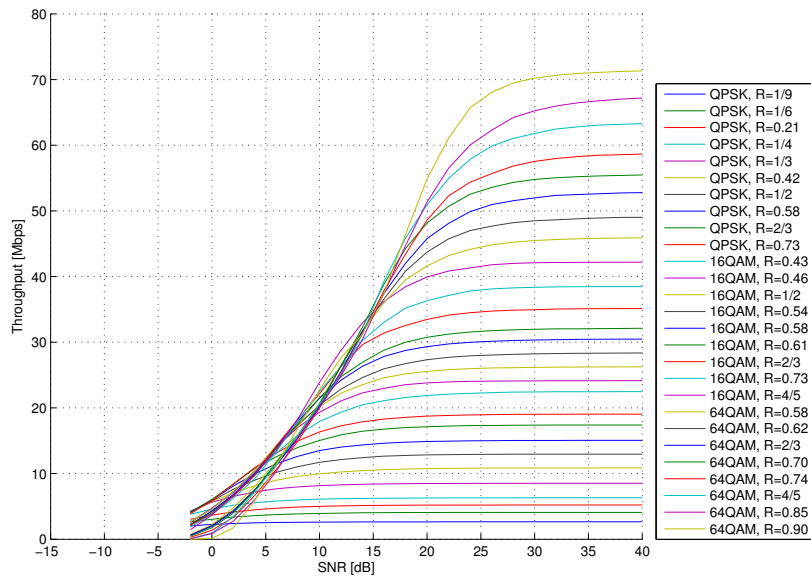
Table 2.2: Downlink SINR requirement for single stream MIMO  $2 \times 2$  LTE-femtocells indoor scenario with 20 MHz bandwidth

| SINR (dB)                   | Rate (Mbps) | Modulation | Code rate | $N_{\text{bits/subcarrier}}$ |
|-----------------------------|-------------|------------|-----------|------------------------------|
| $-1.02 \leq \gamma < 0.93$  | 5.33        | QPSK       | 1/4       | 0.32                         |
| $0.93 \leq \gamma < 1.38$   | 9.12        | QPSK       | 0.42      | 0.54                         |
| $1.38 \leq \gamma < 3.23$   | 10.92       | QPSK       | 1/2       | 0.65                         |
| $3.23 \leq \gamma < 3.55$   | 12.69       | QPSK       | 0.58      | 0.76                         |
| $3.55 \leq \gamma < 4.23$   | 14.67       | QPSK       | 2/3       | 0.87                         |
| $4.23 \leq \gamma < 6.71$   | 16.16       | QPSK       | 0.73      | 0.96                         |
| $6.71 \leq \gamma < 6.79$   | 18.97       | 16QAM      | 0.43      | 1.13                         |
| $6.79 \leq \gamma < 7.50$   | 20.46       | 16QAM      | 0.46      | 1.22                         |
| $7.50 \leq \gamma < 8.02$   | 22.29       | 16QAM      | 1/2       | 1.33                         |
| $8.02 \leq \gamma < 8.65$   | 26.09       | 16QAM      | 0.58      | 1.55                         |
| $8.65 \leq \gamma < 9.57$   | 27.11       | 16QAM      | 0.61      | 1.61                         |
| $9.57 \leq \gamma < 10.84$  | 29.84       | 16QAM      | 2/3       | 1.78                         |
| $10.84 \leq \gamma < 12.30$ | 31.83       | 16QAM      | 0.73      | 1.89                         |
| $12.30 \leq \gamma < 13.41$ | 35.94       | 16QAM      | 4/5       | 2.14                         |
| $13.41 \leq \gamma < 14.35$ | 39.27       | 64QAM      | 0.58      | 2.34                         |
| $14.35 \leq \gamma < 14.69$ | 41.83       | 64QAM      | 0.62      | 2.49                         |
| $14.69 \leq \gamma < 15.71$ | 46.86       | 64QAM      | 0.70      | 2.79                         |
| $15.71 \leq \gamma < 18.19$ | 50.34       | 64QAM      | 0.74      | 3.00                         |
| $18.19 \leq \gamma < 18.45$ | 54.17       | 64QAM      | 4/5       | 3.22                         |
| $18.45 \leq \gamma < 19.30$ | 57.56       | 64QAM      | 0.85      | 3.43                         |
| $19.30 \leq \gamma < 20.46$ | 60.84       | 64QAM      | 0.90      | 3.62                         |
| $20.46 \leq \gamma < 21.15$ | 63.54       | 64QAM      | 0.90      | 3.78                         |
| $21.15 \leq \gamma < 22.43$ | 64.61       | 64QAM      | 0.90      | 3.85                         |
| $22.43 \leq \gamma < 24.34$ | 66.20       | 64QAM      | 0.90      | 3.94                         |
| $24.34 \leq \gamma < 27.22$ | 67.20       | 64QAM      | 0.90      | 4.00                         |
| $\gamma \geq 27.22$         | 67.72       | 64QAM      | 0.90      | 4.03                         |

## 2. RADIO ACCESS TECHNOLOGY COMPARISON



(a) BLER vs. SNR WINNER II A1 SISO

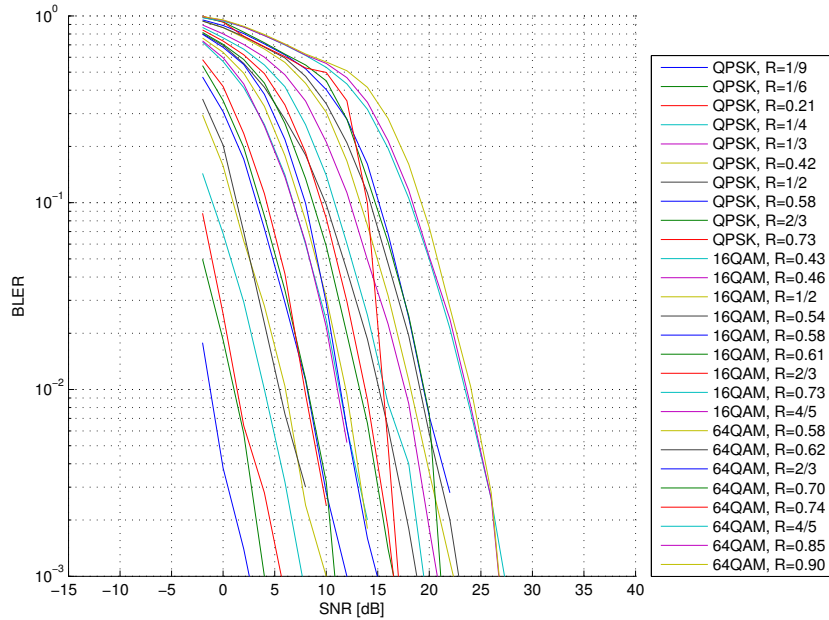


(b) Throughput vs. SNR WINNER II A1 SISO

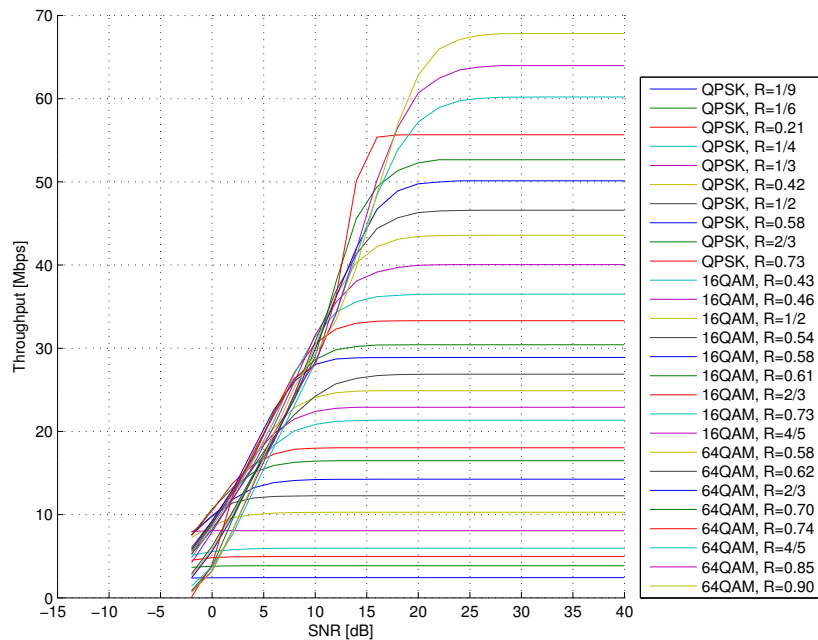
Figure 2.6: BLER and throughput versus SNR plots for the 27 MCSs with SISO and MIMO Alamouti  $2 \times 2$  antenna configurations



## 2. RADIO ACCESS TECHNOLOGY COMPARISON



(a) BLER vs. SNR WINNER II A1 MIMO



(b) Throughput vs. SNR WINNER II A1 MIMO

Figure 2.6: BLER and throughput versus SNR plots for the 27 MCSs with SISO and MIMO Alamouti  $2 \times 2$  antenna configurations

### 2.3.6 Scheduling

The purpose of the scheduler is to determine which users to transmit data (time domain scheduler) and on which set of resource blocks (frequency domain scheduler). For simplicity in this simulator, the time domain scheduler treats each user fairly and accepts all the connected users to the frequency scheduler. The frequency scheduler implemented in each femtocell AP manages and allocates network resources using a Round-Robin' (RR) policy. This scheduler assigns resource blocks to the users in a closed loop circular manner regardless the users' Channel State Information (CSI) or SINR. It has the property of allocating resource blocks fairly to all the users without using power control. At any time slot, a user will be allocated as many RBs that are sufficient to transmit the offered load bits and then the next user will do the same. Once all the RBs have been assigned, any users left will be discarded. For the purpose of fairness, users who have the least RBs in the last TTI will be prioritised in the next TTI.

### 2.3.7 QoS

The instantaneous user data rate in each TTI is calculated by the multiplication of the number of bits per resource element obtained from the relative link adaptation table and the number of resource elements that a user has been assigned. Overall QoS requirements are set in two respects: 1) a minimum target data rate for individual users in the network; 2) a threshold on the percentage of users that can achieve the target data rate. From the network service point of view, a technology (LTE-femtocells or 802.11n) with a specific network configuration can be said to satisfy the network QoS requirement only if the percentage of users that achieve the targeted data rate is larger than the percentage threshold, under any given network topology. In this thesis, the **user QoS** achieved for the network service is defined as the highest 95%-ile threshold of the user data rate, thus if the user QoS achieves 2 Mbit/s then at least 95% of users achieve a minimum data rate of 2 Mbit/s.

## 2.4 802.11n Analytical Model for Energy Efficiency Evaluation

To obtain meaningful results for this comparison study, an analytical model approach has been used for simplicity and scalability. The analytical modelling of the Medium Access Control (MAC) layer throughput performance has been studied by other researchers. Bianchi proposes a classic two-dimensional Markov chain to determine the saturation throughput of a Wireless Local Area Network (WLAN) using the Distributed Coordination Function (DCF) [27]. Tay and Chua propose a model based on average value analysis and study the effects of contention window sizes on the throughput performance [28]. Both of the above models assume an ideal wireless channel with no physical layer channel errors.

In fact, wireless channels are usually error-prone and the effects of packet errors have an impact on the system performance. Several papers extend the above system models to study the throughput performance under different channel error conditions. In this chapter, an approach has been introduced to study the saturated throughput, user QoS (same definition as FAP) and energy consumption performances of 802.11n networks under error-prone channels by extending Bianchi's model. Two ways to perform frame aggregation at the MAC layer are specified in 802.11n standard, which has also been considered in this model. [29].

A mature and widely-accepted extensive throughput analytical model is needed for this energy performance comparison over LTE-femtocells. Thus Bianchi's model was selected and extended to propose an energy analytical model for 802.11n, and several assumptions have been made. The model is concerned with infrastructure mode WLANs that use the DCF MAC protocol. There are a number of APs operating on 3 different frequency channels deployed and a fixed number of 50 client stations in the WLAN. Each user is associated with exactly one AP which provides the highest SINR to that user and each AP with its associated stations defines a cell. Therefore, DCF is used for single-hop only communication within the cells and users access data through their serving APs. Each user is assumed to have saturated traffic. The wireless channel Bit Error Rate (BER) is  $P_b$ . The minimum contention window size is  $\mathfrak{W}$  and the maximum backoff stage is  $m$ . In 802.11 WLANs, control frames are transmitted at the basic rate

## 2. RADIO ACCESS TECHNOLOGY COMPARISON

---

which is more robust in combating errors. They have a much lower frame error rate as the size of these control frames are much smaller than an aggregated data frame. Therefore, the frame error probabilities for control frames and preambles are assumed to be zero.

The system time is divided into small time slots where each slot is the time interval between two consecutive countdowns of backoff timers by stations which are not transmitting.

From Bianchi's model, transmission probability  $\tau$  in a virtual time slot is given by:

$$\tau = \frac{2(1 - 2p)}{(1 - 2p)(\mathfrak{W} + 1) + p\mathfrak{W}(1 - 2p)^m}, \quad (2.18)$$

where  $p$  is the unsuccessful transmission probability conditioned on that there is a transmission in a time slot. When considering both collisions and errors,  $p$  can be expressed as:

$$p = 1 - (1 - p_c)(1 - p_e), \quad (2.19)$$

where  $p_c = 1 - (1 - \tau)^{N_s - 1}$  is the packet conditional collision probability and  $p_e$  is the packet error probability on condition that there is a successful transmission in the time slot and is given by (2.20),  $N_s$  is the total number of contending stations.

$$p_e = 1 - (1 - p_b)^L, \quad (2.20)$$

where  $L$  is the packet size in bits and  $p_b$  is the BER of a particular MCS level. Therefore, the network saturation throughput can be calculated as:

$$S = \frac{\mathbb{E}(l_p)}{\mathbb{E}(t)}, \quad (2.21)$$

where  $\mathbb{E}(l_p)$  is the average packet payload bits successfully transmitted in a virtual time slot, and  $\mathbb{E}(t)$  is the expected length of a time slot.  $\mathbb{E}(l_p)$  and  $\mathbb{E}(t)$  are computed by (2.22) and (2.23):

$$\mathbb{E}(l_p) = Lp_s = Lp_{tr}p_{s.nc}(1 - p_e), \quad (2.22)$$

$$\mathbb{E}(t) = T_\sigma p_\sigma + T_c p_{tr}(1 - p_{s.nc}) + T_e p_e + T_s p_s, \quad (2.23)$$

where the probability of an idle slot  $p_\sigma$  is  $(1 - \tau)^{N_s}$ , the probability of a non-collided transmission  $p_{s.nc}$  is  $\frac{N_s(1-\tau)^{N_s-1}}{p_{tr}}$ , the probability for a transmission in a time slot  $p_{tr}$  is  $1 - p_\sigma = 1 - (1 - \tau)^{N_s}$ , the probability of a successful transmission (without collisions and transmission errors) is  $p_{tr}p_{s.nc}(1 - p_e)$  and  $\tau$  is computed by (2.18).  $T_\sigma$  is equal to the system's empty slot time of 9  $\mu$ s.  $T_\sigma$ ,  $T_c$ ,  $T_s$  and  $T_e$  are the idle, collision, successful and error virtual time slot's length and are defined as follows:

$$T_c = \text{EIFS}, \quad (2.24)$$

$$T_s = \text{DATA} + \text{BACK} + 3\text{SIFS} + \text{DIFS}, \quad (2.25)$$

$$T_e = \text{DATA} + \text{EIFS} + 2\text{SIFS}, \quad (2.26)$$

where  $\text{BACK} = 5.63 \mu$ s and  $\text{DATA}$  are the transmission time for backoff stage and the transmission time for aggregated data frame,  $\text{SIFS} = 16 \mu$ s,  $\text{DIFS} = \text{SIFS} + T_\sigma$ ,  $\text{EIFS} = \text{SIFS} + \text{DIFS} + \text{BACK}$ , respectively.

48 of the 52 OFDM sub-carriers are for data and the remaining 4 are for pilot sub-carriers. Each of these sub-carriers can be a BPSK, QPSK, 16QAM or 64QAM. Table 2.3 lists all valid modes and MCS indexes for 802.11n systems in both SISO and MIMO transmission mode.

## 2.5 Energy Metrics

The power consumption of an indoor AP or indeed any cell is dependent on the hardware technology and the traffic load. Given a fixed hardware technology, the power consumed by a cell comprises a transmission/load dependent Radio-Head (RH) part, and an independent fixed overhead (OH) part. Together the RH and OH constitute the operational (OP) power consumption. During transmission,

## 2. RADIO ACCESS TECHNOLOGY COMPARISON

---

Table 2.3: Valid modes for 802.11n WLANS for SISO and MIMO operation with 20 MHz bandwidth

(a) SISO

| Mode | Rate (Mbit/s) | Code Rate | Modulation |
|------|---------------|-----------|------------|
| 1    | 6             | 1/2       | BPSK       |
| 2    | 9             | 3/4       | BPSK       |
| 3    | 12            | 1/2       | QPSK       |
| 4    | 18            | 3/4       | QPSK       |
| 5    | 24            | 1/2       | 16QAM      |
| 6    | 36            | 3/4       | 16QAM      |
| 7    | 48            | 2/3       | 64QAM      |
| 8    | 54            | 3/4       | 64QAM      |

(b) MIMO

| Mode | Rate (Mbit/s) | Code Rate | Modulation |
|------|---------------|-----------|------------|
| 1    | 6.5           | 1/2       | BPSK       |
| 2    | 13            | 1/2       | QPSK       |
| 3    | 19.5          | 3/4       | QPSK       |
| 4    | 26            | 1/2       | 16QAM      |
| 5    | 39            | 3/4       | 16QAM      |
| 6    | 52            | 2/3       | 64QAM      |
| 7    | 58.5          | 3/4       | 64QAM      |
| 8    | 65            | 5/6       | 64QAM      |

the RH is active, and irrespective of transmission, the OH is always active. The load is defined as the ratio between the traffic demanded and the capacity of the cell across the coverage area denoted as  $\mathcal{L} = \frac{R_{\text{traffic}}}{R_j}$  (where  $J \in \{\text{test, reference}\}$  referring to a test and reference network, respectively). Thus, for a fixed traffic demand, the greater the capacity, the lower the load, and the lower the energy consumption. This is to say, the network with a higher capacity is more energy efficient.

In order to compare the energy consumption of the same system operating in different conditions, the concept of transmission duration and operational duration are defined. Consider an indoor AP with users that demand a traffic amount of  $M$  bits of data over a finite time duration of  $T_{\text{AP}}^{\text{OH}}$ . Two systems are considered: a reference and a test system as the values that  $J$  can take from, both of which

have a capacity that exceeds the offered traffic amount. Due to the fact that the reference and the test system might have different capacities and scheduling mechanisms, the duration which the radio-head spends in transmitting the same  $M$  bits is different. In order to compare two systems, a useful Figure of Merit (FoM) is the **Energy Reduction Gain (ERG)**, which is the reduction in energy consumption when a test system is compared with a reference system:

$$\text{ERG}_{\text{RAN}}^{\text{OP}} = 1 - \frac{E_{\text{test}}^{\text{OP}}}{E_{\text{ref.}}^{\text{OP}}} = 1 - \frac{N_{\text{test}}(P_{\text{test}}^{\text{RH}}\mathcal{L}_{\text{test}} + P_{\text{test}}^{\text{OH}})}{N_{\text{ref.}}(P_{\text{ref.}}^{\text{RH}}\mathcal{L}_{\text{ref.}} + P_{\text{ref.}}^{\text{OH}})}, \quad (2.27)$$

where  $P_j^{\text{RH}} = P_j^{\text{RF}}/\mu_{\Sigma}$ ,  $\mu_{\Sigma}$  is the RH efficiency [30] and  $N_j$  is the number of APs. The capacity of the system is defined as  $R_j = M/T_j^{\text{RH}}$ , which is greater or equal to the offered traffic demand,  $R_{\text{traffic}} = M/T_j^{\text{OH}}$  and  $\mathcal{L}_j = \frac{R_{\text{traffic}}}{R_j}$  is the ratio of the offered traffic demand to the network capacity. The term  $\frac{P_j^{\text{RH}}}{R_j}$  in (2.27) is an indication of the average radio transmission efficiency, which does not consider the overhead energy. This is commonly used to measure energy consumption in literature [31], and is known as the **Energy-Consumption-Ratio (ECR)**. By employing the same definition as Eq. (2.27), the **radio-head Energy Reduction Gain (ERG<sub>RAN</sub><sup>RH</sup>)** can be expressed as:

$$\text{ERG}_{\text{RAN}}^{\text{RH}} = 1 - \frac{E_{\text{test}}^{\text{RH}}}{E_{\text{ref.}}^{\text{RH}}} = 1 - \frac{N_{\text{test}}P_{\text{test}}^{\text{RH}}\frac{R_{\text{traffic}}}{R_{\text{test}}}}{N_{\text{ref.}}P_{\text{ref.}}^{\text{RH}}\frac{R_{\text{traffic}}}{R_{\text{ref.}}}} = 1 - \frac{N_{\text{test}}\text{ECR}_{\text{test}}}{N_{\text{ref.}}\text{ECR}_{\text{ref.}}}, \quad (2.28)$$

The aforementioned energy metrics are based on the SISO scenario. It can be simply extended to MIMO scenario by considering proportional OH power to the number of transmitting antennas as MIMO requires the incorporation of several transceiver chains, one for each antenna link, which may be particularly costly for low power applications. This leads to the conclusion that a MIMO system with more than 2 transmitting antennas at the AP is unlikely to provide any energy efficiency gain, or may even be less efficient than a SISO system, which coincides with the following results.

For a given offered load demanded by users, a more spectral efficient deployment is able to transmit the same data for a short transmission time. Over time,

this amounts to a reduction of the RH energy consumption. The energy saving caused by spectral efficiency alone is **upper-bounded (ERG threshold)** by the ratio of OH energy to OP energy. This upper-bound ( $\text{ERG}_{\text{RANupper-bound}}^{\text{OP}} = 1 - \frac{P_{\text{test}}^{\text{OH}}}{P_{\text{ref.}}^{\text{RH}} + P_{\text{ref.}}^{\text{OH}}} = 1 - \frac{P_{\text{test}}^{\text{OH}}}{P_{\text{ref.}}^{\text{OP}}}$ ) can be obtained when  $R_j$  in Eq. (2.27) approaches infinity on the condition that the same number of APs deployed for both reference and test systems is considered. In order to significantly reduce energy consumption further, a reduction in the number of APs is required to meet the QoS needed. This can only be accomplished by significantly improving the overall throughput of the AP deployment, which will be covered in Chapter. 4.

## 2.6 Network Simulations and Results

In this section, energy efficient performance evaluation results for the downlink LTE femtocells and 802.11n network are presented. The details of the system parameters and model assumptions are listed in Table 4.1 [32].

### 2.6.1 Baseline Results

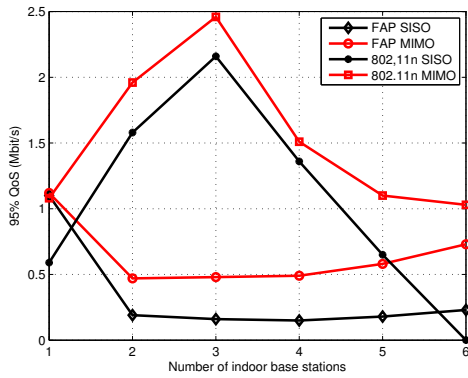
In this section, simulation results obtained from the conventional scenario in Fig. 2.2(a) are presented. As the FAPs are co-channel deployed, interference from outdoor BSs is not currently considered in these baseline results and will be discussed in the following section. Fig. 2.7 illustrates the maximum downlink user QoS and average user data rate versus different number of indoor BSs for both LTE-femtocells and 802.11n network with SISO and MIMO antenna configurations.



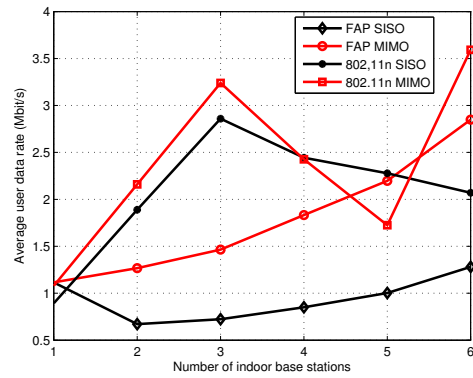
## 2. RADIO ACCESS TECHNOLOGY COMPARISON

Table 2.4: Simulation parameters and model assumptions

| Parameter             | Value (FAP)       | Value (802.11n)   |
|-----------------------|-------------------|-------------------|
| Scenario              | 20 m × 16 m       | 20 m × 16 m       |
| System bandwidth      | 20 MHz            | 20 MHz & 60 MHz   |
| Carrier frequency     | 2130 MHz          | 2400 MHz          |
| Frequency reuse       | 1, 3              | 1, 3              |
| Number of FAPs        | 1-6               | 1-6               |
| Total number of users | 50                | 50                |
| User Distribution     | Uniform           | Uniform           |
| Sub carriers per PRB  | 12                | /                 |
| Total number of RBs   | 100               | /                 |
| Total transmit power  | 0.1 watts         | 0.1 watts         |
| Radio-head efficiency | 6.67%             | 6.67%             |
| Overhead power        | 5.2 watts         | 5.2 watts         |
| Pathloss model        | WINNER II A1      | WINNER II A1      |
| Multipath model       | WINNER II A1      | WINNER II A1      |
| Scheduler             | Round Robin       | Contention        |
| Antenna configuration | SISO MIMO (2 × 2) | SISO MIMO (2 × 2) |
| Traffic mode          | Full buffer       | Full buffer       |



(c) User QoS rate



(d) Average user data rate

Figure 2.7: User QoS and average user data rate vs. the number of indoor base stations for LTE-femtocells and 802.11n with SISO and MIMO deployment without outdoor interference

### 2.6.1.1 1 Access Point

It is shown that 1 FAP can achieve the maximum downlink user QoS of just over 1 Mbit/s in both SISO and MIMO deployment owing to the absence of any interference. It is worth mentioning that there is a 43% improvement in the spectral efficiency when using 1 FAP as compared to 1 AP. This can be seen from Fig. 2.8(a). This gain is due to the different scheduler mechanism as well as the link level MCS between LTE-femtocell and 802.11n network. For the same bandwidth, LTE-femtocell employs a more spectral efficient adaptive modulation and coding scheme than 802.11n. 1 FAP offers 4.44% and only 0.40% ERG against 1 baseline 802.11n AP with SISO and MIMO deployment, respectively. This is shown in Fig. 2.9(a). It was found that for a single AP deployment, a single FAP is more spectral and energy efficient than a single 802.11n AP.

### 2.6.1.2 2 or More Access Points

As the number of APs increases, the 802.11n deployment is always more spectrally and energy efficient due to the increased operating bandwidth of 60 MHz with frequency reuse pattern 3, compared to the LTE bandwidth of 20 MHz with frequency reuse pattern 1. The maximum downlink user QoS decreases dramatically after one FAP scenario and steadily increases until the last number of FAP observed in this investigation. On the other hand, when the number of APs is less than or equal to 3, maximum downlink user QoS of 802.11n network has a linear growth due to the utilisation of the frequency reuse pattern 3 and acquires the maximum downlink user QoS in the scenario of using 3 APs as shown in Fig. 2.8(b), after which the user QoS starts decreasing due to the inter-AP interference that arises between the APs causing a degradation of overall performance. Comparing Fig. 2.7(c) and Fig. 2.7(d), the average user data rate trend is roughly same as the QoS trend but the QoS data rate is lower. The operational ERG performance for LTE-femtocell and baseline 802.11n network is shown in Fig. 2.9(a). For the number of APs greater than 2, 802.11 APs provides 2.61% to 16.72% ERG over FAP when utilising more bandwidth than FAP.

### 2.6.1.3 SISO vs. MIMO

Fig. 2.8(c) and Fig. 2.8(d) show that Alamouti MIMO  $2 \times 2$  provides benefit in spectral efficiency relative to conventional SISO deployment by exploiting the transmit and receive diversity, leading to a higher data rate for both technologies. However, MIMO is less energy efficient than SISO. This is because Alamouti MIMO  $2 \times 2$  consumes double OH power compared to SISO deployment with reference to Eq. (2.27) [30]. For a fair comparison, the RH power for MIMO has already been halved in the derivation of Eq. (2.13) and the ERG performance between SISO and MIMO is illustrated in Fig. 2.9(b). SISO yields an ERG of roughly 40% and 45% for FAP and 802.11n, respectively. This suggests that the overhead power dominates the energy performance for this study. Therefore, there is a possibility for MIMO to outperform SISO in the energy perspective when the QoS is the driven factor. For example, if the QoS of FAP is set around 0.5 Mbit/s, it can be observed in Fig. 2.7(c), 2 MIMO FAPs is sufficient to meet this requirement while more than 6 SISO FAPs is needed assuming the trend of QoS remains steadily increasing after the number of FAPs reaches 6.

## 2.6.2 Results with Outdoor Interference

There is an interest to explore how the interference from an outdoor microcell BS will affect the performance for indoor co-channel deployed FAPs. Fig. 2.10 shows the QoS and average user data rate comparison between LTE-femtocells and 802.11n with SISO deployment in the presence of outdoor microcell interference. This interference is modelled by placing a microcell 150–200 m away from the office with 20 watts transmit power. The interference is calculated in sub-carrier level with WINNER II B4 multipath model considered [26]. With reference to Fig. 2.10, only 1 FAP suffers from the microcell interference and its relating maximum downlink user QoS drops by 0.25 Mbit/s and the average data rate has a decrease of only 0.08 Mbit/s compared to Fig. 2.8(a). However 1 AP still cannot outperform 1 FAP even with the outdoor interference. This shows that LTE scheduling is significantly more efficient over 802.11 contention based MAC and the MCS control is much better in LTE. The results of the number of AP greater than 2 up to 6 remain same as that of in the baseline scenario.

## 2. RADIO ACCESS TECHNOLOGY COMPARISON

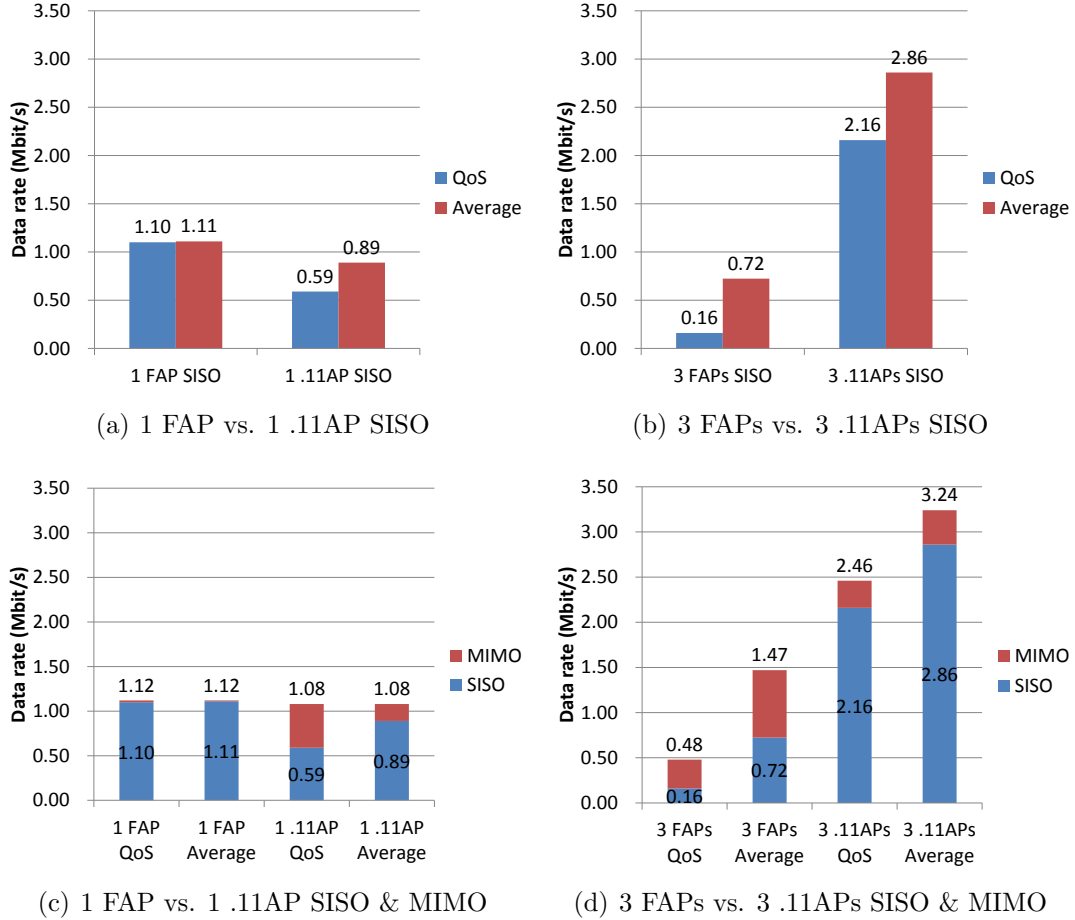


Figure 2.8: Maximum downlink user QoS and average user data rate comparison between LTE-femtocells and 802.11n with SISO and MIMO deployment without outdoor interference

Therefore, for a single AP deployment, an LTE FAP is more spectrally and energy efficient than an 802.11n AP. This is true both with and without a fully loaded micro-cell interference source. In order to achieve a higher maximum downlink user QoS performance, deploying more 802.11n APs is more spectrally and energy efficient. No more than 3 802.11n APs with SISO antenna configuration should be deployed in the same room; any more causes mutual interference and degrades the aggregate QoS received by the users.

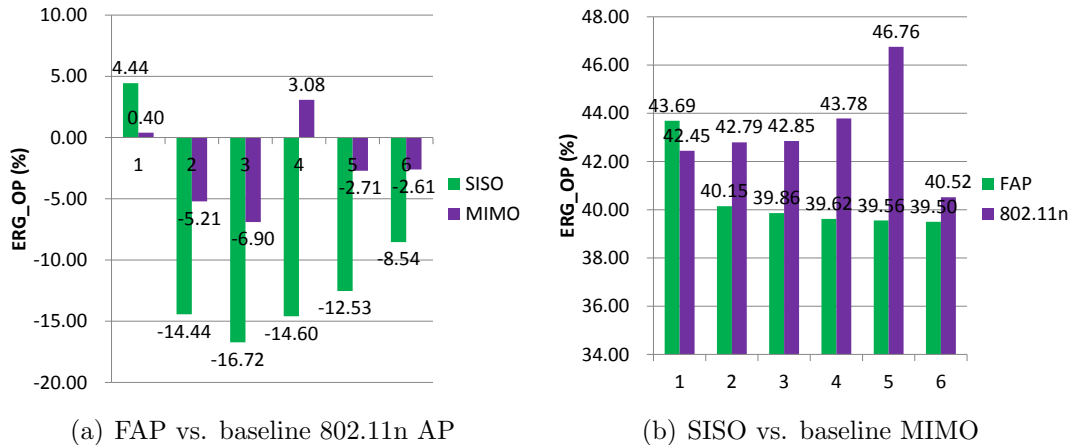


Figure 2.9: ERG comparison for LTE-femtocells and 802.11n with SISO and MIMO deployment without outdoor interference

### 2.6.3 Shannon Capacity Equation vs. Adaptive MCS table

Fig. 2.11 illustrates the QoS and average user data rate comparison between the Shannon capacity equation and MCS tables in the baseline scenario. The user data rate saturates at high SINR regime according to the MCS table while the throughput calculated from the Shannon Capacity equation is significantly greater and is not likely to be bounded. The value derived from Shannon equation of either user data rate or gross RAN throughput is far beyond the realistic scenario although the ERG trends for both throughput calculation methods are roughly the same as shown in Fig. 2.12. The impact of the energy results using Shannon capacity equation is not too obvious in this study. However, it is still worth noting that there exist capacity discrepancies between the Shannon bound and a realistic system. These discrepancies and the associated impacts will be further discussed in the following chapters.

## 2. RADIO ACCESS TECHNOLOGY COMPARISON

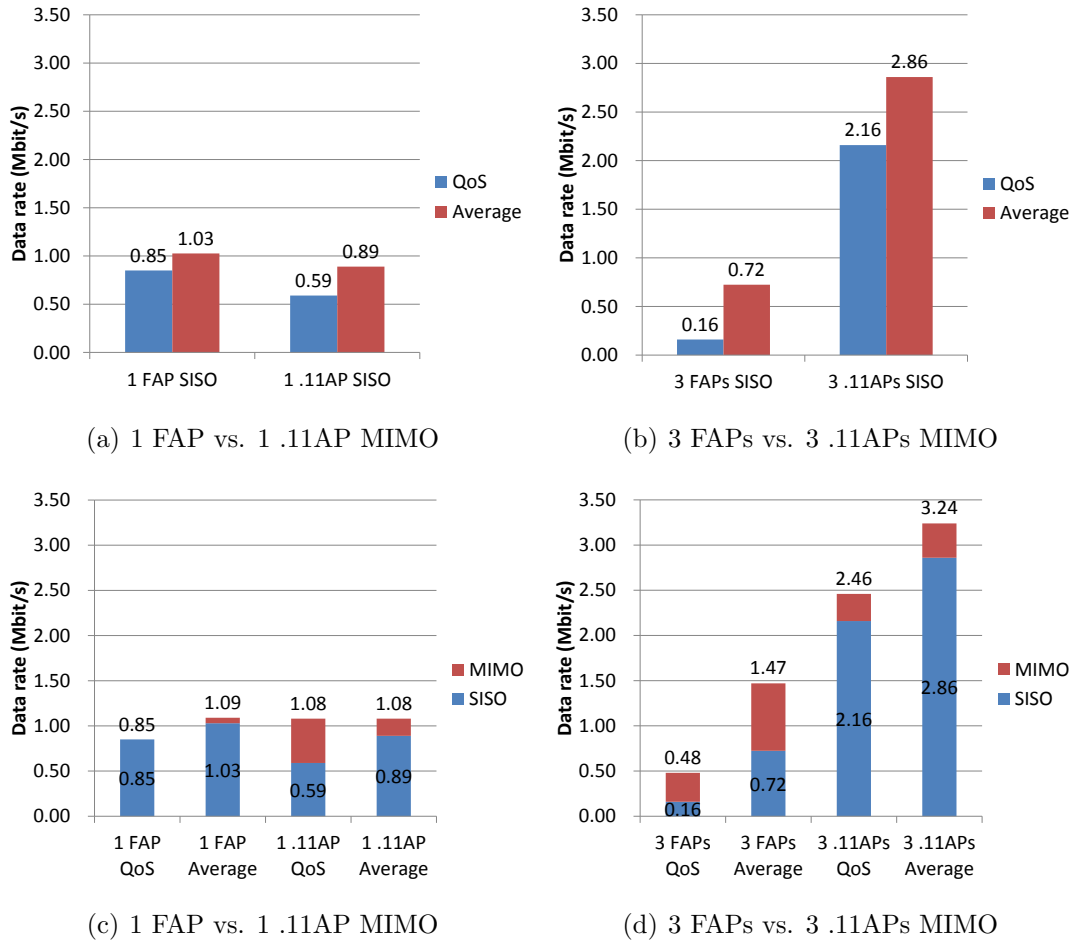


Figure 2.10: QoS and average user data rate comparison between LTE-femtocells and 802.11n with SISO and MIMO deployment with outdoor interference

## 2. RADIO ACCESS TECHNOLOGY COMPARISON

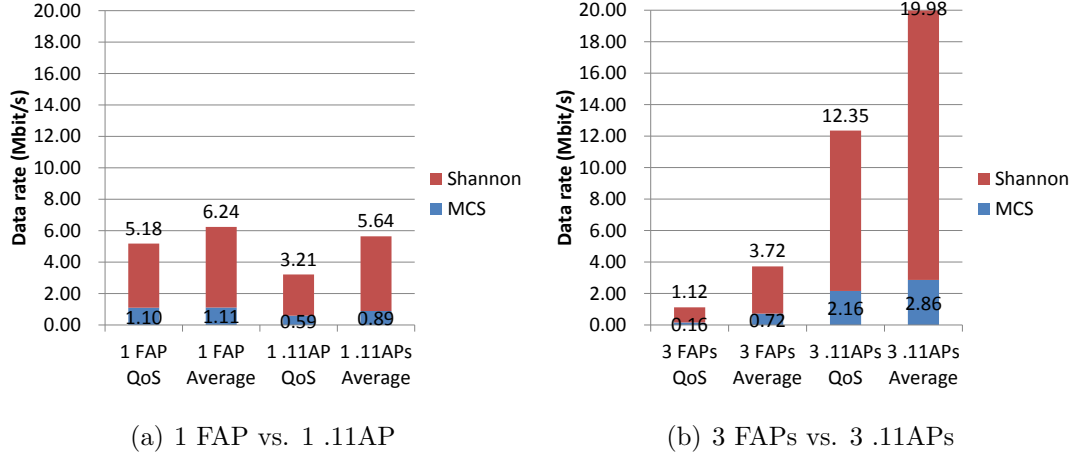


Figure 2.11: QoS and average user data rate comparison between Shannon capacity equation and MCS tables with SISO deployment without outdoor interference

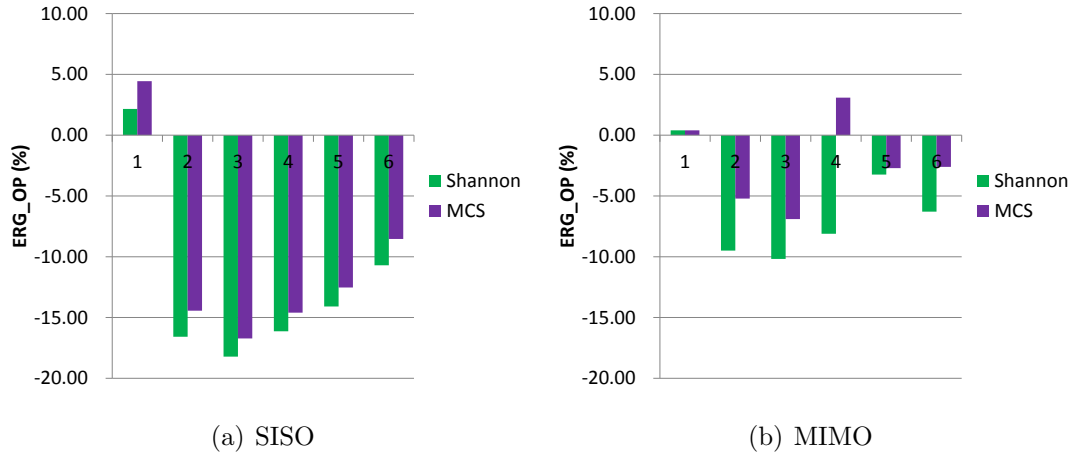


Figure 2.12: ERG comparison between Shannon and look-up table with SISO and MIMO deployment without outdoor interference

### 2.6.4 Alternative (Frequency Reuse) Scenario

The alternative scenario is defined in Section 2, in which both FAPs and 802.11n APs have a total bandwidth of 20 MHz with a frequency reuse pattern 3 and 1, respectively. Fig. 2.13 shows the QoS, average data rate and ERG performance between conventional and alternative scenarios. The case of 1 FAP and 1 802.11n

## 2. RADIO ACCESS TECHNOLOGY COMPARISON

AP for both conventional and alternative scenarios are identical. In the alternative scenario, FAP outperforms 802.11 AP when the number of access points is 3. The average user data rate for 3 FAPs is 1.12 Mbit/s while this value for 3 802.11APs is 0.22 Mbit/s. This is because 802.11 AP suffers server interference from other APs in the alternative scenario and its physical (PHY) layer adopts convolution codes which is less efficient than turbo codes used in LTE-femtocell. Fig. 2.13(b) indicates 3 FAPs provides an ERG of 20.08% in alternative scenario while 3 802.11n APs offers an ERG of 21.80% in conventional scenario. Hence FAP investigation is particularly more interested in the following chapters.

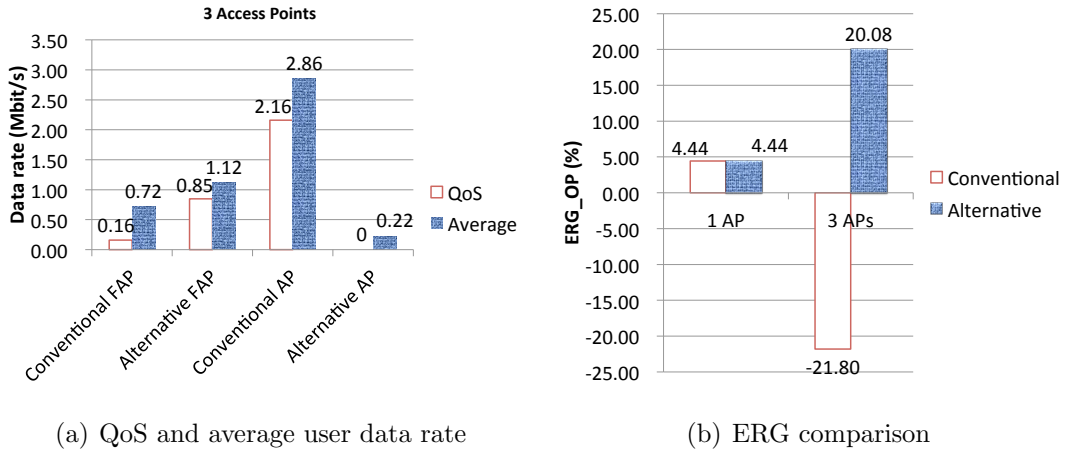


Figure 2.13: User data rate and ERG comparison vs. 3 FAPs and 3 APs SISO deployment between conventional and alternative scenarios

### 2.6.5 Remarks

The results in Fig. 2.8(a) covers the results of all four possible combinations of comparison between one FAP and one 802.11n AP in either conventional or alternative scenario while the results in Fig. 2.13(a) contains the same number of combinations results for the case of 3 FAPs and 3 802.11n AP. These four possible combinations are conventional FAP vs. alternative AP and conventional AP vs. alternative FAP besides the other two which have already been covered in the above sections. It is worth mentioning that 3 FAPs in conventional scenario is more energy efficient than 3 APs in alternative scenario. This is due to the



## *2. RADIO ACCESS TECHNOLOGY COMPARISON*

---

mutual impact from the the different scheduler mechanism and coding scheme applied in both systems.

## 2.7 Conclusions

This chapter addresses the question on the energy comparison of femtocell technology versus 802.11n technology, the methodology and results on the energy efficiency comparison between LTE-femtocells and 802.11n technologies have been presented.

A co-channel LTE-femtocell multi-user and multi-cell simulator has been developed while for 802.11n networks an analytical energy model extended from Bianchi's has been developed. Results indicate that 1 FAP is always more energy efficient than 1 802.11n AP for both SISO and MIMO antenna configurations no matter whether there is outdoor microcell interference in both conventional and alternative scenarios. 802.11n AP achieves the maximum downlink user QoS and average user data rate when fully utilising its 60 MHz bandwidth (i.e., 3 APs) without any interference whereas FAP suffers severe interfering effects and the QoS drops dramatically when the number of FAP is greater than 1 in conventional baseline scenario. For the number of APs greater than 2, 802.11n APs provides an ERG of 2.61% to 16.72% over FAP when utilising more bandwidth than FAP.

It is also illustrated that FAP are always more energy efficient than 802.11n in alternative scenario where their bandwidth are constrained to same 20 MHz. This suggests that using more bandwidth reduces energy consumption. The Alamouti MIMO  $2 \times 2$  scheme yields higher spectral efficiency but at the cost of consuming twice the overhead power which on balance leads to a less energy efficient performance. Nevertheless, using less MIMO APs than SISO to achieve a certain targeted QoS can reduce OH power, which effectively means MIMO will provide a positive value of ERG (OP) against SISO deployment.

ERG(OP) results obtained from both the Shannon Capacity equation and MCS look-up tables were roughly same. However, the absolute values of the QoS and the RAN throughput calculated using Shannon's Capacity equation were significantly greater than those obtained from the MCS look-up tables. This shows that the Shannon expression can only yield reasonable ratio analysis.

## Chapter 3

# Femtocell Interference Avoidance

Having established the relative merits of the RATs, the thesis considers radio resource management (RRM) techniques. Hard frequency reuse patterns were explored as well as time-division (TD) based interference avoidance between neighbouring FAPs. The investigation of co-channel interference mitigation techniques, such as, interference cancellation through receiver processing, interference randomisation by frequency hopping, and interference avoidance through resource usage restrictions imposed by frequency and power planning have become a key focus area in achieving dense spectrum reuse in 3GPP LTE cellular systems. When interference cancellation is considered, the interfering signal received is subtracted at the receiver so that the transmitted information can be successfully decoded. The use of these techniques in wireless communications systems has been studied in [33], where the capacity enhancement is achieved from an information-theoretic point of view. Authors in [34, 35] further analysed such techniques with much more complicated processes to estimate the interfering signal and cancel it at the receiver, which may be hardly practical in implementing real communications systems. Webb suggested careful use of interference cancellation in the book [36] due to errors incurred during cancellation.

Interference avoidance has attracted considerably more attention than interference cancellation from both the carrier industry and the academic community since the complexity of the latter is normally higher to afford. The interference avoidance can be defined in this thesis as a technique that attempts to mitigate interference by preventing it from occurring.

This has been widely implemented through power control, planning of antenna downtilt, optimal FAP placement and RRM. The thesis will now exploit the balance between spectral efficiency and energy efficiency by employing a new RRM and hard frequency reuse approach.

## 3.1 Review of Existing Work

Numerous papers have been published on resource allocation in OFDMA systems, which is employed by standards such as the 3GPP LTE cellular network [37], as well as IEEE 802.16 wireless broadband and IEEE 802.20 mobile broadband wireless access (MBWA). However, most of them focused on single cell scheduling and typically failed to consider the effect of inter-cell interference. Several existing research studies [38,39] have focused on the improvement of the spectral efficiency for femtocell network. The author in [38] outlines the cognitive radio technologies for the future mobile broadband era by proposing a cognitive femtocell solution for indoor communications in order to increase the network capacity in serving indoor users and to solve the spectrum-scarcity problems. The aggregate throughput of two-tier femtocell networks has been improved by a beamforming codebook restriction strategy and an opportunistic channel selection strategy [39]. However, little work in the above studies has been devoted to energy consumption.

However, there also have been various approaches to investigate the power consumption and interference avoidance of the cellular networks. Much of the previous work [40–42] has focused on minimising the transmit power of BS. The authors in [43] proposed a new automated method of simultaneously maximising coverage while minimising the interference for a desired level of coverage overlap. However, such an approach is not always practical as network optimisation is constrained by a number of restrictions on BS placements, interference and power emissions. Researches in [44] described an approach of adjusting the transmit power for fixed positions of FAPs in the enterprise offices to achieve coverage optimisation and load balance, but did not consider the evaluation of effect on user's QoS. In [45], the authors derived the downlink SINR formula for the residential femtocell but the formula had not taken the throughput into account. A theoretical framework was proposed in [46] to analyse the interference char-

acteristics of different femtocell sub-bands for OFDMA systems employing the Fractional Frequency Reuse (FFR) scheme which can be extended to optimise power and frequency allocation, but the path loss model employed in this framework is far too simple to reflect the real characteristics of the indoor scenario. Moreover, this method mostly relies on static pre-planned frequency allocations that slowly evolve through time. As a consequence, it failed to cope with traffic spatial distribution, user QoS requirement and channel conditions [47].

More understandable, realistic and tailored approaches to OFDMA networks have been proposed in [48-50]. A dynamic frequency allocation scheme for a FFR OFDMA-based network was proposed in [48]. This technique improved the performance of conventional FFR schemes by taking cell load conditions into account. Nevertheless, no minimum user data rate was guaranteed since the resource assignment demanded that users were allocated to one sub-channel. Another centralised dynamic FFR approach for OFDMA networks was presented in [49] to maximise the long-term throughput of the network. Furthermore, a minimum user data rate was guaranteed, which was an improvement from the previous study. However, a great deal of uplink feedback was demanded due to the need of inter-cell interference data of every user-sub-carrier pair. In contrast, the authors in [50] employed the same MCS to all RBs of a certain user and proposed a sub-optimal reduced complexity multiuser scheduler which maximised cell throughput in scenarios where users had distinct fading in each RB, but inter-cell interference is neglected.

## 3.2 Research Contribution

The following sections of this chapter further the study of interference avoidance for a network where both the micro-cell and the LTE-femtocells use OFDMA signalling. It is necessary for network planners to carefully analyse the interference to the observed FAP as the interference from the dominated source severely affects system capacity and energy consumption. From an interference management point of view, the granularity of resource allocation in OFDMA makes it possible to estimate the interference thus providing the opportunities to mitigate the interference on a sub-carrier basis. In this study, a novel interference manage-

ment approach is proposed and the channel quality improvements derived from there are shown to improve the energy efficiency of the E-UTRAN.

## 3.3 System Model

### 3.3.1 Introduction

The dynamic LTE system level simulator introduced in Chapter 2 is used to evaluate the proposed scheme for an enterprise office area. Fig. 4.1 illustrates the system model. Two **paired FAPs**, which will employ the new algorithm, are placed in the middle of the left half of the two office rooms and a number of users are randomly and evenly distributed within the same places. FAPs in other rooms are defined as ‘**other FAPs**’ in the rest of this chapter unless otherwise specified. Rectangular rooms with light internal walls are also considered. The assumptions made are as follows:

- There is only one outdoor micro-cell interference considered. This is reasonably accurate for this study as proved in Section 5.3.
- The micro-cell is fully loaded and persistently interfere with the FAPs.
- The paired FAPs are not fully loaded and so do not interfere with the observed FAPs.
- The effect of FAP interference onto the micro-cell is not considered in this body of investigation as the scope of this study only concerns indoor coverage.

The path loss models implemented in the simulator are adopted from WINNER A1 and B4 [26]. The indoor line-of-sight (LOS) and non-line-of-sight (NLOS) path loss model  $PL_{in}^{LOS}$  and  $PL_{in}^{NLOS}$  (between the FAP and the mobile user) and the outdoor-to-indoor  $PL_{out-to-in}$  (between the micro-cell BS and the mobile user) are defined as follows, respectively:

$$PL_{in}^{LOS} = 18.7 \log_{10}(d_{FAP}) + 46.8 + 20 \log_{10}\left(\frac{f}{5}\right), \quad (3.1)$$

$$PL_{in}^{NLOS} = 20 \log_{10}\left(\frac{d_{FAP}f}{5}\right) + 46.4 + 5n_{wall}^{FAP}, \quad (3.2)$$

### 3. FEMTOCELL INTERFERENCE AVOIDANCE

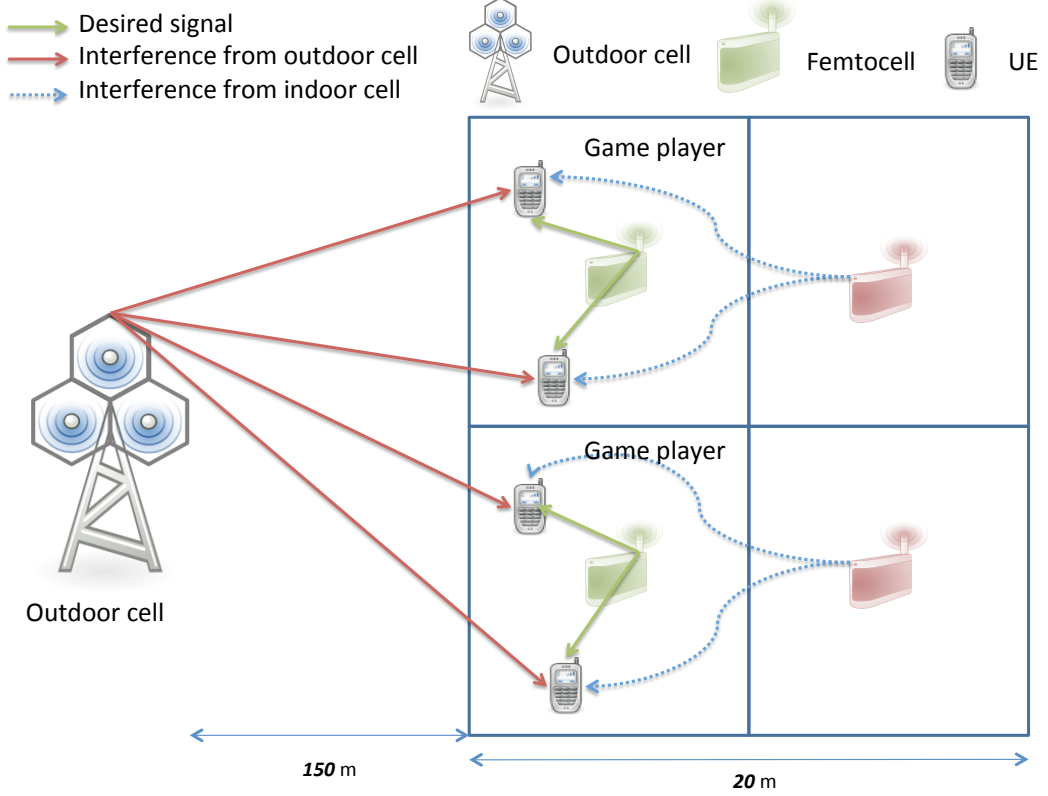


Figure 3.1: Simulation model

$$PL_{\text{out-to-in}} = 36.7 \log_{10}(d_{\text{micro}}) + 22.7 + 26 \log_{10}\left(\frac{f}{5}\right) + PL_{\text{wall}} + 0.5d_{\text{in}}, \quad (3.3)$$

where  $f$  is the frequency of transmission in GHz.  $d_{\text{FAP}}$ ,  $d_{\text{micro}}$  and  $d_{\text{in}}$  are FAP-to-user, micro-cell-to-user and outdoor wall-to-user distance in metres.  $PL_{\text{wall}}$  is the wall loss penetration factor in dBs.  $n_{\text{wall}}^{\text{FAP}}$  is the number of internal walls. The received Signal to Interference-plus-Noise Ratio (SINR) is calculated as below:

$$\gamma = \frac{|h_i|^2 P_i}{\sum_{k=1, k \neq i}^K |h_k|^2 P_k + |h_{\text{micro}}|^2 P_{\text{micro}} + \sigma^2}, \quad (3.4)$$

where  $h_i$ ,  $h_k$  and  $h_{\text{micro}} \sim \mathcal{CN}(0, 1)$  are the channel coefficient of the observed FAP, interfering FAPs and micro-cell BS, respectively. They are modelled as independent and identically distributed (i.i.d.) circularly symmetric complex Gaussian random variables with zero mean and a variance of one.  $P_i$  is the received power

of one sub-carrier from the observed FAP,  $P_k$  and  $P_{\text{micro}}$  are the received power of the same sub-carrier from the interfering FAPs and micro-cell BS and  $\sigma^2$  is the noise power. Without considering more advanced techniques of scheduler, the study considers a round-robin scheduler, which evenly partitions the resource blocks between users.

### 3.3.2 Sequential Game Coordinated Radio Resource Management (SGC/RRM) Algorithm

The motivation of the SGC/RRM algorithm is to exploit the communication between the FAPs, via the X2 interface, with a vision of exchanging instantaneous offered traffic information with the objective of reducing the neighbouring FAP interference thus reducing the required transmit power thereby reducing the energy consumption. In this study, the SGC/RRM algorithm is defined as a dynamic radio resource allocation functionality modelled as a two player sequential game in which both players are independent FAPs. A two player sequential game generally involves the first player choosing a strategy and then the second player deciding what strategy to adopt based on the strategy of the first player. In this study the sequential game was played out between the two FAPs closer to the micro-cell as shown in Fig. 4.1.

#### 3.3.2.1 Player Status Assignment (PSA)

PSA determines the principal player FAP and the agent player FAP. PSA is formulated as follows:

$$\text{maximise} \quad \sum_{\mathfrak{t} \in \{0,1\}} \mathcal{L}_{\mathfrak{t}}(1 - \beta_{\mathfrak{t}}), \quad (3.5a)$$

$$\text{subject to} \quad \sum_{\mathfrak{t} \in \{0,1\}} \beta_{\mathfrak{t}} = 1. \quad (3.5b)$$



where  $\mathfrak{k}$  is the FAP index,  $\mathcal{L}_{\mathfrak{k}}$  is the offered traffic (Mbit/s) of FAP  $\mathfrak{k}$ .  $\beta_{\mathfrak{k}}$  are binary values,  $\beta_{\mathfrak{k}} \in \{0, 1\}$ , which represent the PSA. The value of  $\beta_{\mathfrak{k}}$  is 1 if cell  $\mathfrak{k}$  is the agent player and 0 if cell  $\mathfrak{k}$  is the principal player [51].

#### 3.3.2.2 Game Strategy Definition

The game strategy of each player (principal or agent) defines the choice of transmission frequency bands. The transmission frequency band strategy set  $S_t$  for both the principal player and the agent player was carefully chosen to adhere to the possible LTE bandwidth utilisation specifications i.e. 1.4, 3, 5, 10, 15 and 20 MHz.  $S_t$  is defined as:

$$S_t = \{\text{Idle, VLow, Low, MediumL, MediumH, High, VHigh}\}. \quad (3.6)$$

Considering a maximum LTE transmission bandwidth of 20 MHz, Fig. 3.2 presents the SGC/RRM algorithm definition of the individual FAP strategies. Furthermore the individual strategies of the principal player and the agent player were designed to avoid interference between the players.

#### 3.3.2.3 Player Interference Rank Measurement

The FAP interference rank measurement  $R_{\mathfrak{k}}$  is a classification of the amount of interference to FAP  $\mathfrak{k}$  due to the paired FAP participating in the SGC/RRM algorithm. The FAP interference rank measurement of each player is a function of the transmission frequency strategies adopted by both the principal ( $s_t^P$ ) and agent ( $s_t^A$ ) players [10].

$$R_{\mathfrak{k}} = f(s_t^P, s_t^A), \mathfrak{k} \in \{0, 1\}, \quad (3.7)$$

where  $s_t^P$  and  $s_t^A$  are the transmission frequency strategies of principal and agent players respectively, defined in Eq. (3.6). Higher FAP interference rank values represent greater interference between the players. Thus the FAP interference rank  $R_{\mathfrak{k}}$  is proportional to the number of interfering frequency bands. In this study the constant of proportionality was chosen as unity, however any positive constant may be utilised.

### 3. FEMTOCELL INTERFERENCE AVOIDANCE















| Player Strategy      | Principle Player  | Agent Player   | Comment          |
|----------------------|---|--|------------------|
| $s_t$ <i>Idle</i>    |    |    | 0 MHz Utilised   |
| $s_t$ <i>VLow</i>    |    |    | 1.4 MHz Utilised |
| $s_t$ <i>Low</i>     |    |    | 3 MHz Utilised   |
| $s_t$ <i>MediumL</i> |   |   | 5 MHz Utilised   |
| $s_t$ <i>MediumH</i> |  |  | 10 MHz Utilised  |
| $s_t$ <i>High</i>    |  |  | 15 MHz Utilised  |
| $s_t$ <i>VHigh</i>   |  |  | 20 MHz Utilised  |

Figure 3.2: SGC/RRM algorithm player strategy definition

$$R_{\mathfrak{k}} = \mathcal{F}, \mathfrak{k} \in \{0, 1\}, \quad (3.8)$$

where  $\mathcal{F}$  is the number of interfering frequency bands in MHz.

### 3.3.3 Player Strategy Selection

First the principal player decides what strategy to adopt based on the offered traffic presented, and then the agent player decides what strategy to adopt given the strategy of the principal player. The SISO capacities of the LTE Physical Downlink Shared Channel (PDSCH) for 1.4, 3, 5, 10, 15 and 20 MHz are 4.26, 10.65, 17.75, 35.51, 53.26, 71.01 Mbit/s, respectively using the highest modulation and coding scheme (MCS). In order to achieve these capacity values, SINR values greater than 35.94 dB are required. Since the users on average experience SINR values of 30 dB, this thesis utilised a reduction factor of  $\frac{10^3}{10^{3.594}} = 0.25$  from the capacity values in order to characterise the instantaneous offered traffic, e.g. offered traffic between 0 Mbit/s and 1.1 Mbit/s ( $4.26 \times 0.25$ ) are characterised as low loads whereas the threshold of high load starts at 2.13 Mbit/s ( $4.26 \times 0.5$ ). The agent player chooses a transmission strategy from the set of transmission frequency strategies that minimises its FAP interference with the principal player given the transmission frequency strategy adopted by the principal player, defined by Eq. (3.9).

$$s_t^A = \min_{s \in S_t} (R_A(s) | S_t^P). \quad (3.9)$$

Table 3.1: Interference Rank Pay Off Matrix

|                 | $s_t^A$<br>Idle | $s_t^A$<br>VLow | $s_t^A$<br>Low | $s_t^A$<br>MediumL | $s_t^A$<br>MediumH | $s_t^A$<br>High | $s_t^A$<br>VHigh |
|-----------------|-----------------|-----------------|----------------|--------------------|--------------------|-----------------|------------------|
| $s_t^P$ Idle    | 0               | 0               | 0              | 0                  | 0                  | 0               | 0                |
| $s_t^P$ VLow    | 0               | 0               | 0              | 0                  | 0                  | 0               | 1.4              |
| $s_t^P$ Low     | 0               | 0               | 0              | 0                  | 0                  | 0               | 3                |
| $s_t^P$ MediumL | 0               | 0               | 0              | 0                  | 0                  | 0               | 5                |
| $s_t^P$ MediumH | 0               | 0               | 0              | 0                  | 0                  | 5               | 10               |
| $s_t^P$ High    | 0               | 0               | 0              | 0                  | 5                  | 10              | 15               |
| $s_t^P$ VHigh   | 0               | 1.4             | 3              | 5                  | 10                 | 15              | 20               |

The best response strategies are the strategies that result in a FAP interference rank measurement of zero. From the player FAP interference rank payoff matrix (Table. 3.1), it is observed that there are multiple best responses (roll back equilibriums) that the agent player can adopt given the strategy of the principal player. In situations where the agent player has multiple best response strategies

to the strategy adopted by the principal player, the agent's best response strategy that utilises more of the transmission band is chosen as the agent players strategy. It is worth noting that the principal player will only play the idle strategy if and only if the offered traffic presented is 0 Mbit/s; by definition this implies that the agent player can adopt the strategy up to a very high regime. The SGC/RRM algorithm is repeated periodically to capture the dynamic characteristics of the instantaneous offered traffic and ensure that no single player (FAPs) dominates the principal player status.

## 3.4 Simulation Results

In this section, the thesis presents the performance of the interference avoidance techniques in terms of the SINR performance, the spectral efficiency, the radio-head ECR and the operational ERG. The details of the system parameters and model assumptions also listed in Table. 3.2 are: Room size (10 m × 20 m), system bandwidth (20 MHz), carrier frequency (2130 MHz), total number of users (21), user distribution (Uniform), FAP transmit power (0.1 W), FAP radio-head efficiency (6.67%), FAP overhead power (5.2 W), micro-cell antenna gain (10 dBi),  $d_{\text{micro}}$  (150 m), outdoor wall loss (10 dB), indoor wall loss (5 dB) and interference from other FAPs (0–10 W).

The SINR performance is used to quantify the expected channel quality experienced by a user measured in dBs. The spectral efficiency is used to analyse the efficiency of the FAP networks in bit/s/Hz. The radio-head ECR performance and the operational ERG are used to measure the energy efficiency of the FAP networks in Joules/bit and the operational energy comparison in percentage, respectively.

The SGC/RRM algorithm dynamically mitigates the effects of FAP interference based on the instantaneous offered traffic presented to the individual FAP in the E-UTRAN. Fig. 3.3(a) illustrates the comparison of the SINR performance of the user grids with and without using SGC/RRM algorithm. It can be found that the SGC/RRM algorithm produced a higher SINR range compared to the baseline scenario without eliminating any FAP interference. The SINR performance improvement of the SGC/RRM is due to the fact that a user in a particular FAP

### 3. FEMTOCELL INTERFERENCE AVOIDANCE

---

Table 3.2: Simulation parameters and model assumptions

| Parameter                    | Value       |
|------------------------------|-------------|
| Room size                    | 10 m × 20 m |
| System bandwidth             | 20 MHz      |
| Carrier frequency            | 2130 MHz    |
| Total number of users        | 21          |
| User Distribution            | Uniform     |
| FAP transmit power           | 0.1 W       |
| FAP radio-head efficiency    | 6.67%       |
| FAP overhead power           | 5.2 W       |
| Micro-cell transmit power    | 20 W        |
| Micro-cell antenna gain      | 10 dBi      |
| $d_{\text{micro}}$           | 150 m       |
| Outdoor wall loss            | 10 dB       |
| Indoor wall loss             | 5 dB        |
| Interference from other FAPs | 0–10 W      |

will not experience interference from one of the dominant neighbouring FAP due to the fact that the user’s serving FAP is engaged in the SGC/RMM algorithm with one of the dominant interfering FAP. An improvement in SINR translates to utilisation of fewer resource blocks for a given offered traffic, thus reducing the required transmit power and radio-head energy.

The comparison of the spectral efficiency for the FAP network is presented in Fig. 3.3(b). It can be seen that the spectral efficiency decreases in both baseline and SGC/RRM algorithm scenarios along with the increase of total interference from those which are not paired into this particular group. However the difference in spectral efficiency of the two scenarios reduces steadily with the increase of the interference. Due to the fact that most of the user’s SINRs are usually in the high regime as shown in Fig. 3.3(a), all the users can be scheduled in the first TTI. That is to say, the targeted QoS for each user is met.

The radio-head and operational energy performance of the SGC/RRM al-

### 3. FEMTOCELL INTERFERENCE AVOIDANCE

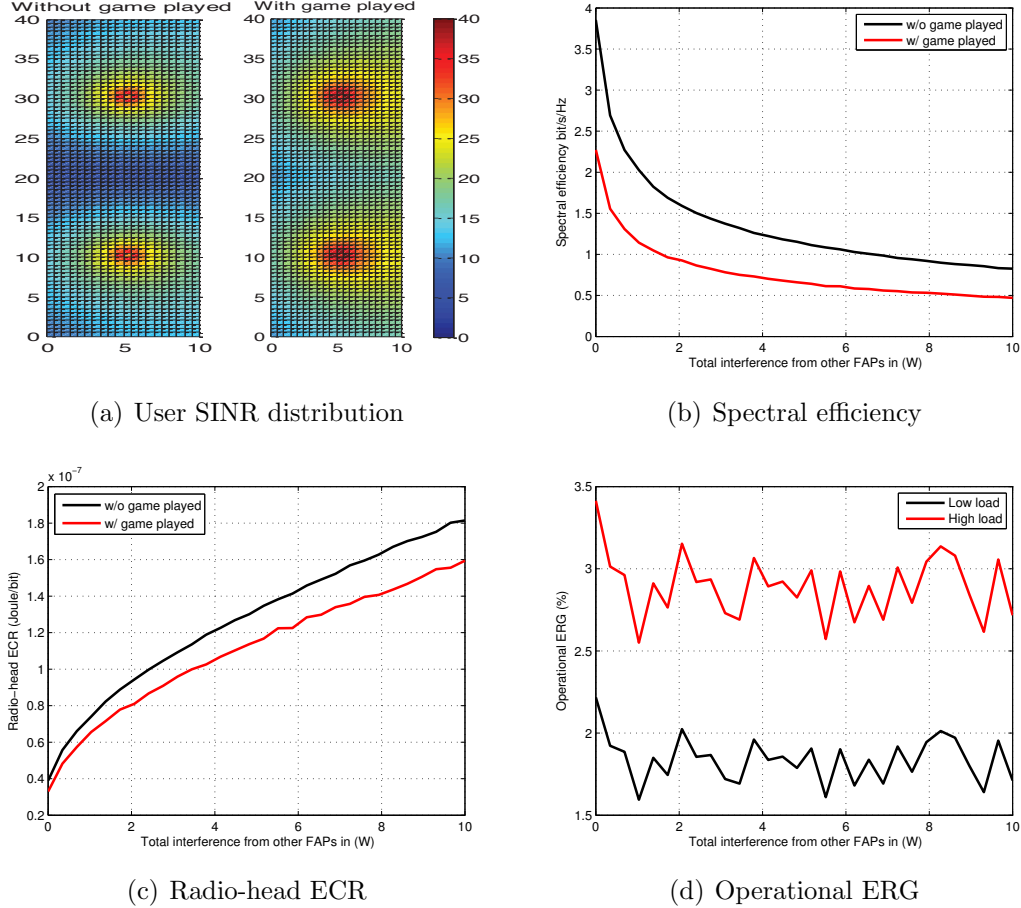


Figure 3.3: Trade-off of spectral efficiency and energy efficiency

gorithm were compared with the baseline scenario as shown in Fig. 3.3(c) and Fig. 3.3(d). The SGC/RRM algorithm is more energy efficient than the baseline case. This can be explained that the SGC/RRM algorithm provides the two players a chance to use only half of the total radio power in the whole network compared to the baseline scenario to produce more than half of the total RAN throughput. It can be found that the SGC/RRM algorithm works more effectively when the strength of the surrounding interference becomes stronger (i.e. larger than 15 dB). It should also be noted that this algorithm can offer 2.5%–3.5% and 1.6%–2.2% of the operational energy reduction in high load and low load scenarios.

## 3.5 Conclusions

This body of investigation has applied a strategy of interference avoidance to an indoor LTE-femtocell network of 2 FAPs, which mitigates the effects of interference through a sequential game play between FAPs in the E-UTRAN based on the offered traffic presented to the individual FAP. This is done for a 2-D office scenario. The comparisons of the simulation results have shown that up to 12% in radio-head energy and 3% in operational energy can be saved by consuming less than half the radio-head power while maintaining the user offered traffic unchanged. It is worth noting that the proposed scheme can be extended to be played by more than 2 FAPs as long as the extra care is provided in designing the interference rank pay off matrix.

## Chapter 4

# Deployment Location Optimisation of Indoor Femtocells

Having presented one way to boost throughput and the associated energy efficiency by interference mitigation using frequency domain restriction and transmit power limit of a FAP, the thesis will now examine how to create an algorithm that optimises the location of FAP with respect to the dominant interference. This distributed self-deployment solution includes a novel theoretical throughput framework which considers the effects of capacity saturation of realistic modulation and coding schemes and a statistical indoor propagation model. The results demonstrated that by knowing the strength and direction of the dominant interference source, significant throughput and energy savings gains can be made by optimising the location of FAPs. Furthermore, it shows that optimising the location of access points both within a building and within the individual rooms is critical to minimise the energy consumption.

Whilst the location and transmission of outdoor BSs are controlled by operators to meet throughput and coverage targets, there is less understanding and control on where indoor FAPs can be placed. Conventionally, indoor FAPs are located in areas of convenience (i.e., near an electricity socket or in the corner of a room). Indeed, the end-user cannot always arbitrarily decide where a FAP can



be placed, but this investigation shows that given a choice of regions in a room, there are regions which are more beneficial than others. The detection of the beneficial regions can be implemented as a distributed solution, embedded inside the FAPs. It requires no significant effort on the end-user's part as the study also demonstrates that the optimisation algorithm is rapid, automated and is a one-off process.

## 4.1 Review of Existing Work

There have been various approaches to investigate the optimal BS placement to achieve the operator's desired downlink user QoS or coverage targets, but there is some lack of knowledge about optimal indoor FAP deployment in the research community. Optimal placement of wireless nodes have been previously investigated in [52–55], whereby iterative computational techniques were used to find the optimal location of multiple nodes. Given that the diverse variations in buildings, such a model requires knowledge of: the building structure, electromagnetic properties of materials, and user locations. This is not a practically distributable solution for homes and small enterprise scenarios. Alternatively, other research has assumed that the coverage of the FAP is circular and the user locations are fixed. To the best of the author's knowledge, no middle-ground has been found between a deterministic and the statistical modelling approach. Given a general building structure, no explicit rule has been devised for where a FAP should be placed, as a function of statistical network parameters and co-channel interference.

A global optimisation approach in commercial buildings has been proposed in two recently published articles [56, 57]. However, the literature over-simplified the role of capacity saturation and the effect of interference, which will lead to a misleading result. On the contrary, the work in this chapter will show that by jointly considering the effects of interference and capacity saturation, the optimisation solution is significantly different from those of noise-limited channels without capacity saturation. When the capacity saturation is considered, placing FAP closer to those saturated users will not increase their data rate any more.

## 4.2 Research Contribution

Given the large number of propagation variables in indoor buildings and its relation to the outdoor cellular network, this work provides a best practice in optimising FAP deployment with very little SINR degradation for micro-cell users. In the first part of this investigation, this thesis optimises one indoor FAP position with the aim of achieving the highest mean network throughput in the presence of co-channel interference from a dominant source (either a micro-cell or a FAP in an adjacent room). In contrast with previous research, the analytical approach is corroborated by means of a Monte Carlo simulation which encapsulates sub-carrier level interference and user mobility modelling. The novel contribution is the simulation results and the proposed theoretical framework that reinforces the key deployment solutions. Moreover, for a given building size, the trade-off between increased user QoS and power consumption, as well as the capacity saturation points are demonstrated in the second part of the study. Finally, it is shown by simulation that the key results hold for a generic building with multiple rooms on multiple floors with an outdoor interference source. The reason why only one dominant outdoor micro-cell interference has been considered is because given that a building is inside the coverage of a cell, the interference of that cell will be far greater than neighbouring cells that are further away (this excludes the extreme case that the building is right at the boundary of two cells). The combined results of the three scenarios will lead to a general low energy indoor deployment rule.

## 4.3 Single Room Single FAP Placement

### 4.3.1 System Model

Previously in Chapter 2, the optimal number of APs to deploy in a single room has been considered. The conclusion was that for a low maximum downlink user QoS target, 1 FAP is the most energy efficient deployment. For higher maximum downlink user QoS targets, 2–3 802.11n APs should be deployed. In this section, simulation is used to determine where to place this 1 FAP given that there is

#### 4. DEPLOYMENT LOCATION OPTIMISATION OF INDOOR FEMTOCELLS

an outdoor interference source from a micro-cell. Furthermore, result of 1 FAP optimal placement with a theoretical background has been reinforced. Fig. 4.1 illustrates the system model. A number of users are randomly and uniformly distributed within the indoor office area. The mean user downlink throughput is considered as the objective metric for optimisation. Two single rectangular rooms with internal light walls are considered. The path loss models implemented in the simulator are the same as those used in Chapter 3 (Eq.(3.1) to (3.3)). The investigation considers the scenario of 1 FAP with 1 interfering outdoor micro-BS, followed by the scenario of 1 FAP with 1 adjacent interfering FAP. The common assumptions made are [58]:

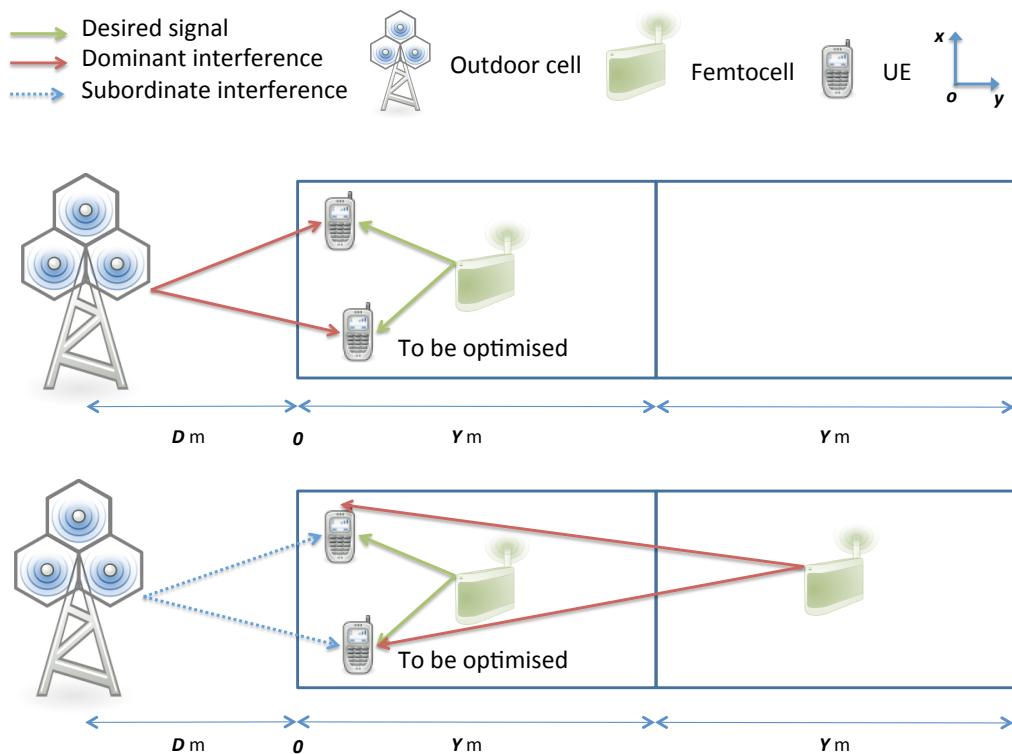


Figure 4.1: Simulation and theoretical model

- There is only one outdoor micro-cell interference considered. This is reasonably accurate for this study as proved in Section 5.3.
- The dominant interfering cell(s) (micro-BS in the first scenario and micro-BS plus FAP in the other room in the second scenario) have a full buffer

and persistently interfere with the serving-FAP on all channels.

- The channel mode is statistical in order to yield generalised insights into indoor FAP placement.
- The building is not right at the boundary of two cells.

### 4.3.2 Simulation Framework

In the simulation framework, the FAP location is varied across the room. For each location, a sufficiently high number of user positions are considered to yield converging results. The traditional brute-force exhaustive grid-search is employed to find the optimal FAP placement that yields the highest mean user throughput. The simulator supports adaptive MCS based on the channel quality (i.e., SINR). The link level MCS is generated from the Vienna LTE simulator [25] under the WINNER II A1 multipath model [26]. The corresponding throughput versus SNR curves of the look-up tables and the Shannon bound are illustrated in Fig. 4.2. It can be seen that simply using the Shannon Capacity expression will result in a huge discrepancy compared to a realistic wireless cellular system.

## 4.4 Theoretical Framework

In order to verify the simulation result of the optimal coordinate for a FAP to maximise the mean averaged area throughput in a particular office, an extensive theoretical model to solve this optimal problem has been developed under certain assumptions. The theoretical throughput expressions take into account the effects of capacity saturation, whereby any improvements in the channel quality yields no improvements in the throughput. This is due to the mutual information saturation of realistic transmission modulation schemes. The theoretical framework's assumptions are as follows [59]:

- The variation of throughput is predominantly along the interference alignment between the serving-FAP and the interference source.
- A modified Shannon expression is used for throughput, which accounts for the mutual information saturation of modulation and coding schemes.

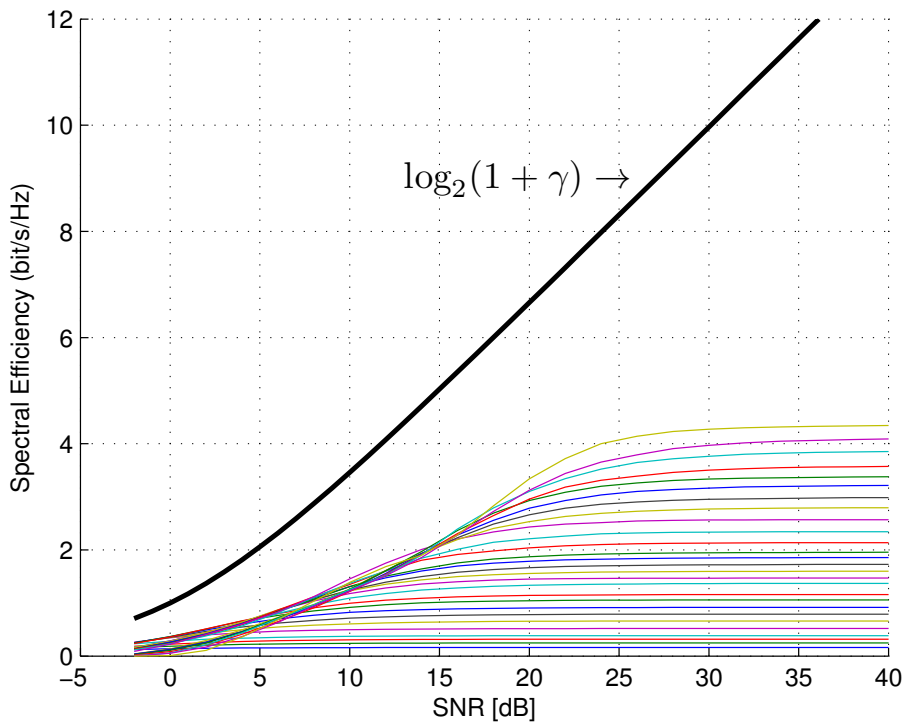


Figure 4.2: Throughput vs. SNR from WINNER\_II A1 SISO configuration and Shannon bound

#### 4.4.1 Dominant Micro-BS Interference

Consider a FAP network with one dominated micro-BS interference, where a FAP is located at  $(a, b)$  in the Cartesian co-ordinate system, a micro-BS is located at  $D$  m away from the nearest office wall and a user is located at  $(x, y)$ . The  $\gamma_{x,y}$  defined as the received SINR for a user at a particular position can be expressed as,

#### 4. DEPLOYMENT LOCATION OPTIMISATION OF INDOOR FEMTOCELLS

---

$$\begin{aligned}
\gamma_{x,y} &= \frac{\frac{P_{\text{FAP}}}{(d_{x,y,\text{FAP}})^{1.87} \times 10^{46.8/10} \times (\frac{f}{5})^2}}{\frac{P_{\text{micro}} \bar{G}_{\text{micro}}}{(d_{x,y,\text{micro}})^{3.67} \times 10^{(22.7+\text{PL}_{\text{wall}}+0.5d_{x,y,\text{in}})/10} \times (\frac{f}{5})^{2.6}} + \sigma^2}}, \\
&\approx \frac{P_{\text{FAP}} D^{3.67} \times 10^{(22.7+\text{PL}_{\text{wall}})/10} \times (\frac{f}{5})^{2.6} 10^{0.5d_{x,y,\text{in}}/10}}{P_{\text{micro}} \bar{G}_{\text{micro}} \times 10^{46.8/10} \times (\frac{f}{5})^2} \frac{1}{d_{x,y,\text{FAP}}^{1.87}}, \\
&= K_\gamma \frac{10^{\beta d_{x,y,\text{in}}}}{d_{i,\text{FAP}}^\alpha},
\end{aligned} \tag{4.1}$$

where  $\frac{P_{\text{FAP}} D^{3.67} \times 10^{(22.7+\text{PL}_{\text{wall}})/10} \times (\frac{f}{5})^{2.6}}{P_{\text{micro}} \bar{G}_{\text{micro}} \times 10^{46.8/10} \times (\frac{f}{5})^2}$  is denoted as  $K_\gamma$ ,  $\alpha = 1.87$  and  $\beta = 0.05$ .  $P_{\text{FAP}}$  and  $P_{\text{micro}}$  are the transmit power of FAP and micro-BS, respectively.  $\bar{G}_{\text{micro}}$  is the expected value of the antenna gain from the micro-BS.  $d_{x,y,\text{FAP}}$  is the  $i^{\text{th}}$  FAP-to-grid distance and  $d_{x,y,\text{micro}}$  is the  $i^{\text{th}}$  micro-BS-to-grid distance.  $d_{x,y,\text{in}}$  is the distance between the wall and  $i^{\text{th}}$  grid. As  $D \gg d_{x,y,\text{in}}$ ,  $d_{x,y,\text{micro}}$  can be accurately estimated as  $D$ .  $\gamma_{x,y}$  can then be re-written as  $K_\gamma \frac{10^{\beta d_{x,y,\text{in}}}}{d_{i,\text{FAP}}^\alpha}$ .

For a given FAP position of  $(x = a, y = b)$ , the mean throughput of a user attached to this FAP across all positions is:

$$\begin{aligned}
\bar{C}_{a,b} &= \frac{1}{A} \iint_A \log_2(1 + \gamma_{x,y}) \, dx \, dy, \\
&\approx \frac{1}{A} \iint_A \log_2(\gamma_{x,y}) \, dx \, dy, \\
&= \frac{1}{A} \iint_A \log_2 \left[ K_\gamma \frac{10^{\beta|y|}}{\left( \sqrt{(x-a)^2 + (y-b)^2} \right)^\alpha} \right] \, dx \, dy.
\end{aligned} \tag{4.2}$$

It can be seen from Fig. 4.3 (the same structure and layout as Fig. 4.1) that the typical SINR  $\gamma_{x,y}$  is in the high regime ranging from 15 to 45 dB so that a high SINR approximation is reasonable. According to the MCS physical-layer capacity simulations, the capacity will saturate when  $\gamma_{x,y} > \gamma_s = 35.94$  dB, **where  $\gamma_s$  is defined as the saturation SNR threshold**. Hence, the throughput values ( $\bar{C}_{a,b}$ ) across the room is not continuously increased and should be modified to reflect this saturated region, which is shown as  $d_{bp1}$  and  $d_{bp2}$  in Fig. 4.4. It is also

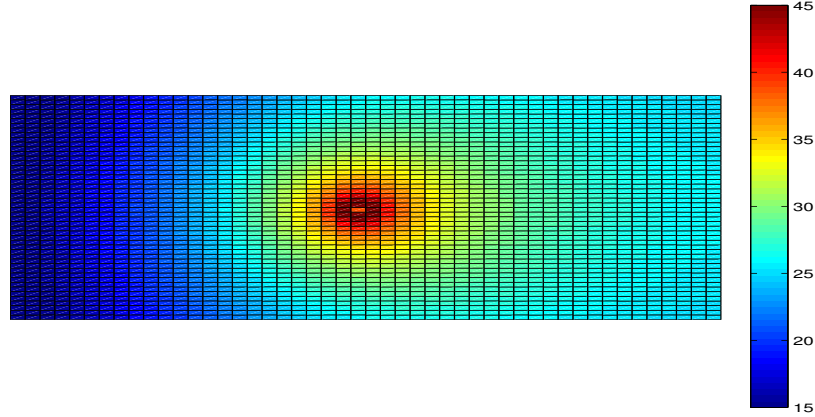


Figure 4.3: SINR grid map

worth pointing out that  $\gamma_{x,y}$  hardly fluctuates along the  $x$  axis, which is the axis orthogonal to the direction of the dominant interference. Therefore, Eq. (4.2) can be re-written as Eq. (4.3):

$$\bar{C}^b = \frac{1}{Y_s + Y_{ns}} \left[ C_s Y_s + \int_{Y_{ns}} \log_2 \left( K_\gamma \frac{10^{\beta y}}{|y-b|^\alpha} \right) dy \right], \quad (4.3)$$

where  $C_s = \log_2(1 + 10^{\frac{\gamma_s}{10}})$  bit/s/Hz.  $Y_s$  and  $Y_{ns}$  are the length of saturated and non-saturated capacity ranges, respectively.

It is important to note that due to capacity saturation, the mean throughput of the indoor users has to be broken up into the following 3 scenarios:

1. Scenario 1 ( $0 < b \leq b_1$ ): the FAP is close to the outdoor interfering-BS (window), so that the only non-saturated throughput region is away from the FAP and interfering-BS.
2. Scenario 2 ( $b_1 < b \leq b_2$ ): the FAP is in the middle region of the room so that the non-saturated throughput regions exist both towards and away from the interfering-BS.
3. Scenario 3 ( $b_2 < b \leq Y$ ): the FAP is far from the interfering-BS, so that the only non-saturated throughput region is towards the interfering-BS.

#### 4. DEPLOYMENT LOCATION OPTIMISATION OF INDOOR FEMTOCELLS

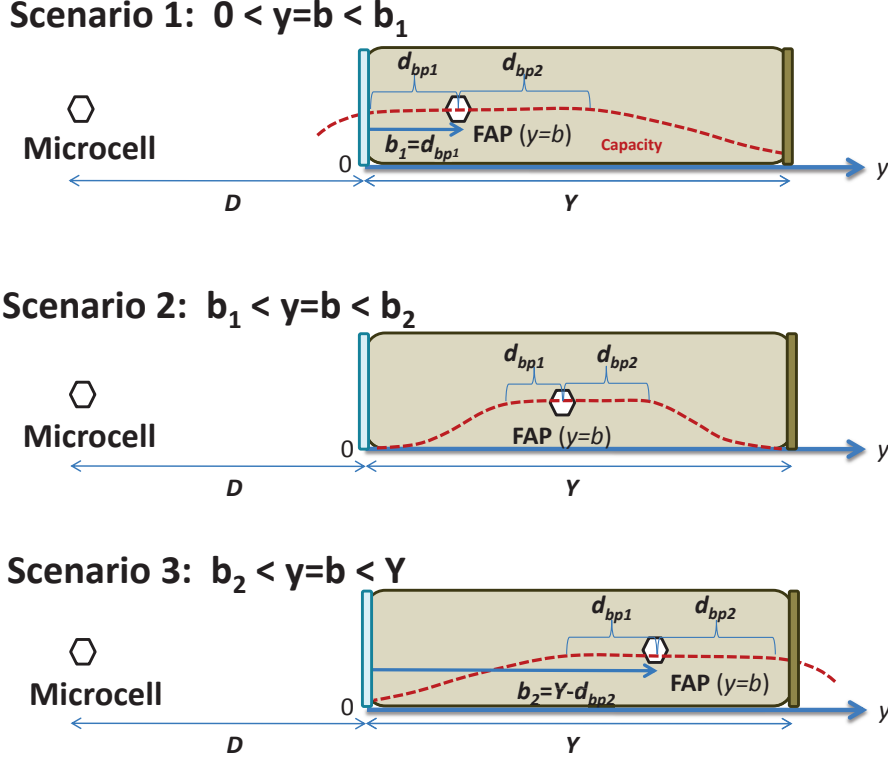


Figure 4.4: Illustration of the analytical scenarios in terms of the saturated throughput region with respect to different FAP positions inside the room.

##### 4.4.1.1 Formulation Scenario 1

In **scenario 1**, the farthest coordinate for FAP cannot exceed  $b_1$  where the SINR value at the wall close to the micro-BS side (i.e.  $d_{x,y,in} = 0$ ) should just achieve the saturation SNR threshold  $\gamma_s$ . Hence,  $b_1$  can be calculated as:

$$\begin{aligned}
 K_\gamma \frac{10^{\beta d_{y,in}}}{b_1^\alpha} &= 10^{\frac{\gamma_s}{10}}, \\
 \Rightarrow b_1 &= \sqrt[\alpha]{\frac{K_\gamma}{10^{\frac{\gamma_s}{10}}}}.
 \end{aligned} \tag{4.4}$$



The throughput can therefore be expressed by:

$$\begin{aligned}
 \bar{C}_1^b &= \frac{1}{Y} \int_0^{b+d_{bp2}} C_s \, dy + \frac{1}{Y} \int_{b+d_{bp2}}^Y \log_2 \left[ K_\gamma \frac{10^{\beta y}}{(y-b)^\alpha} \right] \, dy, \\
 &= \underbrace{\frac{(b+d_{bp2})C_s}{Y}}_{= P_1} + \underbrace{\frac{(Y-b-d_{bp2}) \log_2 K_\gamma}{Y}}_{= Q_1}, \\
 &\quad \underbrace{\phantom{\frac{(Y-b-d_{bp2}) \log_2 K_\gamma}{Y}}}_{= S_1} \\
 &+ \frac{\beta \log_2 10}{Y} \int_{b+d_{bp2}}^Y y \, dy - \frac{\alpha}{Y} \int_{b+d_{bp2}}^Y \log_2(y-b) \, dy, \\
 &= P_1 + Q_1 + \underbrace{\frac{\beta \log_2 10}{2Y} [Y^2 - (b+d_{bp2})^2]}_{= R_1} - \frac{\alpha}{Y} S_1.
 \end{aligned} \tag{4.5}$$

The breaking-point term  $d_{bp2}$  can be solved by the following equation:

$$\begin{aligned}
 K_\gamma \frac{10^{\beta(b+d_{bp2})}}{d_{bp2}^\alpha} &= 10^{\frac{\gamma_s}{10}}, \\
 \Rightarrow d_{bp2} &= B \exp[-W(-F)],
 \end{aligned} \tag{4.6}$$

where  $B = 10^{\frac{b}{20\alpha}} \left( \frac{K_\gamma}{10^{\frac{\gamma_s}{10}}} \right)^{\frac{1}{\alpha}}$ ,  $F = \frac{\ln 10}{20\alpha} B$ ,  $W$  is the **Lambert W** function, namely the branches of the inverse relation of the function  $f(W) = W \exp(W)$ .  $S_1$  can then be calculated in (4.7). By substituting Eq. (4.7) for  $S_1$  in Eq. (4.5),  $\bar{C}_1^b$  can be finalised as:

$$\bar{C}_1^b = P_1 + Q_1 + R_1 - \frac{\alpha}{Y}(T_1 - U_1). \tag{4.8}$$

#### 4.4.1.2 Formulation Scenario 2

When the position of FAP is on the coordinate  $b_2$ , the user's SINR at the other end of the office is equal to  $\gamma_s$ .  $b_2$  needs to be determined before assigning the proper limits for the mean throughput integral. With reference to Eq. (4.4),  $b_2$  can be found to be:

$$K_\gamma \frac{10^{\beta Y}}{(Y-b_2)^\alpha} = 10^{\frac{\gamma_s}{10}}, \Rightarrow b_2 = Y - \sqrt[\alpha]{\frac{K_\gamma 10^{\beta Y}}{10^{\frac{\gamma_s}{10}}}}. \tag{4.9}$$

4. DEPLOYMENT LOCATION OPTIMISATION OF INDOOR FEMTOCELLS

---

$$\begin{aligned}
S_1 &= \int_{b+d_{bp2}}^Y \log_2(y-b) dy = y \log_2(y-b) \Big|_{b+d_{bp2}}^Y - \int_{b+d_{bp2}}^Y \frac{y}{(y-b) \ln 2} dy, \\
&= \underbrace{Y \log_2(Y-b) - (b+d_{bp2}) \log_2 d_{bp2}}_{= T_1} - \frac{1}{\ln 2} \int_{b+d_{bp2}}^Y \frac{y-b+b}{y-b} dy, \\
&= T_1 - \frac{1}{\ln 2} [y + b \ln(y-b)] \Big|_{b+d_{bp2}}^Y = T_1 - \frac{1}{\ln 2} [Y-b-d_{bp2} + b \ln(Y-b) - b \ln d_{bp2}], \\
&= T_1 - \underbrace{\left( \frac{Y-b-d_{bp2}}{\ln 2} + b \log_2 \frac{Y-b}{d_{bp2}} \right)}_{U_1}.
\end{aligned} \tag{4.7}$$

After  $b_2$  is solved, the mean throughput in this scenario can therefore be expressed by:

$$\begin{aligned}
\bar{C}_2^b &= \frac{1}{Y} \int_0^{b-d_{bp1}} \log_2 \left[ K_\gamma \frac{10^{\beta y}}{(b-y)^\alpha} \right] dy + \frac{1}{Y} \int_{b-d_{bp1}}^{b+d_{bp2}} C_s dy \\
&+ \frac{1}{Y} \int_{b+d_{bp2}}^Y \log_2 \left[ K_\gamma \frac{10^{\beta y}}{(y-b)^\alpha} \right] dy, \\
&= P_2 + Q_2 + R_1 + R_2 - \frac{\alpha}{Y} (T_1 + T_2 - U_1 - U_2),
\end{aligned} \tag{4.10}$$

where  $d_{bp1}$  can be solved by the following equation:

$$\begin{aligned}
K_\gamma \frac{10^{\beta(b-d_{bp1})}}{d_{bp1}^\alpha} &= 10^{\frac{\gamma_s}{10}}, \\
\Rightarrow d_{bp1} &= B \exp[-W(F)],
\end{aligned} \tag{4.11}$$

and

$$P_2 = \frac{(d_{bp1} + d_{bp2})C_s}{Y}, \tag{4.12}$$

$$Q_2 = \frac{(Y - d_{bp1} - d_{bp2}) \log_2 K_\gamma}{Y}, \tag{4.13}$$

$$\bar{C}^b = \begin{cases} P_1 + Q_1 + R_1 - \frac{\alpha}{Y}(T_1 - U_1), & 0 < b \leq b_1 \\ P_2 + Q_2 + R_1 + R_2 - \frac{\alpha}{Y}(T_1 + T_2 - U_1 - U_2), & b_1 < b \leq b_2 \\ P_3 + Q_3 + R_2 - \frac{\alpha}{Y}(T_2 - U_2), & b_2 < b < Y \end{cases}. \quad (4.20)$$

$$R_2 = \frac{\beta \log_2 10}{2Y}(b - d_{bp1})^2, \quad (4.14)$$

$$T_2 = (b - d_{bp1}) \log_2 d_{bp1}, \quad (4.15)$$

$$U_2 = \frac{b - d_{bp1}}{\ln 2} + b \log_2 \frac{d_{bp1}}{b}. \quad (4.16)$$

#### 4.4.1.3 Formulation Scenario 3

In the last scenario, the mean throughput expression is very similar to that in scenario 1 and is given by:

$$\begin{aligned} \bar{C}_3^b &= \frac{1}{Y} \int_0^{b-d_{bp1}} \log_2 \left[ K_\gamma \frac{10^{\beta y}}{(b-y)^\alpha} \right] dy \\ &+ \frac{1}{Y} \int_{b-d_{bp1}}^Y C_s dy, \\ &= P_3 + Q_3 + R_2 - \frac{\alpha}{Y}(T_2 - U_2), \end{aligned} \quad (4.17)$$

where

$$P_3 = \frac{(Y - b + d_{bp1})C_s}{Y}, \quad (4.18)$$

$$Q_3 = \frac{(b - d_{bp1}) \log_2 K_\gamma}{Y}. \quad (4.19)$$

#### 4.4.2 Formulation Summary and Convex Optimisation

Equations (4.5), (4.10) and (4.17) complete the expression of the mean throughput of the network with respect to the position of the FAP  $b$  shown in Eq. (4.20). By combining the previously mentioned 3 scenarios together, the indoor mean and aggregate throughput for an interference-limited deployment have been formulated. The **benefit** of this **novel expression** is that it can be used to portray

the dominant trends which govern the throughput performance. The thesis will now combine the scenarios and perform convex optimisation to find the theoretical optimal FAP location and the resulting mean throughput.

It can be shown that the function is convex and that according to the first rule of finding the maximum value of a function, stationary points can be determined by differentiating Eq. (4.20) (Note:  $\frac{\partial d_{bp1}}{\partial b} = \frac{B \exp[-W(F)] \ln 10}{20\alpha[1+W(F)]}$  and  $\frac{\partial d_{bp2}}{\partial b} = \frac{B \exp[-W(-F)] \ln 10}{20\alpha[1+W(-F)]}$ ) and then solving the differentiated function for zeros. The resulting expression is a closed form expression and the solutions can be evaluated by straightforward analytical techniques. All the stationary points are tested in order to verify the type of the stationary points (maxima) by checking if the corresponding value in the second-order differential function of Eq. (4.20) is negative. Finally, the mean throughput value(s) corresponding to all the stationary points are compared with all endpoints of the interval of each sub-function in Eq. (4.20) and the global maximum value is selected as the maximum of mean throughput. The solution  $b_{\text{opt}}$  is the optimal coordinate for FAP placement.

#### 4.4.3 Dominant FAP Interference

A similar formulation exists when the dominant co-channel interference source is from a neighbouring FAP. Consider the same scenario as above with an extra in-building neighbouring FAP interference located at  $D_F$  m away from the wall close to the micro-BS. With reference to Eq. (3.2) ( $n_{\text{wall}} = 1$ ) and Eq. (4.1), the received SINR  $\gamma_{x,y}^F$  can be expressed in Eq. (4.21) by neglecting the subordinate micro-BS interference (on average 14 dB less than the dominant FAP interference):

$$\gamma_{x,y}^F = \left( K_F \frac{d_{x,y,\text{FAPint}}}{d_{x,y,\text{FAP}}} \right)^{\alpha_F}, \quad (4.21)$$

where  $d_{x,y,\text{FAPint}}$  is distance between the interfering FAP and the serving user,  $\alpha_F = 2$  and  $K_F = 10^{-0.25}$ . Therefore the mean throughput can be computed using the same methodology derived for Eq. (4.20). The three sub-functions of the mean throughput  $\bar{C}^F$  are given as in Eq. (4.22).

Where  $D_F$  is the distance between the interfering FAP and the nearest room

#### 4. DEPLOYMENT LOCATION OPTIMISATION OF INDOOR FEMTOCELLS

---

$$\overline{C}^F = \begin{cases} P_1^F + Q_1^F + R_1^F - \frac{\alpha_F}{Y} S_1, & 0 < b \leq b_1^F \\ P_2^F + Q_2^F + R_1^F + R_2^F - \frac{\alpha_F(S_1 - S_2)}{Y}, & b_1^F < b \leq b_2^F \\ P_3^F + Q_3^F + R_2^F - \frac{\alpha_F}{Y} S_2, & b_2^F < b < Y \end{cases} \quad (4.22)$$

wall,

$$P_1^F = \frac{(b + d_{bp2F})C_s}{Y}, \quad (4.23)$$

$$P_2^F = \frac{(d_{bp1F} + d_{bp2F})C_s}{Y}, \quad (4.24)$$

$$P_3^F = \frac{(Y - b + d_{bp1F})C_s}{Y}, \quad (4.25)$$

$$Q_1^F = \frac{(Y - b - d_{bp2F}) \log_2 K_F}{Y}, \quad (4.26)$$

$$Q_2^F = \frac{(Y - d_{bp1F} - d_{bp2F}) \log_2 K_F}{Y}, \quad (4.27)$$

$$R_1^F = \frac{\alpha_F}{Y} \left[ (Y - D_F) \log_2(D_F - Y) + (D_F - b - d_{bp2F}) \log_2(D_F - b - d_{bp2F}) - \frac{Y - b - d_{bp2F}}{\ln 2} \right], \quad (4.28)$$

$$R_2^F = \frac{\alpha_F}{Y} \left[ D_F \log_2 D_F - (D_F - b + d_{bp1F}) \log_2(D_F - b + d_{bp1F}) - \frac{b - d_{bp1F}}{\ln 2} \right], \quad (4.29)$$

$$b_1^F = \frac{K_F D_F}{\alpha_F \sqrt[10]{10^{\frac{\gamma_s}{10}}}}, \quad (4.30)$$

$$b_2^F = Y - \frac{K_F(D_F - Y)}{\alpha_F \sqrt[10]{10^{\frac{\gamma_s}{10}}}}, \quad (4.31)$$

$$d_{bp1F} = \frac{K_F D_F}{K_F + \alpha_F \sqrt[10]{10^{\frac{\gamma_s}{10}}}}, \quad (4.32)$$

$$d_{bp2F} = \frac{K_F D_F + \alpha_F \sqrt[10]{10^{\frac{\gamma_s}{10}}} b}{K_F + \alpha_F \sqrt[10]{10^{\frac{\gamma_s}{10}}}}. \quad (4.33)$$

Table 4.1: Simulation parameters and model assumptions

| Parameter                     | Value             |
|-------------------------------|-------------------|
| Scenario                      | 10 m × 20 m       |
| System bandwidth              | 20 MHz            |
| Carrier frequency             | 2130 MHz          |
| Frequency reuse               | 1                 |
| Number of FAPs                | 1                 |
| Total number of users         | 10                |
| User Distribution             | Uniform           |
| Total number of PRBs          | 100               |
| FAP transmit power            | 0.01–0.1 watts    |
| Micro-cell transmit power     | 5–40 watts        |
| FAP Radio-head efficiency     | 6.67%             |
| Overhead power                | 5.2 watts         |
| Pathloss model                | WINNER II A1 & B4 |
| Distance between Micro-to-FAP | 150–400 m         |
| Wall loss                     | 0–20 dB           |
| Scheduler                     | Round Robin       |
| Antenna configuration         | SISO              |
| Traffic mode                  | Full buffer       |

After solving the differentiated function of Eq. (4.22), the solution  $b_{\text{opt}}^F$  is the optimal coordinate for FAP placement in this scenario.

## 4.5 Simulation and Theoretical Results

The optimal placement is judged according to salient system variables, namely: the micro-BS location, the electromagnetic properties of the walls, and the ratio of micro-BS and FAP transmit power. A baseline conventional FAP deployment has been considered for comparison purposes, whereby the reference FAP is placed at the corner of the room where the power socket is typically located. The param-

ters used in the investigation are as follows and also contained in Table. 4.1: Office size ( $10 \times 20$  m), System bandwidth (20 MHz), Carrier frequency (2130 MHz), Total number of users (10), Sub-carriers per Physical Resource Block (12), FAP transmit power (0.01–0.1 W), micro-BS transmit power (5–40 W), FAP radio-head efficiency (6.67%), FAP overhead power (5.2 W), Micro-BS distance away from the office (150–450 m), and Wall loss (0–20 dB).

The result of the comparison between the optimal and the conventional is illustrated in the sub-plots of Fig. 4.5(a), Fig. 4.5(c) and Fig. 4.5(e). The theoretical results are shown as lines and are compared with the simulation results shown as symbols.

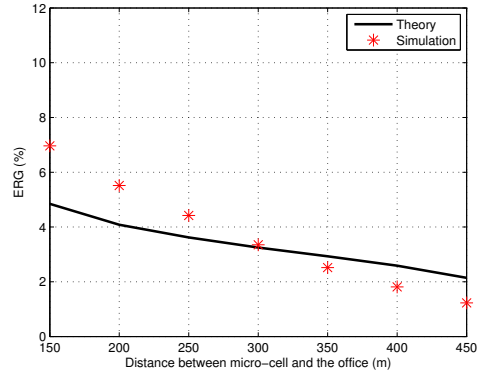
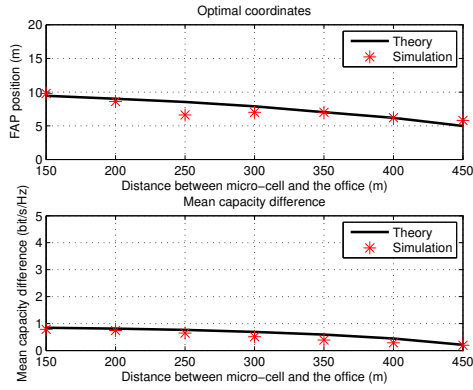
### 4.5.1 Dominant Micro-BS Interference

#### 4.5.1.1 Throughput Results

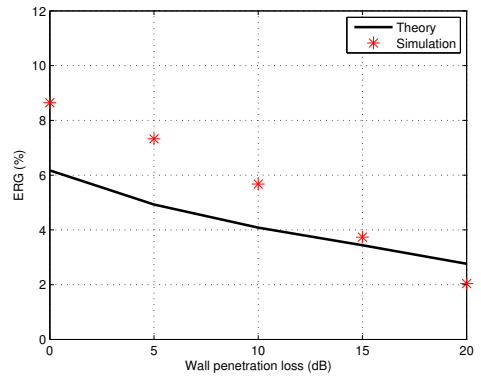
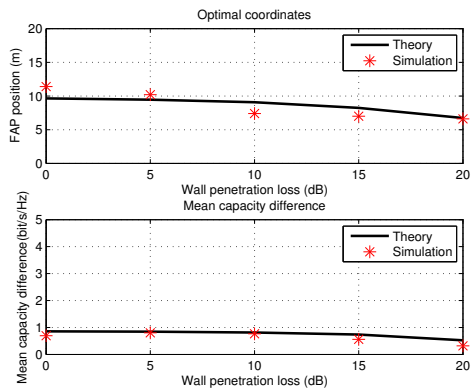
The impact of the micro-BS to office distance  $D$  on the performance of finding the optimal position is shown in Fig. 4.5(a), when  $PL_{\text{wall}} = 10$  dB,  $P_{\text{FAP}} = 0.1$  W and  $P_{\text{micro}} = 20$  W. The influence of the wall penetration loss is depicted in Fig. 4.5(c) when  $D = 200$  m,  $P_{\text{FAP}} = 0.1$  W and  $P_{\text{micro}} = 20$  W. And Fig. 4.5(e) shows the power ratio of micro-BS to FAP effect on the optimal placement decision.

When the users in the office suffer the most severe interference from the outdoor micro-BS, the optimal FAP position tends to be in the middle of the enterprise office. This position steadily moves towards the interfering micro-BS direction and converges to approximately 5–6 m away from the wall close to the micro-BS. The black curves in the optimal coordinate plots provide an accurate match to the results obtained from the Monte-Carlo simulator. The mean throughput difference between the optimal FAP position and the worst position (i.e. the smallest mean throughput) is illustrated in the lower half of Fig. 4.5(a), Fig. 4.5(c) and Fig. 4.5(e). The worst position is always at the corner of the far ending of the office. It can be seen that the difference calculated both in the theoretical model by Shannon’s capacity equation and the simulation with a MCS look-up table range from 0.2 bit/s/Hz to 0.8 bit/s/Hz. The following section will describes how much operational (OP) energy can be saved for an optimal FAP position compared to the worst scenario.

#### 4. DEPLOYMENT LOCATION OPTIMISATION OF INDOOR FEMTOCELLS

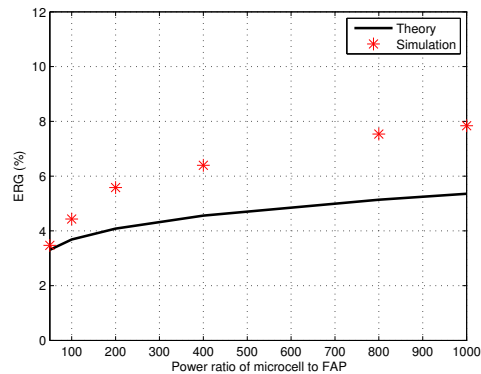
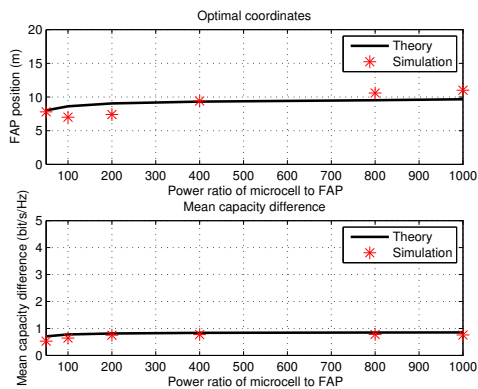


(a) Impact of distance between micro-BS and the office (b) Impact of distance between micro-BS and the office



(c) Wall penetration loss effect

(d) Wall penetration loss effect



(e) Power ratio of micro-BS to FAP

(f) Power ratio of micro-BS to FAP

Figure 4.5: Mean throughput difference (between optimal scenario and the baseline) and operational energy reduction gain (ERG): Theoretical (line) and simulation (symbols) results for optimal FAP placement.



#### 4. DEPLOYMENT LOCATION OPTIMISATION OF INDOOR FEMTOCELLS

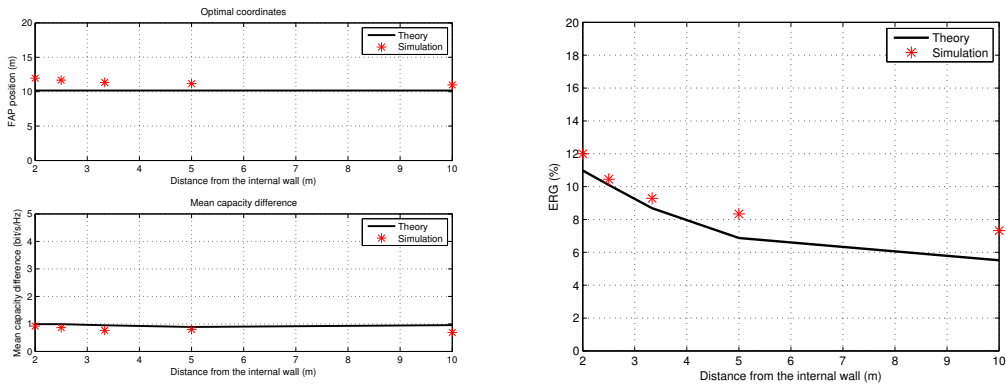
---

It can be noted that this solution of optimising the FAP location does not significantly degrade the outdoor network performance. By moving the FAP from 0 to 5 m closer to the cell-site, the interference to the outside network is increased by 0–2.5 dB, compared to when the FAP is placed in the middle of the room. When compared to the FAP randomly placed closer to the window, the interference is not significantly increased.

##### 4.5.1.2 Energy Results

Fig. 4.5(b), Fig. 4.5(d) and Fig. 4.5(f) show the ERG performance for the same three sets of equivalent investigation in Fig. 4.5(a), Fig. 4.5(c) and Fig. 4.5(e). Approximately 8% of OP energy can be saved when the source of the interference is close to the FAP (150 m), and 1% OP energy reduction can be made when the interference source is far from the FAP (450 m). The reason being that in the latter case, no matter where the FAP is located, all user locations in the room will experience a saturated throughput. Thus, the challenge of optimal FAP placement is non-existent.

##### 4.5.2 Dominant FAP Interference



(a) Impact of distance between interfering FAP and the internal wall

(b) ERG with FAP interference

Figure 4.6: Mean capacity gain and ERG comparison: Theoretical (line) and simulation (symbols) results of optimal FAP placement with a dominant FAP interference from adjacent room.

#### 4.5.2.1 Throughput Results

The impact of the micro-BS to office distance  $D$  on the performance of finding the optimal indoor FAP position is shown in the sub-plot Fig. 4.5(a), with parameters  $PL_{\text{wall}} = 10$  dB,  $P_{\text{FAP}} = 0.1$  W and  $P_{\text{micro}} = 20$  W. The influence of the extra FAP interference is depicted in the sub-plot Fig. 4.6(a) when  $D = 200$  m,  $P_{\text{FAP}} = 0.1$  W and  $P_{\text{micro}} = 20$  W.

In the presence of the FAP interference, this position almost remains in the middle as the saturated region is too small to contribute to the non-saturated ones. The lines provide an accurate match to the results obtained from the simulator (symbols). The mean throughput difference between the optimal FAP position and the worst position (i.e. the smallest mean throughput) is illustrated in the bottom sub-plots Fig. 4.6(a). The worst position is always at the corner of the far end of the office.

#### 4.5.2.2 Energy Results

Following the same logic as in the previous macro-cell only scenario, the thesis now quantifies how much energy can be saved relating to the improvement in capacity just shown. Fig. 4.6(b) depicts the ERG performance for these two scenarios shown in Fig. 4.1. Approximately 12% of OP energy can be saved when the source of the interference is close to the FAP (150 m), and 1% OP energy reduction can be made when the interference source is far from the FAP (450 m). In terms of the global context, there are 1 billion people in developed countries and if each house with 5 people has 1 FAP of a persistent 10 W operational power consumption, the annual electricity energy consumed is 17-20 TWh ( $10^{12}$  Wh). This is a lower bound as those duplicate FAPs in un-developed nations, shops, outdoors and workplace are not considered. With the optimal FAP placement, 1.6 TWh can be saved, which translates to the power generated by two 1000 MW power plants.

#### 4.5.2.3 Comparison with 3GPP Simulator

In Fig. 4.7(a), the optimal placement results from an industrial indoor network planning simulator based on 3GPP standards, RANPLAN iBuildNet, are con-

#### 4. DEPLOYMENT LOCATION OPTIMISATION OF INDOOR FEMTOCELLS

---

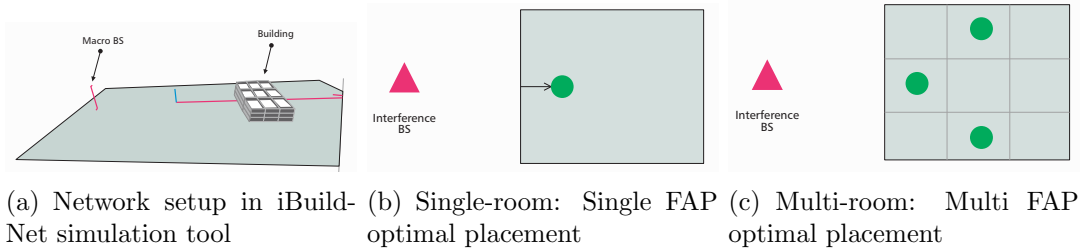


Figure 4.7: Optimal FAP deployment for maximum uniform coverage in: a) investigation setup in iBuildNet; b) a single room; c) multiple rooms.

sidered. The results from the simulation apply to a large building: Fig. 4.7(b) without internal walls and Fig. 4.7(c) with internal walls [14]. The results show that there is a FAP that is always deployed close to the outdoor macro-cell interference source, which is identical to the result found theoretically in the previous sub-sections. The key advantage of the method this study presents is that one can use a simple yet tractable expression to calculate the optimal placement of FAP without having to run a computationally intense simulator.

### 4.6 Single Room Multiple FAPs Placement

The thesis now turns its attention to observe how to place more than one FAP in one single room. The results in Fig. 4.8 shows that when more than 1 co-frequency AP is deployed in the same room, the mutual interference between them dominate. The meaning of dots in different colours in the plots is the association of users to different FAPs. Their location is a trade-off between: being in the central area to reduce path-loss distance to the users, and being further away from each other to reduce mutual interference. The **RAN throughput** for both optimal and conventional scenarios (placement policy stated in Chapter. 2) increases as more FAPs are deployed. It reaches a saturation region when 6 FAPs are optimally placed as shown in Fig. 4.9(a). Compared to the baseline elliptical deployment discussed in Chapter. 2, there is an average 6% ERG obtained from the optimal deployment shown in Fig. 4.9(b). The ERG threshold is defined in the second paragraph under Eq. (2.28).

#### 4. DEPLOYMENT LOCATION OPTIMISATION OF INDOOR FEMTOCELLS

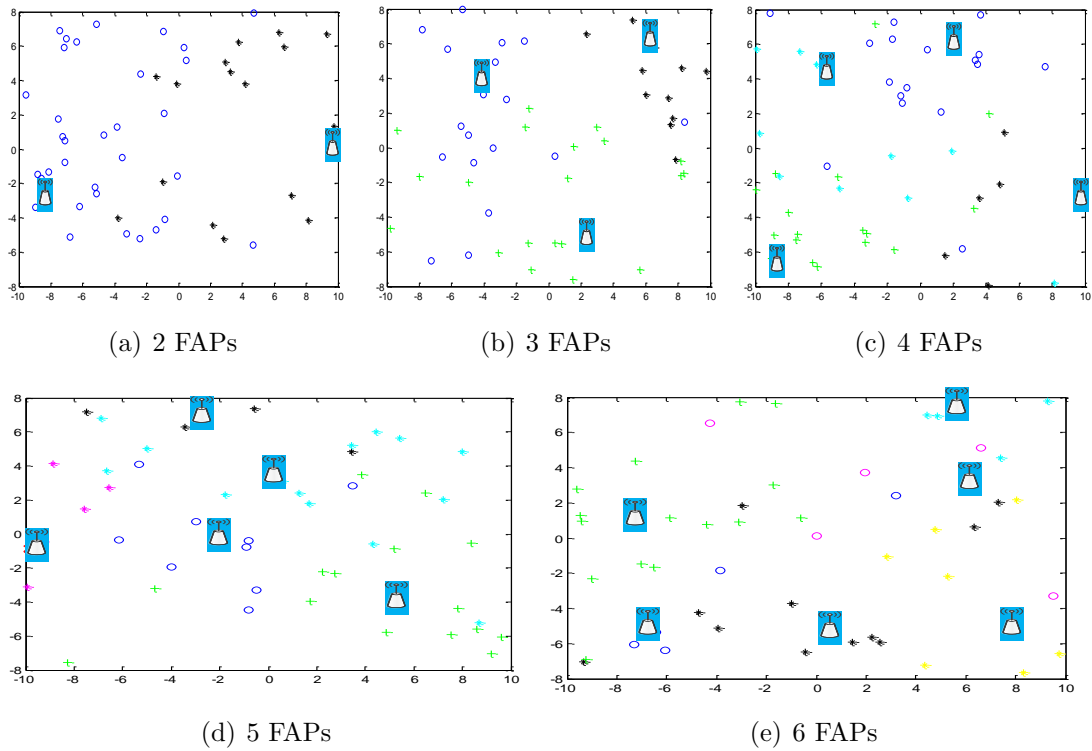
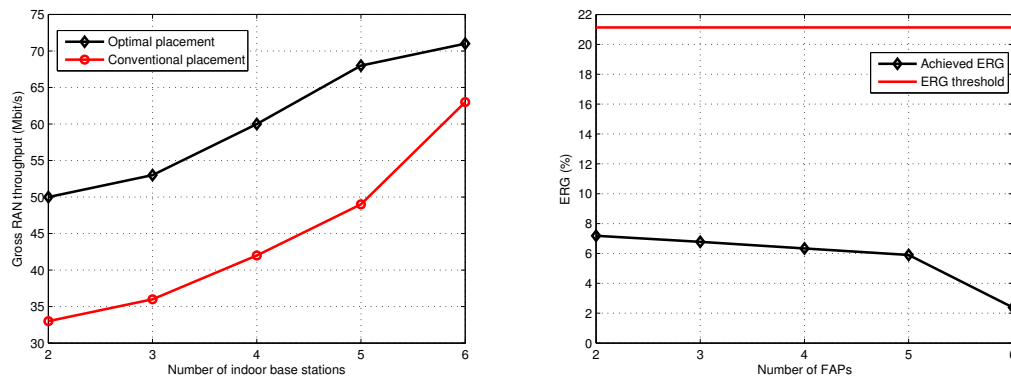


Figure 4.8: 2 to 6 FAPs optimal location with respect to mutual interference



(a) Average RAN throughput vs. number of FAPs

(b) ERG vs. number of FAPs

Figure 4.9: Average RAN throughput and ERG performance for 2 to 6 FAPs between optimal and conventional deployment

## 4.7 Multi-Room Multi-Floor FAP Placement

The study now considers a building with  $F$  floors and  $R$  rooms per floor as shown in Fig. 4.10. The framework of this comparison is how much energy is saved when the location of a FAP is optimised compared to an even distribution of FAPs across the building. This investigation is done for FAPs in the presence of an outdoor micro-cell interference source. A series of **RAN QoS** offered loads on the system is considered and what the minimum number of FAPs is required to meet this targeted load is examined. The parameters used in the investigation are as follows: number of floors (3), number of rooms per floor (9), room size (10 m  $\times$  20 m  $\times$  4 m), system bandwidth (20 MHz), carrier frequency (2130 MHz), total number of users per building (300), sub-carriers per Physical Resource Block (12), FAP transmit power (0.1 W), micro-cell transmit power (20 W), FAP RH efficiency (6.67%), FAP overhead power (5.2 W), micro-cell distance away from the room (200 m), and wall loss (10 dB). Fig. 4.11 shows the optimal locations of FAPs for different numbers of FAPs required and the associated capacity and energy consumption improvements. The rooms on the top floor have been numbered 1–9 followed by the rooms on the middle floor (10–18) and the ones on the ground floor (19–27). The micro-cell base station is located close to the side of rooms numbered (7–9, 16–18 and 25–27). FAP positions in yellow indicate that the system performance will be almost the same when deploying a FAP at either of these positions. FAP positions in blue are the recommended optimal ones in each scenario.

The results in Fig. 4.11(a) shows that at least 1-2 FAP(s) are always required near the wall that faces the outdoor interference source, and this should be on a floor with a similar height to the height of the interfering micro-cell-site. The other FAPs should be deployed on other floors at the far corners in alternating pattern to minimise the interference. The positions of the FAPs in blue have to be fixed while one of the FAPs in yellow can be selected as the last FAP position. A design principle can be summarised as follows:

1. In the presence of no strong outdoor interference, deploy a single FAP at centre of building. In the presence of outdoor micro-cell interference, deploy the FAP near the wall that is closest to the outdoor interference

#### 4. DEPLOYMENT LOCATION OPTIMISATION OF INDOOR FEMTOCELLS

---

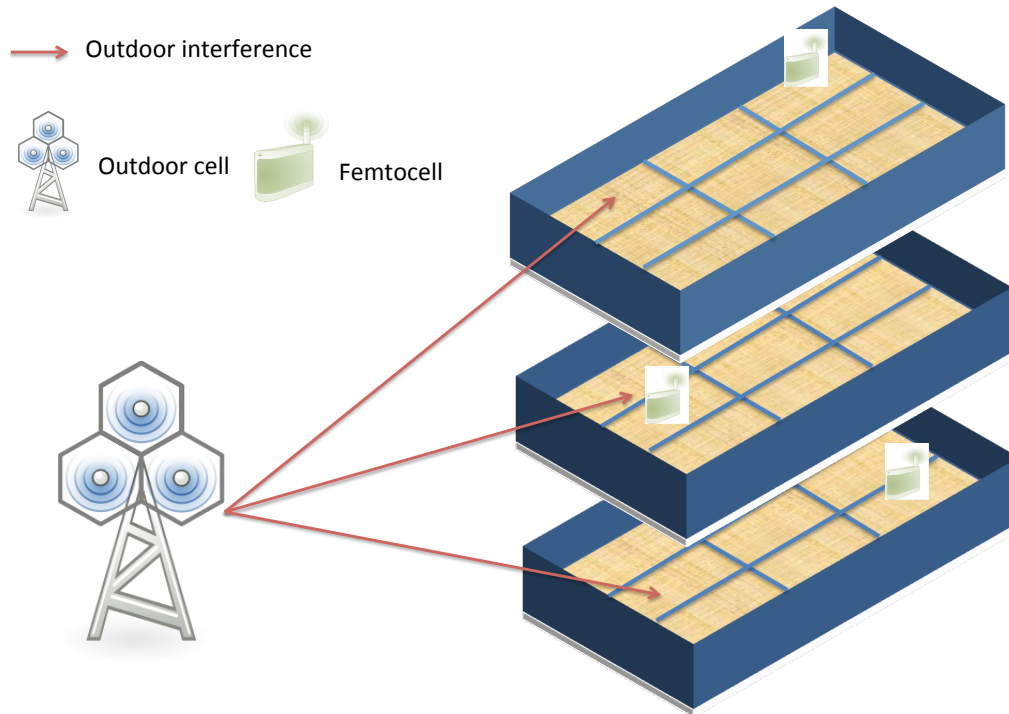


Figure 4.10: Simulation model of 3D multi-floors-multi-rooms (each grid on every floor represents a room)

source. The floor level should be one that is closest to the height of the micro-cell.

2. Any single additional FAP should be deployed also near the aforementioned wall on the same floor, but not in the same room as the first FAP.
3. Any multiple additional FAPs should be deployed not on the same floor, and at the opposite side of the building in corner rooms. These FAPs should not be on the same floor as FAPs placed in Steps 1 and 2 and with each other in Step 3.
4. Any additional FAP that do not satisfy rule 3. is likely to cause energy inefficiency.

Generally speaking, this rule can cover the optimisation of FAP placement for up to 6 FAPs, which can provide a sufficiently high QoS. The **RAN QoS** increases as the number of FAPs increases. This optimal deployment offers an average 12%

ERG compared to the baseline even distributional deployment. This is shown in Fig. 4.11(b). Fig. 4.11(c) illustrates how much energy can be reduced while deploying the optimal FAPs in this building when comparing to the baseline scenario for a certain **RAN QoS**. As the number of FAPs needed for different targeted **RAN QoS** is not always the same for optimal and baseline deployment, **ERG threshold** is omitted in this comparison.

## 4.8 Practical Implementation

To achieve this distributed FAP placement solution in reality, the thesis proposes that each FAP employs an in-built algorithm that estimates the following parameters:

- Dominant interference strength: either via pre-knowledge of where the nearest outdoor BS is, or alternatively via a *walk-and-scan* method to locate the strength and direction of the nearest co-channel interference source.
- Distance exponents of path loss model: can be an in-built knowledge, which is estimated from known literature by knowing the type of environment that the building is in.
- Length of building or room and the wall penetration loss: can be derived by associating the type of wall material and known literature on their penetration loss.

In the current technological-economic environment, any indoor AP placement optimisation solution is indeed more suited towards large venues, such as shopping malls, conference centres and enterprise offices. For home users, given a choice of *convenient* locations, the AP can at least advise which is better. This is achieved by knowing the location of the nearest interference source (macro-cell from cell planning web-site for example) and applying the proposed algorithm. The optimisation algorithm is a **one-off and rapid process** and has been theoretically predicted to yield improvements to the throughput and energy efficiency of indoor networks.

One of the key challenges with deployment optimisation generally is that the optimal capacity location of a cell, may not be available for practical and economic reasons. In that case, each FAP should be equipped with certain self-

optimisation features such that sub-optimal placement does not exacerbate the network performance.

## 4.9 Conclusions

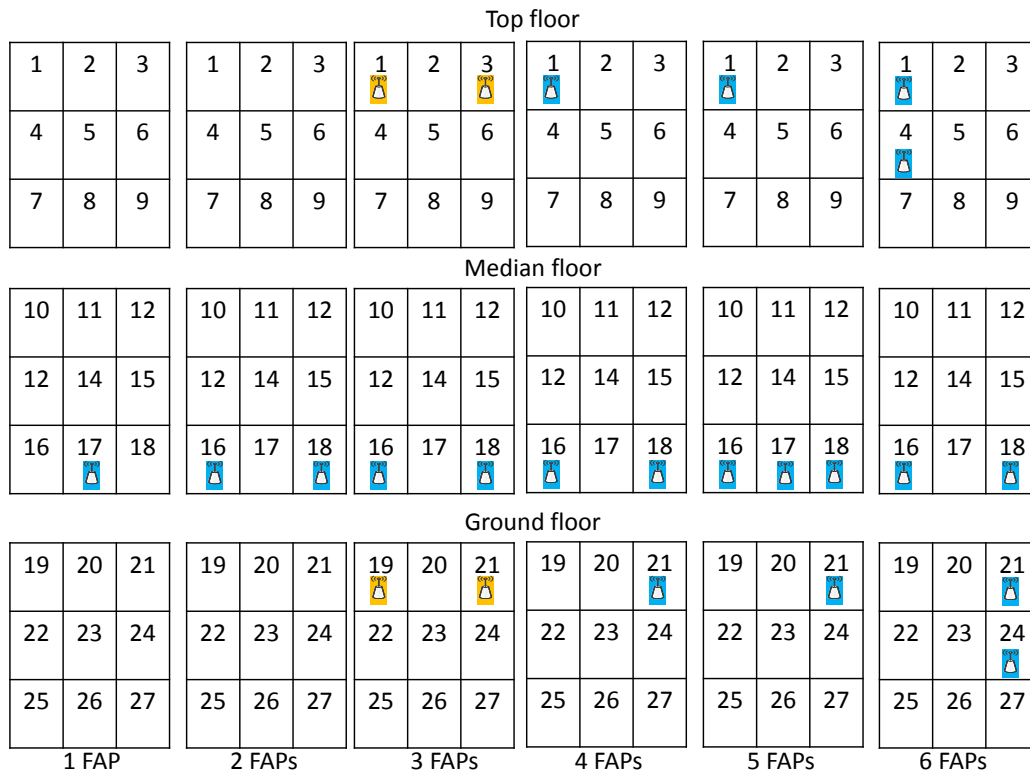
In this chapter, a theoretical and simulated optimisation framework has been proposed to find the optimal placement of an indoor FAP in the presence of either a micro-BS or an in-building FAP interference source. The framework takes into account statistical propagation parameters, transmitted power levels, mutual information saturation and the relative position of the indoor room with respect to the outdoor micro-BS. This work can be extended to consider multiple FAPs and outdoor macro-cells.

The comparison between theory and simulation shows good agreement, which indicates that the theoretical model can yield useful insights into the interaction between the location of FAPs and the resulting throughput and energy consumption performances. This chapter has demonstrated that optimising placement of indoor FAP location can significantly boost throughput and this should be an incentive for customers to consider placing the FAPs at certain regions of a room.

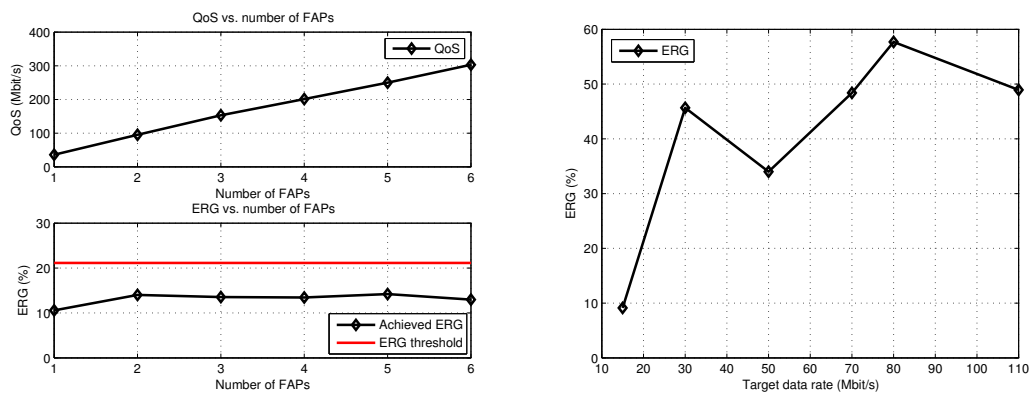
The key result is that the optimal FAP position varies between the centre of the room and towards the interfering source depending on the scenario. Compared to the conventional FAP placement, a performance improvement of up to 20% in mean throughput and 5 to 40% operational energy reduction have been achieved. Given the large number of indoor access points in the world, this leads to a significant world-wide energy reduction. The baseline simulation results are reinforced with a novel theoretical framework, which can be used to develop and optimise indoor deployment while causing very little SINR degradation for micro-cell users.



#### 4. DEPLOYMENT LOCATION OPTIMISATION OF INDOOR FEMTOCELLS



(a) Optimal position for 1–6 FAPs



(b) RAN QoS and ERG vs. number of FAPs

(c) ERG vs. targeted RAN QoS

Figure 4.11: Optimising indoor femtocell deployment and the capacity and energy consumption improvements

## Chapter 5

# Heterogeneous Network: Capacity, Coverage and Interference Performance Characterisation

The investigation has so far mainly considered the indoor network performance with dominant outdoor interference from one outdoor cell. By considering the Macro-cell BS (MBS) and co-channel indoor FAPs, the system-level performance will be characterised using both the dynamic system simulator and a stochastic-geometry theoretical framework, namely a Spatial-Poisson-Point-Process (SPPP) analysis. By introducing the interference from all the outdoor MBSs, there exists a historical open issue of how to analytically model the performance of the heterogeneous cellular network accurately [60]. The mathematical intractability mainly arises from the difficulty of precisely modelling adjacent interference by taking into account the spatial locations of the MBSs and the stochastic character of the wireless channel [61]. An alternative and popular approach of conducting such analysis is the use of costly, time-consuming and often proprietary system-level simulators [62]. However, this usual method seldom provides insightful information on system design and the results of optimisation vary from case to case in terms of the dependency of the system parameters. With the introduction of

new infrastructure elements to the conventional single tier cellular network, e.g., femto/pico BSs, fixed/mobile relays, cognitive radios, and distributed antennas, the downside of excessive reliance on simulations is even more exacerbated in the future cellular network, which is becoming more heterogeneous [8, 63–65]. Therefore, accurate and tractable models for downlink capacity and coverage, considering full network interference is needed in order not to impede the development of techniques to combat the other-cell interference.

## 5.1 Existing Common Analytical Models

To tackle the other-cell interference, communications researchers usually abstract tractable but overly simple spatial models of the BSs' locations for performance analysis. In particular, there are four abstraction models widely used by information theorists in this community.

- The Wyner model [66–68]: which is only accurate if there is a very large amount of interference averaging over the space because this model is normally one-dimensional and assumes a unit gain from each BS to the associated user and an equal gain that is less than one to the two users in the two neighbouring cells. It is highly inaccurate due to the fact that other-cell interference was modelled as a constant factor of the aggregate interference. For evolving cellular systems, such as LTE and Worldwide Interoperability for Microwave Access (WiMAX) using OFDMA, the Wyner model and related mean-value methods are highly inaccurate as the SINR values over a cell vary dramatically for irregular cell deployment. However, some of the latest discussions were still conducted via this model to evaluate the capacity of multi-cell systems [69–71].
- 1-D single interference cell model [72]: which is at least correct for the two cell case, where SINR does vary for different user position and possibly fading. Nevertheless, most sources of interference in the network with this approach are still neglected and therefore it is highly idealised. A recent work of such a model for the purposes of BS cooperation to reduce interference is given in [73]. That such a simplified approach to other-cell interference modelling was still considered state-of-the-art for analysis

## 5. HETEROGENEOUS NETWORK: CAPACITY, COVERAGE AND INTERFERENCE PERFORMANCE CHARACTERISATION

---

speaks to the difficulty in finding more realistic tractable approaches.

- 2-D regular hexagonal lattice or square grid model [74]: tractable analysis can sometimes be achieved for a fixed user with only a small number of interfering BSs, for example by considering the “worst-case” user location -the cell edge- and finding the SINR which is still a random variable in terms of shadowing and/or fading. The performance metrics such as average user rate and network outage probability can be determined only for this “worst-case” scenario [75, 76]. These are very pessimistic results which do not provide much insight into the performance of most users in the system. Moreover, such a model still requires either intensive numerical simulations or multi-fold Monte Carlo integrations done by computers [60]. Tractable expressions for the SINR in general for a random user location in the cell and the probability of outage/coverage over the entire cell are still unavailable in this model and it usually provides information for specific BSs deployments, and typically fails to provide useful guidance for more random, unplanned, emerging underlaid femtocells and picocells heterogeneous cellular networks. In a nutshell, this 2-D model is still highly idealised and may be increasingly inaccurate for the heterogeneous deployments common in urban and suburban areas where cell radii vary considerably.
- Homogeneous Spatial Poisson Point Process (SPPP) model [77–80]: Motivated by the aforementioned considerations, a new abstraction model is currently emerging and gaining popularity, according to which an additional source of randomness is introduced that the positions of the BSs are modelled as points of a Poisson Point Process (PPP) compared to that they are placed deterministically on a regular grid. Powerful tools from applied probability, such as stochastic geometry, are leveraged to develop tractable integrals and tractable mathematical frameworks for several key performance metrics (e.g., network coverage and average rate). Such an approach for BS modelling has been considered as early as 1997 [81]. Subsequently, a similar shotgun-based, PPP-based abstraction model was proposed in [82], and it was shown that, compared with the traditional hexagonal grid model, the shotgun approach provides upper performance bounds, but the key metrics of coverage (SINR distribution) and average

## 5. HETEROGENEOUS NETWORK: CAPACITY, COVERAGE AND INTERFERENCE PERFORMANCE CHARACTERISATION

---

network rate have not been determined. More recently, the SPPP model has been widely accepted for the analysis of spatial and opportunistic Aloha protocol [83], and for the characterisation of the SINR of single tier cellular networks [84]. In particular, a comprehensive framework to compute coverage and average rate of single-tier deployments is provided in [85]. Until then, the random-based abstraction model for the positions of the BSs had not received the attention it deserved. It has been demonstrated that the SPPP model is as accurate as regular grid models, but it has the main advantage of being more analytically tractable.

It can be noted that the homogeneous (or stationary) SPPP model, which benefits from the advantages of stochastic geometry characteristics, will continue being the main tool to study and analyse large networks of essentially randomly deployed nodes. This is more true for the femtocells underlaid heterogeneous network where FAPs are formed due to the end-user deployments which are regarded as falling into a random deployment category. A comprehensive study based on real BSs deployments obtained from the open source project OpenCellID has revealed that the SPPP model can indeed be used for accurate coverage analysis in major cities worldwide [86]. There are many other researchers currently using the SPPP-based abstraction model to study one- and multi-tier cellular networks and interference in a vast literature corresponding to stochastic geometric modelling and analysis of systems with randomly deployed nodes [87–121]. There have been three independent efforts to applying stochastic geometry to study heterogeneous networks: downlink coverage and average network rate in a single-tier cellular network with general fading and minimum distance cell association policy, downlink coverage and average network rate in an open-access multi-tier co-channel cellular network with general fading and maximum average received power cell association policy and uplink interference and power control modelling in a single-tier cellular network with Rayleigh fading. This chapter will incorporate all the modelling details available in the literature for studying the downlink performance of heterogeneous cellular network, introduce a few additional important features (namely the multi-tier property, statistical interference abstraction and non-co-channel network performance), and obtain the complete characterisation of the downlink SINR, and the outage probability (i.e., difference

between 1 and coverage probability) in both open- and closed-access multi-tier co-channel/non-co-channel heterogeneous network, for the original case where the mobile user is tagged to the cell that provides the maximum long-term averaged received power to the user.

## 5.2 System Model

Consider a collection of BSs modelled by SPPP  $\Phi_i$  of intensity  $\lambda_i$  ( $i = 1 \dots k$ ) in the Euclidean plane, respectively. Then, a heterogeneous cellular deployment can be modelled as a  $K$ -tier network where each tier models the BSs of a particular class and the  $k$  SPPPs are assumed to be spatially independent. The mobile users are also arranged according to some independent SPPP  $\Phi_u$  of intensity  $\lambda_u$ . Without loss of generality, the analysis of the model is focused on a typical mobile user located at the origin. The channel coefficient between the typical mobile user and a BS is assumed to be independent and identically distributed (i.i.d.) Rayleigh fading and denoted by  $H_i \sim \exp(1)$ . The standard path loss propagation model is applied with the path loss exponent  $\alpha_i > 2$ . Therefore, the downlink received SINR assuming the user connects to  $l^{\text{th}}$  BS in an  $i^{\text{th}}$ -tier is calculated as below ignoring antenna gain ( $G$ ) and log-normal shadowing ( $\mathcal{S}$ ):

$$\gamma_{il} = \frac{P_{ti} \text{PL}_C h_{il} d_{il}^{-\alpha_i}}{\sum_{k=1}^K \sum_{\substack{j \in \Phi_k \\ \setminus \text{BS}_{il}}} P_{tk} \text{PL}_C h_{kj} d_{kj}^{-\alpha_k} + \sigma^2} = \frac{P_{ti} \text{PL}_C h_{il} d_{il}^{-\alpha_i}}{I_{kj} + \sigma^2}, \quad (5.1)$$

where  $d_{il}$  and  $d_{kj}$  are the distance between the typical mobile user and its associated home BS and the  $j^{\text{th}}$  interfering BSs in the  $k^{\text{th}}$ -tier, respectively.  $h_{il}$  and  $h_{kj}$  follow the defined exponential distribution.  $P_{ti}$  is the transmit power of BSs in the  $i^{\text{th}}$ -tier.  $\text{PL}_C$  is the path loss constant, which is typically equal to  $10^{-4}$  [26]. Define the new random variable  $G_i = P_{ti} \text{PL}_C H_i$  and hence  $G_i \sim \exp(\beta_i)$  where  $\beta_i = \frac{1}{P_{ti} \text{PL}_C}$ .

### 5.2.1 Open Access

The thesis defines open access as a typical user can connect to the BS in any tier while the closed access is defined as the user can only connect to a specific tier. The typical user in an open access network is tagged to the  $i^{\text{th}}$ -tier only if the received power  $P_{ri}$  in  $i^{\text{th}}$ -tier is greater than any received power  $P_{rk}$  ( $k \neq i$ ) in other tiers. Therefore, the probability that the typical user is tagged to the  $i^{\text{th}}$ -tier can be expressed in the following mathematical form:

$$\begin{aligned}
 p_{Ti} &= \mathbb{E}_{R_i} \left\{ \mathbb{P} [P_{ri}(r_i) > \max_{k, k \neq i} P_{rk}(r_k)] \right\}, \\
 &= \mathbb{E}_{R_i} \left\{ \prod_{\substack{k=1 \\ k \neq i}}^K \mathbb{P} [P_{ri}(r_i) > P_{rk}(r_k)] \right\}, \\
 &= \mathbb{E}_{R_i} \left[ \prod_{\substack{k=1 \\ k \neq i}}^K \mathbb{P} \left( P_{ti} r_i^{-\alpha_i} > P_{tk} r_k^{-\alpha_k} \right) \right], \\
 &= \int_0^{+\infty} \prod_{\substack{k=1 \\ k \neq i}}^K \mathbb{P} \left[ R_k > \left( \frac{P_{tk}}{P_{ti}} \right)^{\frac{1}{\alpha_k}} r_i^{\frac{\alpha_i}{\alpha_k}} \right] f_{R_i}(r_i) dr_i,
 \end{aligned} \tag{5.2}$$

where  $f_{R_i}$  is the probability density function (pdf) of the random variable  $R_i$  denoted as the distance between the typical user and the nearest BS in the  $i^{\text{th}}$ -tier. The pdf and cumulative distribution function (CDF) for a random variable  $X$  are denoted, unless otherwise specified, as  $f_X(x)$  and  $F_X(x)$ . The derivation of  $f_{R_i}(r_i)$  is based on the fact that no other BS within the tier is located closer than  $r_i$  which is the distance separating the typical mobile user and its associated closest home BS. Therefore there is no BS at a distance from the typical user smaller than  $r_i$ . This probability can be derived by employing the 2-D Poisson process defined as  $\mathbb{P}[N(\mathcal{D}) = m] = \frac{(\lambda|\mathcal{D}|)^m e^{-\lambda|\mathcal{D}|}}{m!}$ . When  $m = 0$  and  $\mathcal{D} = \pi r^2$ , then the complementary cumulative distribution function (CCDF) of  $R_i$  can be expressed by this definition as

$$\mathbb{P}(R_i > r_i) = \mathbb{P}[(\text{BSs closer than } r_i) = 0] = e^{-\lambda_i \pi r_i^2}, \tag{5.3}$$

## 5. HETEROGENEOUS NETWORK: CAPACITY, COVERAGE AND INTERFERENCE PERFORMANCE CHARACTERISATION

---

so that the pdf of  $R_i$  can be found by differentiating the CDF of  $R_i$ :  $(1 - \mathbb{P}(R_i > r_i)) = 1 - e^{-\lambda_i \pi r_i^2}$  as

$$f_{R_i}(r_i) = \frac{dF_{R_i}(r_i)}{dr_i} = 2\lambda_i \pi r_i e^{-\lambda_i \pi r_i^2}. \quad (5.4)$$

With the reference to Eq. (5.3), the expression  $\prod_{\substack{k=1 \\ k \neq i}}^K \mathbb{P}\left[R_k > \left(\frac{P_{tk}}{P_{ti}}\right)^{\frac{1}{\alpha_k}} r_i^{\frac{\alpha_i}{\alpha_k}}\right]$  in the last step of Eq. (5.2) can be manipulated as  $\prod_{\substack{k=1 \\ k \neq i}}^K e^{-\lambda_k \pi \left(\frac{P_{tk}}{P_{ti}}\right)^{\frac{2}{\alpha_k}} r_i^{\frac{2\alpha_i}{\alpha_k}}}$  which can be used with Eq. (5.4) to further simplify  $p_{T_i}$ :

$$\begin{aligned} p_{T_i} &= \int_0^{+\infty} \prod_{\substack{k=1 \\ k \neq i}}^K \mathbb{P}\left[R_k > \left(\frac{P_{tk}}{P_{ti}}\right)^{\frac{1}{\alpha_k}} r_i^{\frac{\alpha_i}{\alpha_k}}\right] f_{R_i}(r_i) dr_i, \\ &= \int_0^{+\infty} \prod_{\substack{k=1 \\ k \neq i}}^K e^{-\lambda_k \pi \left(\frac{P_{tk}}{P_{ti}}\right)^{\frac{2}{\alpha_k}} r_i^{\frac{2\alpha_i}{\alpha_k}}} \cdot 2\lambda_i \pi r_i e^{-\lambda_i \pi r_i^2} dr_i, \\ &= 2\lambda_i \pi \int_0^{+\infty} r_i \exp\left[-\pi \sum_{\substack{k=1 \\ k \neq i}}^K \lambda_k \left(\frac{P_{tk}}{P_{ti}}\right)^{\frac{2}{\alpha_k}} r_i^{\frac{2\alpha_i}{\alpha_k}} - \pi \lambda_i \left(\frac{P_{ti}}{P_{ti}}\right)^{\frac{2}{\alpha_k}} r_i^{\frac{2\alpha_i}{\alpha_i}}\right] dr_i, \\ &= 2\lambda_i \pi \int_0^{+\infty} r_i \exp\left[-\pi \sum_{k=1}^K \lambda_k \left(\frac{P_{tk}}{P_{ti}}\right)^{\frac{2}{\alpha_k}} r_i^{\frac{2\alpha_i}{\alpha_k}}\right] dr_i, \end{aligned} \quad (5.5)$$

Setting  $\alpha_i = \alpha_k = \alpha$ ,  $p_{T_i}$  yields a more elegant form as



5. HETEROGENEOUS NETWORK: CAPACITY, COVERAGE AND INTERFERENCE PERFORMANCE CHARACTERISATION

---

$$\begin{aligned}
p_{\text{Ti}}(\alpha) &= 2\lambda_i\pi \int_0^{+\infty} r_i \exp \left[ -\pi \sum_{k=1}^K \lambda_k \left( \frac{P_{\text{tk}}}{P_{\text{ti}}} \right)^{\frac{2}{\alpha}} r_i^2 \right] dr_i, \\
&= \lambda_i \int_0^{+\infty} \exp \left[ -\pi \sum_{k=1}^K \lambda_k \left( \frac{P_{\text{tk}}}{P_{\text{ti}}} \right)^{\frac{2}{\alpha}} r_i^2 \right] d(\pi r_i^2), \\
&= \frac{\lambda_i}{\sum_{k=1}^K \lambda_k \left( \frac{P_{\text{tk}}}{P_{\text{ti}}} \right)^{\frac{2}{\alpha}}}.
\end{aligned} \tag{5.6}$$

Eq. (5.6) confirms the intuitive result that a user prefers to connect to a tier with higher BS density and transmit power. Starting with Eq. (5.3) in mind, the probability of the event  $D_i > d_{\text{il}}$  can therefore be achieved. By definition, the event  $D_i > d_{\text{il}}$  is indeed the event of  $R_i > d_{\text{il}}$  conditioned on that the typical user is attached to the  $i^{\text{th}}$ -tier, where the random variable  $D_i$  is denoted as the statistical distance between the typical user and the serving BS. The CCDF of  $D_i > d_{\text{il}}$  can be expressed as

$$\begin{aligned}
\mathbb{P}(D_i > d_{\text{il}}) &= \mathbb{P}[R_i > d_{\text{il}} | \text{User is attached to } i^{\text{th}} \text{ tier}], \\
&= \frac{\mathbb{P}[R_i > d_{\text{il}}, P_{\text{ri}}(R_i) > \max_{k, k \neq i} P_{\text{rk}}(R_k)]}{p_{\text{Ti}}}, \\
&= \frac{\int_{d_{\text{il}}}^{+\infty} \prod_{\substack{k=1 \\ k \neq i}}^K \mathbb{P} \left[ R_k > \left( \frac{P_{\text{tk}}}{P_{\text{ti}}} \right)^{\frac{1}{\alpha_k}} r_i^{\frac{\alpha_i}{\alpha_k}} \right] f_{R_i}(r_i) dr_i}{p_{\text{Ti}}}, \\
&= \frac{2\lambda_i\pi \int_{d_{\text{il}}}^{+\infty} r_i \exp \left[ -\pi \sum_{k=1}^K \lambda_k \left( \frac{P_{\text{tk}}}{P_{\text{ti}}} \right)^{\frac{2}{\alpha_k}} r_i^{\frac{2\alpha_i}{\alpha_k}} \right] dr_i}{p_{\text{Ti}}}.
\end{aligned} \tag{5.7}$$

## 5. HETEROGENEOUS NETWORK: CAPACITY, COVERAGE AND INTERFERENCE PERFORMANCE CHARACTERISATION

---

The CDF  $F_{D_i}(\mathbf{d}_{il})$  of  $D_i$  is  $1 - \mathbb{P}(D_i > \mathbf{d}_{il})$  and the pdf  $f_{D_i}(\mathbf{d}_{il})$  of  $D_i$  is therefore given by

$$\begin{aligned} f_{D_i}(\mathbf{d}_{il}) &= \frac{dF_{D_i}(\mathbf{d}_{il})}{d\mathbf{d}_{il}}, \\ &= \frac{2\lambda_i \pi \mathbf{d}_{il} \exp \left[ -\pi \sum_{k=1}^K \lambda_k \left( \frac{P_{tk}}{P_{ti}} \right)^{\frac{2}{\alpha_k}} \mathbf{d}_{il}^{\frac{2\alpha_i}{\alpha_k}} \right]}{p_{T_i}}. \end{aligned} \quad (5.8)$$

Setting  $\alpha_i = \alpha_k = \alpha$ ,  $f_{D_i}(\mathbf{d}_{il})$  simplifies to

$$f_{D_i}(\mathbf{d}_{il})(\alpha) = 2\pi \sum_{k=1}^K \lambda_k \left( \frac{P_{tk}}{P_{ti}} \right)^{\frac{2}{\alpha}} \mathbf{d}_{il} \exp \left[ -\pi \sum_{k=1}^K \lambda_k \left( \frac{P_{tk}}{P_{ti}} \right)^{\frac{2}{\alpha}} \mathbf{d}_{il}^2 \right], \quad (5.9)$$

for  $K = 1$ , Eq. (5.9) reduces to Eq. (5.4).

The average typical user's data rate of the overall network is taken over both the SPPP  $\Phi_i$  for all tiers and the exponential fading distribution and is defined as follows

$$C = \sum_{i=1}^K C_i p_{T_i}, \quad (5.10)$$

where  $C_i$  is the mean achievable user data rate in the  $i^{\text{th}}$ -tier and is averaged over both the distribution of  $D_i$  and the exponential fading distribution

$$\begin{aligned} C_i &= \mathbb{E}_{D_i} \left\{ \mathbb{E}_{\Gamma_i} \left[ B_{\text{eff}} \log_2 \left( 1 + \frac{\gamma_{il}}{\gamma_{\text{eff}}} \right) \right] \right\}, \\ &= B_{\text{eff}} \int_0^{+\infty} \mathbb{E}_{\Gamma_i} \left[ \log_2 \left( 1 + \frac{\gamma_{il}}{\gamma_{\text{eff}}} \right) \right] f_{D_i}(\mathbf{d}_{il}) d\mathbf{d}_{il}, \end{aligned} \quad (5.11)$$

where the adjustment factor of  $B_{\text{eff}} = 0.56$  is the bandwidth efficiency and  $\gamma_{\text{eff}} = 2$  is the SNR efficiency for LTE with Round Robin scheduling and SISO antenna configuration being applied according to [122]. When a continuous random variable  $X$  takes only non-negative values, the following formula can be used for computing its expectation

5. HETEROGENEOUS NETWORK: CAPACITY, COVERAGE AND INTERFERENCE PERFORMANCE CHARACTERISATION

---

$$\mathbb{E}(X) = \int_0^{+\infty} \mathbb{P}(X > \zeta) \, d\zeta. \quad (5.12)$$

With this approach,  $\mathbb{E}_{\Gamma_i} \left[ \log_2 \left( 1 + \frac{\gamma_{il}}{\gamma_{\text{eff}}} \right) \right]$  can be further developed as follows

$$\begin{aligned} \mathbb{E}_{\Gamma_i} \left[ \log_2 \left( 1 + \frac{\gamma_{il}}{\gamma_{\text{eff}}} \right) \right] &= \int_0^{+\infty} \mathbb{P} \left\{ \log_2 \left[ 1 + \frac{P_{\text{ti}} \text{PL}_C h_{il} \mathbf{d}_{il}^{-\alpha_i}}{(I_{kj} + \sigma^2) \gamma_{\text{eff}}} \right] > \zeta \right\} \, d\zeta, \\ &= \int_0^{+\infty} \mathbb{P} \left[ P_{\text{ti}} \text{PL}_C h_{il} > \gamma_{\text{eff}} \mathbf{d}_{il}^{\alpha_i} (I_{kj} + \sigma^2) (2^\zeta - 1) \right] \, d\zeta, \\ &= \int_0^{+\infty} \int_0^{+\infty} \int_{\gamma_{\text{eff}} \mathbf{d}_{il}^{\alpha_i} (I_{kj} + \sigma^2) (2^\zeta - 1)}^{+\infty} f_{G_i}(\mathbf{g}_{il}) f_{I_{kj}}(I_{kj} | \mathbf{d}_{il}) \, d\mathbf{g}_{il} \, dI_{kj} \, d\zeta, \\ &= \int_0^{+\infty} e^{-\beta_i \gamma_{\text{eff}} (2^\zeta - 1) \sigma^2 \mathbf{d}_{il}^{\alpha_i}} \int_0^{+\infty} e^{-\beta_i \gamma_{\text{eff}} (2^\zeta - 1) \mathbf{d}_{il}^{\alpha_i} I_{kj}} f_{I_{kj}}(I_{kj} | \mathbf{d}_{il}) \, dI_{kj} \, d\zeta, \\ &= \int_0^{+\infty} e^{-\beta_i \gamma_{\text{eff}} (2^\zeta - 1) \sigma^2 \mathbf{d}_{il}^{\alpha_i}} \mathcal{L}_{kj} \left[ -\beta_i \gamma_{\text{eff}} (2^\zeta - 1) \mathbf{d}_{il}^{\alpha_i} \right] \, d\zeta, \end{aligned} \quad (5.13)$$

where  $\mathcal{L}_{kj} \left[ -\beta_i \gamma_{\text{eff}} (2^\zeta - 1) \mathbf{d}_{il}^{\alpha_i} \right]$  is the Laplace transform of the random variable  $I_{kj}$  evaluated at  $-\beta_i \gamma_{\text{eff}} (2^\zeta - 1) \mathbf{d}_{il}^{\alpha_i}$  conditioned on the serving BS being at a distance  $\mathbf{d}_{il}$  from the typical mobile user at the origin and it yields

5. HETEROGENEOUS NETWORK: CAPACITY, COVERAGE AND INTERFERENCE PERFORMANCE CHARACTERISATION

---

$$\begin{aligned}
\mathcal{L}_{\mathbf{g}_{kj}} \left[ -\beta_i \gamma_{\text{eff}} (2^\zeta - 1) \mathbf{d}_{il}^{\alpha_i} \right] &= \int_0^{+\infty} e^{-\beta_i \gamma_{\text{eff}} (2^\zeta - 1) \mathbf{d}_{il}^{\alpha_i} I_{kj}} f_{I_{kj}}(I_{kj} | \mathbf{d}_{il}) \, dI_{kj}, \\
&= \mathbb{E}_{\Phi_k} \left[ \int_0^{+\infty} e^{-\beta_i \gamma_{\text{eff}} (2^\zeta - 1) \mathbf{d}_{il}^{\alpha_i} \sum_{k=1}^K \sum_{\substack{j \in \Phi_k \\ \setminus \text{BS}_{il}}} P_{tk} \text{PLC} h_{kj} \mathbf{d}_{kj}^{-\alpha_k}} f_{\mathbf{G}_k}(\mathbf{g}_{kj}) \, d\mathbf{g}_{kj} \right], \\
&= \mathbb{E}_{\Phi_k} \left[ \int_0^{+\infty} \prod_{k=1}^K \prod_{\substack{j \in \Phi_k \\ \setminus \text{BS}_{il}}} e^{-\beta_i \gamma_{\text{eff}} (2^\zeta - 1) \mathbf{d}_{il}^{\alpha_i} P_{tk} \text{PLC} h_{kj} \mathbf{d}_{kj}^{-\alpha_k}} f_{\mathbf{G}_k}(\mathbf{g}_{kj}) \, d\mathbf{g}_{kj} \right], \\
&= \mathbb{E}_{\Phi_k} \left[ \int_0^{+\infty} \prod_{k=1}^K \prod_{\substack{j \in \Phi_k \\ \setminus \text{BS}_{il}}} e^{-\beta_i \gamma_{\text{eff}} (2^\zeta - 1) \mathbf{d}_{il}^{\alpha_i} \mathbf{g}_{kj} \mathbf{d}_{kj}^{-\alpha_k}} \beta_k e^{-\beta_k \mathbf{g}_{kj}} \, d\mathbf{g}_{kj} \right], \\
&= \mathbb{E}_{\Phi_k} \left[ \prod_{k=1}^K \prod_{\substack{j \in \Phi_k \\ \setminus \text{BS}_{il}}} \frac{\beta_k}{\beta_k + \beta_i \gamma_{\text{eff}} (2^\zeta - 1) \mathbf{d}_{il}^{\alpha_i} \mathbf{d}_{kj}^{-\alpha_k}} \right], \\
&= \mathbb{E}_{\Phi_k} \left[ \prod_{k=1}^K \prod_{\substack{j \in \Phi_k \\ \setminus \text{BS}_{il}}} \frac{P_{ti}}{P_{ti} + P_{tk} \gamma_{\text{eff}} (2^\zeta - 1) \mathbf{d}_{il}^{\alpha_i} \mathbf{d}_{kj}^{-\alpha_k}} \right], \tag{5.14} \\
&= \prod_{k=1}^K \int_{\mathbb{R}^2} \lambda_k \left[ \frac{P_{ti}}{P_{ti} + P_{tk} \gamma_{\text{eff}} (2^\zeta - 1) \mathbf{d}_{il}^{\alpha_i} \mathbf{d}_{kj}^{-\alpha_k}} - 1 \right] \, d\mathbf{d}_{kj}, \\
&= \prod_{k=1}^K \exp \left\{ \int_{\mathbb{R}^2} -\lambda_k \left[ 1 + \frac{\mathbf{d}_{kj}^{\alpha_k}}{P_{tk} \gamma_{\text{eff}} (2^\zeta - 1) \mathbf{d}_{il}^{\alpha_i}} \right]^{-1} \, d\mathbf{d}_{kj} \right\}, \\
&= \prod_{k=1}^K \exp \left\{ \int_0^{+\infty} \left( \frac{P_{tk}}{P_{ti}} \right)^{\frac{1}{\alpha_k}} \mathbf{d}_{il}^{\frac{\alpha_i}{\alpha_k}} - 2\lambda_k \pi \mathbf{v} \left[ 1 + \frac{\mathbf{v}^{\alpha_k}}{P_{tk} \gamma_{\text{eff}} (2^\zeta - 1) \mathbf{d}_{il}^{\alpha_i}} \right]^{-1} \, d\mathbf{v} \right\}, \\
&= \prod_{k=1}^K \exp \left\{ -\lambda_k \pi \left( \frac{P_{tk}}{P_{ti}} \right)^{\frac{2}{\alpha_k}} \mathbf{d}_{il}^{\frac{2\alpha_i}{\alpha_k}} \int_{[\gamma_{\text{eff}} (2^\zeta - 1)]^{-\frac{2}{\alpha_k}}}^{+\infty} \frac{[\gamma_{\text{eff}} (2^\zeta - 1)]^{\frac{2}{\alpha_k}}}{1 + \mathbf{u}^{\frac{\alpha_k}{2}}} \, d\mathbf{u} \right\}, \\
&= \prod_{k=1}^K e^{-\lambda_k \pi \left( \frac{P_{tk}}{P_{ti}} \right)^{\frac{2}{\alpha_k}} \mathbf{d}_{il}^{\frac{2\alpha_i}{\alpha_k}} \mathcal{A}(\zeta, \alpha_k)},
\end{aligned}$$

where the fourth step follows from the i.i.d. distribution of  $\mathbf{G}_k$  and its further independence from the SPPP  $\Phi_k$ , the seventh step follows from the probability

## 5. HETEROGENEOUS NETWORK: CAPACITY, COVERAGE AND INTERFERENCE PERFORMANCE CHARACTERISATION

---

generating functional (PGFL) [123] of the SPPP. In the ninth step, the manipulation results from converting from Cartesian to polar coordinates and the lower limit of the integral is  $\left(\frac{P_{tk}}{P_{ti}}\right)^{\frac{1}{\alpha_k}} d_{il}^{\frac{\alpha_i}{\alpha_k}}$  due to the fact that the closest interferer in the  $k^{\text{th}}$ -tier is at least at a distance  $\left(\frac{P_{tk}}{P_{ti}}\right)^{\frac{1}{\alpha_k}} d_{il}^{\frac{\alpha_i}{\alpha_k}}$  (from the last step in Eq. (5.2)). The variable  $u$  is substituted for  $\frac{v^2}{\left[\frac{P_{tk}}{P_{ti}}\gamma_{\text{eff}}(2^\zeta-1)d_{il}^{\alpha_i}\right]^{\frac{2}{\alpha_k}}}$  in the tenth step.

Combining Eq. (5.13), (5.14) and (5.8),  $C_i$  can be finalised as

$$C_i = B_{\text{eff}} \int_0^{+\infty} \int_0^{+\infty} e^{-\beta_i \gamma_{\text{eff}} (2^\zeta - 1) \sigma^2 d_{il}^{\alpha_i}} \prod_{k=1}^K e^{-\lambda_k \pi \left(\frac{P_{tk}}{P_{ti}}\right)^{\frac{2}{\alpha_k}} d_{il}^{\frac{2\alpha_i}{\alpha_k}} \mathcal{A}(\zeta, \alpha_k)} d\zeta$$

$$\cdot \frac{2\lambda_i \pi d_{il} \exp \left[ -\pi \sum_{k=1}^K \lambda_k \left(\frac{P_{tk}}{P_{ti}}\right)^{\frac{2}{\alpha_k}} d_{il}^{\frac{2\alpha_i}{\alpha_k}} \right]}{P_{Ti}} dd_{il}. \quad (5.15)$$

In an interference-limited network, setting  $\sigma^2 = 0$  and all path loss exponents to  $\alpha$ ,  $C_i$  can be further simplified as

$$C_i(\alpha)|_{\sigma^2=0} = B_{\text{eff}} \int_0^{+\infty} \int_0^{+\infty} \prod_{k=1}^K e^{-\lambda_k \pi \left(\frac{P_{tk}}{P_{ti}}\right)^{\frac{2}{\alpha}} d_{il}^{\frac{2}{\alpha}} \mathcal{A}(\zeta, \alpha)} d\zeta$$

$$\cdot 2\pi \sum_{k=1}^K \lambda_k \left(\frac{P_{tk}}{P_{ti}}\right)^{\frac{2}{\alpha}} d_{il} \exp \left[ -\pi \sum_{k=1}^K \lambda_k \left(\frac{P_{tk}}{P_{ti}}\right)^{\frac{2}{\alpha}} d_{il}^{\frac{2}{\alpha}} \right] dd_{il},$$

$$= 2\pi \sum_{k=1}^K \lambda_k \left(\frac{P_{tk}}{P_{ti}}\right)^{\frac{2}{\alpha}} B_{\text{eff}}$$

$$\cdot \int_0^{+\infty} \int_0^{+\infty} d_{il} \exp \left\{ -\pi \sum_{k=1}^K \lambda_k \left(\frac{P_{tk}}{P_{ti}}\right)^{\frac{2}{\alpha}} d_{il}^{\frac{2}{\alpha}} [1 + \mathcal{A}(\zeta, \alpha)] \right\} d\zeta dd_{il},$$

$$= \int_0^{+\infty} \frac{B_{\text{eff}}}{1 + \mathcal{A}(\zeta, \alpha)} d\zeta. \quad (5.16)$$

Substituting Eq. (5.16) in Eq. (5.10),  $C(\alpha)|_{\sigma^2=0}$  can be obtained as

5. HETEROGENEOUS NETWORK: CAPACITY, COVERAGE AND INTERFERENCE PERFORMANCE CHARACTERISATION

---

$$\begin{aligned} \mathcal{C}(\alpha)|_{\sigma^2=0} &= \int_0^{+\infty} \frac{B_{\text{eff}}}{1 + \mathcal{A}(\zeta, \alpha)} d\zeta \sum_{k=1}^K p_{\text{Ti}}, \\ &= \int_0^{+\infty} \frac{B_{\text{eff}}}{1 + \mathcal{A}(\zeta, \alpha)} d\zeta. \end{aligned} \quad (5.17)$$

For a special case when  $\alpha = 4$ , the mean achievable user data rate of the overall open access LTE heterogeneous network can be computed as

$$\begin{aligned} \mathcal{C}(4)|_{\sigma^2=0} &= \int_0^{+\infty} \frac{B_{\text{eff}}}{1 + \mathcal{A}(\zeta, 4)} d\zeta, \\ &= 0.56 \int_0^{+\infty} \frac{1}{1 + \sqrt{\gamma_{\text{eff}}(2^\zeta - 1)} \arctan \sqrt{\gamma_{\text{eff}}(2^\zeta - 1)}} d\zeta, \\ &\approx 0.92 \text{ bit/s/Hz}. \end{aligned} \quad (5.18)$$

The last step follows the approximate value of the numerical integration by using a method of Gauss-Kronrod quadrature formula and this suggests that the mean downlink spectral efficiency in an LTE heterogeneous cellular network with Rayleigh fading and no AWGN is predicted to be 0.92 bit/s/Hz. It reveals that the average interference-limited network data rate is not affected by BS density, BS transmit power, or even the number of tiers. This means that adding BSs or raising the power increases interference and desired signal power by the same amount, and they eventually offset each other. Therefore, the network sum data rate increases in direct proportion to the total number of BSs.

The last metric of performance characterisation to be studied is the outage probability (i.e., difference between 1 and coverage probability). From the right hand side of Eq. (5.13), the expression inside the integral can be interpreted as the probability that the data rate is greater than  $\zeta$ . A similar expression for the probability that the received SINR is greater than  $\xi$ , namely, the probability of coverage, at any given serving distance  $d_{\text{ii}}$  is given by

5. HETEROGENEOUS NETWORK: CAPACITY, COVERAGE AND INTERFERENCE PERFORMANCE CHARACTERISATION

---

$$\begin{aligned} \mathbf{P}_{\text{cov}}(\mathbf{d}_{\text{il}}) &= \mathbb{P}(\gamma_{\text{il}} > \xi) = e^{-\beta_i \xi \sigma^2 d_{\text{il}}^{\alpha_i}} \mathcal{L}_{\text{kj}}[-\beta_i \xi d_{\text{il}}^{\alpha_i}], \\ &= e^{-\beta_i \xi \sigma^2 d_{\text{il}}^{\alpha_i}} \prod_{k=1}^K e^{-\lambda_k \pi \left(\frac{P_{\text{tk}}}{P_{\text{ti}}}\right)^{\frac{2}{\alpha_k}} d_{\text{il}}^{\frac{2\alpha_i}{\alpha_k}} \mathfrak{A}(\xi, \alpha_k)}, \end{aligned} \quad (5.19)$$

where  $\mathfrak{A}(\xi, \alpha_k) = \xi^{\frac{2}{\alpha_k}} \int_{\xi^{-\frac{2}{\alpha_k}}}^{+\infty} (1 + \mathbf{u}^{\frac{\alpha_k}{2}})^{-1} d\mathbf{u}$ . To obtain the probability of coverage averaging the whole plane in an open access interference-limited heterogeneous network is obtained by integrating with respect to  $\mathbf{d}_{\text{il}}$  (assume  $\alpha_i = \alpha_k = \alpha$ )

$$\begin{aligned} \bar{\mathbf{P}}_{\text{cov}} &= \int_0^{+\infty} \prod_{k=1}^K e^{-\lambda_k \pi \left(\frac{P_{\text{tk}}}{P_{\text{ti}}}\right)^{\frac{2}{\alpha}} d_{\text{il}}^2 \mathfrak{A}(\xi, \alpha)} f_{D_i}(\mathbf{d}_{\text{il}})(\alpha) d\mathbf{d}_{\text{il}}, \\ &= \left( 1 + \xi^{\frac{2}{\alpha}} \int_{\xi^{-\frac{2}{\alpha}}}^{+\infty} \frac{1}{1 + \mathbf{u}^{\frac{\alpha}{2}}} d\mathbf{u} \right)^{-1}, \end{aligned} \quad (5.20)$$

and the probability of outage averaging the whole plane is given by

$$\begin{aligned} \bar{\mathbf{P}}_{\text{out}} &= 1 - \bar{\mathbf{P}}_{\text{cov}}, \\ &= 1 - \left( 1 + \xi^{\frac{2}{\alpha}} \int_{\xi^{-\frac{2}{\alpha}}}^{+\infty} \frac{1}{1 + \mathbf{u}^{\frac{\alpha}{2}}} d\mathbf{u} \right)^{-1}. \end{aligned} \quad (5.21)$$

Not surprisingly, the probability of outage and coverage is not a function of the BS density, transmit power or the number of tiers in an open access heterogeneous cellular network.

### 5.2.2 Closed Access

In this subsection, expressions for metrics derived in the open access network will be provided for the closed access scenario, accordingly. The user can only be associated with a specific tier. The probability that the typical user is tagged in the specific  $i^{\text{th}}$ -tier is 1 and to an other tier is 0 by definition. It should be noted that the pdf of random variable  $D_i$  is the same as that for  $R_i$  in a closed access

## 5. HETEROGENEOUS NETWORK: CAPACITY, COVERAGE AND INTERFERENCE PERFORMANCE CHARACTERISATION

---

network. From Eq. (5.11), the mean achievable user data rate in the  $i^{\text{th}}$ -tier with closed access can be expressed as

$$\begin{aligned}
C_i^{\text{CA}} &= B_{\text{eff}} \int_0^{+\infty} \mathbb{E}_{\Gamma_i} \left[ \log_2 \left( 1 + \frac{\gamma_{\text{il}}}{\gamma_{\text{eff}}} \right) \right] f_{R_i}(\mathbf{d}_{\text{il}}) \, \mathbf{d}\mathbf{d}_{\text{il}}, \\
&= B_{\text{eff}} \int_0^{+\infty} \int_0^{+\infty} e^{-\beta_i \gamma_{\text{eff}} (2^\zeta - 1) \sigma^2 \mathbf{d}_{\text{il}}^{\alpha_i}} \prod_{k=1}^K e^{-\lambda_k \pi \left( \frac{P_{\text{tk}}}{P_{\text{ti}}} \right)^{\frac{2}{\alpha_k}} \mathbf{d}_{\text{il}}^{\frac{2\alpha_i}{\alpha_k}} \mathcal{B}(\zeta, \alpha_k)} \, \mathbf{d}\zeta \\
&\quad \cdot 2\lambda_i \pi \mathbf{d}_{\text{il}} e^{-\lambda_i \pi \mathbf{d}_{\text{il}}^2} \, \mathbf{d}\mathbf{d}_{\text{il}},
\end{aligned} \tag{5.22}$$

where  $\mathcal{B}(\zeta, \alpha_k)$  comes from the last two steps of Eq. (5.14) setting the lower limit of the integral to 0 since the interferer from the  $k^{\text{th}}$ -tier can be arbitrary close to the typical user and yielding

$$\begin{aligned}
\mathcal{B}(\zeta, \alpha_k) &= \int_0^{+\infty} \frac{[\gamma_{\text{eff}}(2^\zeta - 1)]^{\frac{2}{\alpha_k}}}{1 + \mathbf{u}^{\frac{\alpha_k}{2}}} \, \mathbf{d}\mathbf{u}, \\
&= \frac{2\pi [\gamma_{\text{eff}}(2^\zeta - 1)]^{\frac{2}{\alpha_k}}}{\alpha_k \sin\left(\frac{2\pi}{\alpha_k}\right)}.
\end{aligned} \tag{5.23}$$

For an interference-limited network, setting  $\sigma^2 = 0$  and all path loss exponent to  $\alpha$ ,  $C_i^{\text{CA}}$  can be further simplified as



5. HETEROGENEOUS NETWORK: CAPACITY, COVERAGE AND INTERFERENCE PERFORMANCE CHARACTERISATION

---

$$\begin{aligned}
C_i^{\text{CA}}(\alpha)|_{\sigma^2=0} &= 2\lambda_i\pi B_{\text{eff}} \int_0^{+\infty} d_{\text{il}} \int_0^{+\infty} \prod_{k=1}^K e^{-\lambda_k\pi\left(\frac{P_{\text{tk}}}{P_{\text{ti}}}\right)^{\frac{2}{\alpha}} d_{\text{il}}^2 \mathcal{B}(\zeta, \alpha)} e^{-\lambda_i\pi d_{\text{il}}^2} d\zeta dd_{\text{il}}, \\
&= 2\lambda_i\pi B_{\text{eff}} \int_0^{+\infty} \int_0^{+\infty} d_{\text{il}} \exp \left\{ -\pi d_{\text{il}}^2 \left[ \lambda_i + \sum_{k=1}^K \lambda_k \left( \frac{P_{\text{tk}}}{P_{\text{ti}}} \right)^{\frac{2}{\alpha}} \mathcal{B}(\zeta, \alpha) \right] \right\} d\zeta dd_{\text{il}}, \\
&= B_{\text{eff}} \int_0^{+\infty} \frac{\lambda_i}{\lambda_i + \sum_{k=1}^K \lambda_k \left( \frac{P_{\text{tk}}}{P_{\text{ti}}} \right)^{\frac{2}{\alpha}} \mathcal{B}(\zeta, \alpha)} d\zeta, \\
&= B_{\text{eff}} \int_0^{+\infty} \left[ 1 + \sum_{k=1}^K \frac{\lambda_k}{\lambda_i} \left( \frac{P_{\text{tk}}}{P_{\text{ti}}} \right)^{\frac{2}{\alpha}} \mathcal{B}(\zeta, \alpha) \right]^{-1} d\zeta.
\end{aligned} \tag{5.24}$$

For a special case when  $\alpha = 4$ , the mean achievable user data rate of the  $i^{\text{th}}$ -tier in a closed access LTE heterogeneous network can be computed as

$$\begin{aligned}
C_i^{\text{CA}}(4)|_{\sigma^2=0} &= B_{\text{eff}} \int_0^{+\infty} \left[ 1 + \sum_{k=1}^K \frac{\lambda_k}{\lambda_i} \sqrt{\frac{P_{\text{tk}}}{P_{\text{ti}}}} \mathcal{B}(\zeta, 4) \right]^{-1} d\zeta, \\
&= B_{\text{eff}} \int_0^{+\infty} \left[ 1 + \frac{\pi}{2} \sum_{k=1}^K \frac{\lambda_k}{\lambda_i} \sqrt{\frac{P_{\text{tk}}}{P_{\text{ti}}}} \gamma_{\text{eff}}(2\zeta - 1) \right]^{-1} d\zeta.
\end{aligned} \tag{5.25}$$

The last step of the expression involves an improper integral which can be computed to any specified precision by using the method of Gauss-Kronrod quadrature formula. It is also an intuitive result that the higher BS density and transmit power provide a higher mean achievable user data rate. Fig. 5.1 depicts the average spectral efficiency versus different FAP density to macro-cell BS density ratio in a two-tier interference-limited LTE heterogeneous network. The power of MBS to FAP is set to 400. The cross-over point occurs at the density ratio of around 20, which means the closed access network of any tier provides the same network performance in terms of the average data rate when the the number of FAPs is 20 times more than the number of MBSs.

Recall Eq. (5.21), the  $i^{\text{th}}$ -tier probability of outage averaging over the whole

## 5. HETEROGENEOUS NETWORK: CAPACITY, COVERAGE AND INTERFERENCE PERFORMANCE CHARACTERISATION

---

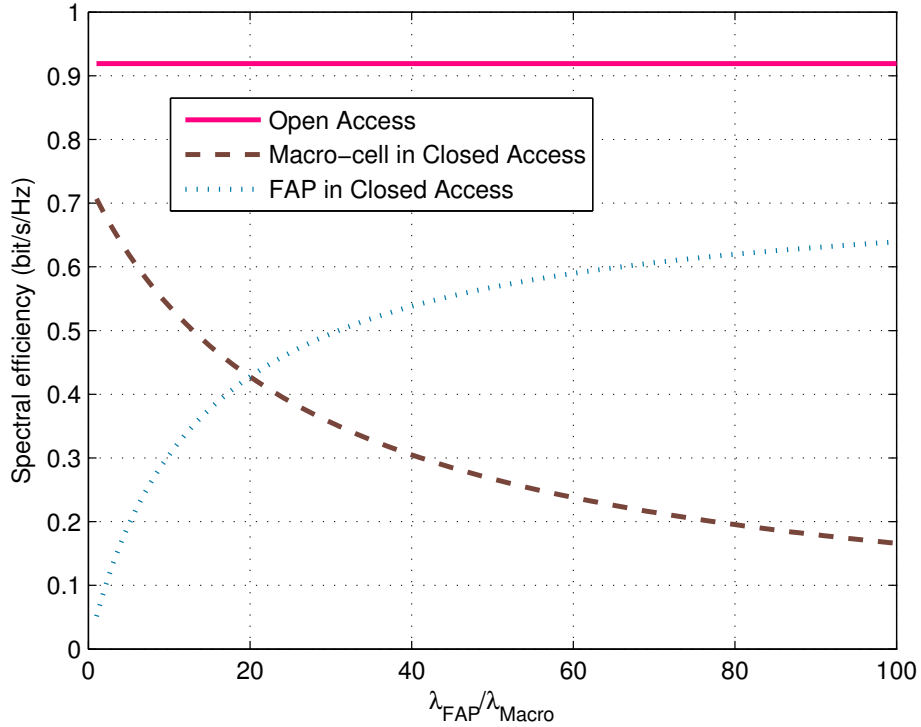


Figure 5.1: Average LTE spectral efficiency versus the ratio of FAP density to the macro-cell BS density comparison between open access and closed access policy in a two-tier interference-limited heterogeneous network

plane in an interference-limited heterogeneous network (assume  $\alpha_i = \alpha_k = \alpha$ ) can be achieved and yields

$$\begin{aligned} \bar{P}_{\text{out}}^{\text{CA}} &= 1 - \bar{P}_{\text{icov}}^{\text{CA}}, \\ &= 1 - \left( 1 + \frac{\pi}{2} \sum_{k=1}^K \frac{\lambda_k}{\lambda_i} \sqrt{\frac{P_{\text{tk}}}{P_{\text{ti}}}} \xi \right)^{-1}. \end{aligned} \quad (5.26)$$

Fig. 5.2 shows the probability of outage versus SNR threshold comparison between open access and closed access policy in a two-tier interference-limited heterogeneous network, with three different FAP to MBS density ratio. It is expected that the closed access model to gives pessimistic results compared to an open access

deployment due to the strong interference generated by nearby BS.

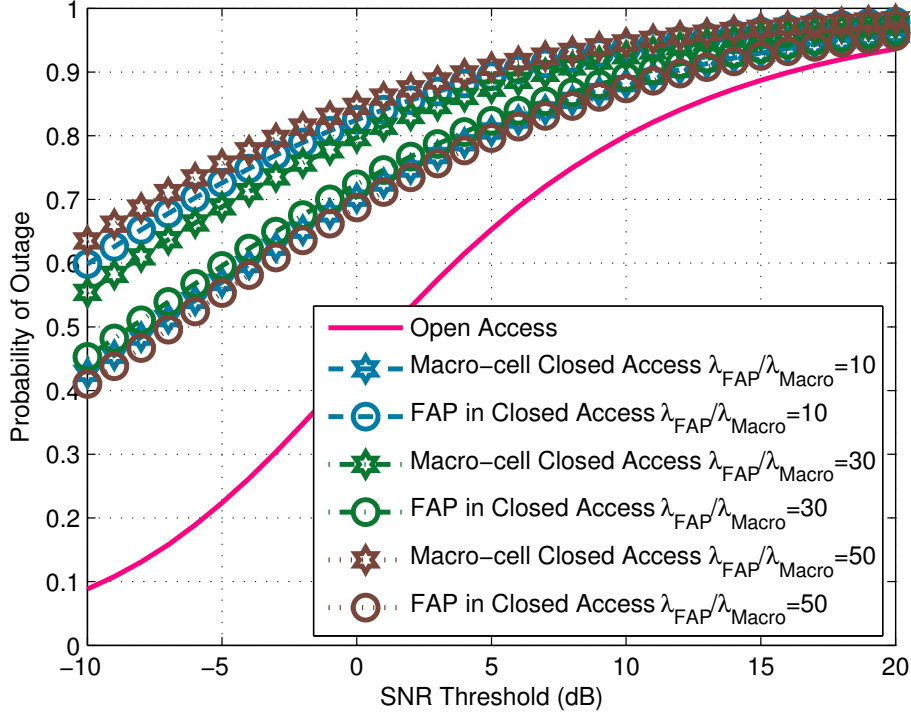


Figure 5.2: Probability of outage vs. SNR threshold comparison between open access and closed access policy in a two-tier interference-limited heterogeneous network, with FAP to MBS ratio 10, 30 and 50

### 5.2.3 Non-co-channel Deployment

In this sub-section, a brief discussion on the average user data rate and the probability of outage in non-co-channel deployment with open and closed access policy will be given. The term “non-co-channel” means there is no existence of inter-tier interference. The mean achievable user data rate of the  $i^{\text{th}}$ -tier network under open access policy is equivalent to the result of one-tier network under open access policy and therefore the mean achievable user data rate of a  $K$ -tier open access interference-limited network with the same path loss exponent is the same as Eq. (5.17). Moreover, the mean achievable user data rate of the  $i^{\text{th}}$ -tier network under closed access policy is equal to average spectral efficiency of any  $i^{\text{th}}$

network under closed access policy as Eq. (5.24). Thus the probability of outage in an open access network and the probability of outage in any  $i^{\text{th}}$ -tier closed network are identical to Eq. (5.21) and Eq. (5.26). That is to say, while using more radio resource in non-co-channel deployment, this scenario does not provide a more significant enhancement of the mean achievable user data rate nor does it offer a lower probability of outage as a whole.

### 5.3 Statistical Interference Model

Owing to the tractability of the above framework using SPPP, it provides a method to have a deeper look into the statistics of the aggregate interference. This section will take the aggregate interference in a  $K$ -tier closed access heterogeneous network as an example to demonstrate the concept of how to derive the statistics of such random variables through the moment generating function (MGF). Using the same notation  $I_{kj}$  of Eq.(5.1) to denote the aggregate interference received for a typical user. The MGF of the random variable  $\mathfrak{I}_{kj}$  is defined as follows

$$M_{\mathfrak{I}_{kj}}(\mathbf{s}) \triangleq \mathbb{E}(e^{sI_{kj}}) \quad (I_{kj} > 0). \quad (5.27)$$

Since the Laplace transform of a function  $f(t)$ , defined for all real numbers  $t \geq 0$ , is the function  $F(s)$ , defined by

$$F(s) \triangleq \mathcal{L}[f(t)](s) = \int_0^{+\infty} e^{-st} f(t) dt, \quad (5.28)$$

Eq. (5.27) evaluated at  $-s$  can be re-written as the Laplace transform of the pdf of  $\mathfrak{I}_{kj}$

5. HETEROGENEOUS NETWORK: CAPACITY, COVERAGE AND INTERFERENCE PERFORMANCE CHARACTERISATION

---

$$\begin{aligned}
M_{\mathfrak{I}_{kj}}(-s; \alpha_k) &= \mathcal{L}[f_{\mathfrak{I}_{kj}}(I_{kj})](I_{kj}), \\
&= \mathbb{E}(e^{-sI_{kj}}), \\
&= \mathbb{E}_{\Phi_k} \left\{ \mathbb{E}_{G_k} \left[ \exp \left( -s \sum_{k=1}^K \sum_{\substack{j \in \Phi_k \\ \setminus \text{BS}_i}} P_{tk} \text{PLC} h_{kj} d_{kj}^{-\alpha_k} \right) \right] \right\}, \\
&= \mathbb{E}_{\Phi_k} \left\{ \prod_{k=1}^K \prod_{\substack{j \in \Phi_k \\ \setminus \text{BS}_i}} \mathbb{E}_{G_k} \left[ \exp \left( -s g_{kj} d_{kj}^{-\alpha_k} \right) \right] \right\}, \\
&= \mathbb{E}_{\Phi_k} \left( \prod_{k=1}^K \prod_{\substack{j \in \Phi_k \\ \setminus \text{BS}_i}} \frac{\beta_k}{\beta_k + s d_{kj}^{-\alpha_k}} \right) \tag{5.29} \\
&= \prod_{k=1}^K \exp \left[ -2\pi \lambda_k \int_0^{+\infty} \left( 1 - \frac{\beta_k}{\beta_k + s v^{-\alpha_k}} \right) v \, dv \right], \\
&= \prod_{k=1}^K \exp \left[ -\pi \lambda_k \left( \frac{s}{\beta_k} \right)^{\frac{2}{\alpha_k}} \int_0^{+\infty} \frac{1}{1 + u^{\frac{\alpha_k}{2}}} \, du \right], \\
&= \prod_{k=1}^K \exp \left[ -\frac{2\pi^2 \lambda_k \csc \left( \frac{2\pi}{\alpha_k} \right)}{\alpha_k} \left( \frac{s}{\beta_k} \right)^{\frac{2}{\alpha_k}} \right].
\end{aligned}$$

Therefore, the pdf of  $\mathfrak{I}_{kj}$  is obtained by taking the inverse Laplace transform as

$$\begin{aligned}
f_{\mathfrak{I}_{kj}}(I_{kj}; \alpha_k) &= \mathcal{L}^{-1}[M_{\mathfrak{I}_{kj}}(-s)](I_{kj}), \\
&= \mathcal{L}^{-1} \left\{ \prod_{k=1}^K \exp \left[ -\frac{2\pi^2 \lambda_k \csc \left( \frac{2\pi}{\alpha_k} \right)}{\alpha_k} \left( \frac{s}{\beta_k} \right)^{\frac{2}{\alpha_k}} \right] \right\} (I_{kj}), \tag{5.30} \\
&= \left( \frac{\pi}{I_{kj}} \right)^{\frac{3}{2}} \sum_{k=1}^K \frac{\lambda_k \csc \left( \frac{2\pi}{\alpha_k} \right)}{\alpha_k \sqrt{\beta_k}} \exp \left[ -\frac{\pi^4}{I_{kj}} \sum_{k=1}^K \frac{\lambda_k^2 \csc^2 \left( \frac{2\pi}{\alpha_k} \right)}{\alpha_k^2 \beta_k} \right].
\end{aligned}$$

The CDF of  $\mathfrak{I}_{kj}$  is thus given by

5. HETEROGENEOUS NETWORK: CAPACITY, COVERAGE AND INTERFERENCE PERFORMANCE CHARACTERISATION

---

$$\begin{aligned}
F_{\mathfrak{I}_{kj}}(I_{kj}; \alpha_k) &= \int_0^{I_{kj}} f_{\mathfrak{I}_{kj}}(t; \alpha_k) dt, \\
&= \int_0^{I_{kj}} \left(\frac{\pi}{t}\right)^{\frac{3}{2}} \sum_{k=1}^K \frac{\lambda_k \csc\left(\frac{2\pi}{\alpha_k}\right)}{\alpha_k \sqrt{\beta_k}} \exp\left[-\frac{\pi^4}{t} \sum_{k=1}^K \frac{\lambda_k^2 \csc^2\left(\frac{2\pi}{\alpha_k}\right)}{\alpha_k^2 \beta_k}\right] dt \quad (5.31) \\
&= \operatorname{erfc}\left[\frac{\pi^2}{\sqrt{I_{kj}}} \sum_{k=1}^K \frac{\lambda_k \csc\left(\frac{2\pi}{\alpha_k}\right)}{\alpha_k \sqrt{\beta_k}}\right].
\end{aligned}$$

For a special case where all the path loss exponents are equals to 4, the pdf and CDF of the aggregate interference reduce to

$$f_{\mathfrak{I}_{kj}}(I_{kj}; 4) = \left(\frac{\pi}{I_{kj}}\right)^{\frac{3}{2}} \sum_{k=1}^K \frac{\lambda_k}{4\sqrt{\beta_k}} \exp\left[-\frac{\pi^4}{I_{kj}} \sum_{k=1}^K \frac{\lambda_k^2}{16\beta_k}\right], \quad (5.32)$$

$$F_{\mathfrak{I}_{kj}}(I_{kj}; 4) = \operatorname{erfc}\left[\frac{\pi^2}{\sqrt{I_{kj}}} \sum_{k=1}^K \frac{\lambda_k}{4\sqrt{\beta_k}}\right]. \quad (5.33)$$

The last metric of the statistical interference is the expected value of the aggregated interference received at the typical user end. Since the largest value of  $I_{kj}$  cannot be decided from the receiver, only the upper bounded expectation can be attained. From the first principal and Eq. (5.12), the upper bound of expectation where  $\alpha_k = 4$  should be defined as

$$\begin{aligned}
 \mathbb{E}(\mathfrak{I}_{kj})(z; 4) &\leq \lim_{I_{kj} \rightarrow z} \int_0^{I_{kj}} 1 - F_{\mathfrak{I}_{kj}}(\omega; 4) \, d\omega, \\
 &= \frac{\pi^{3/2}}{2} \sqrt{I_{kj}} \sum_{k=1}^K \frac{\lambda_k}{\sqrt{\beta_k}} \exp \left[ -\frac{\pi^4}{16 I_{kj}} \left( \sum_{k=1}^K \frac{\lambda_k}{\sqrt{\beta_k}} \right)^2 \right] \\
 &\quad - \frac{\pi^4}{8} \left( \sum_{k=1}^K \frac{\lambda_k}{\sqrt{\beta_k}} \right)^2 \operatorname{erfc} \left( \frac{\pi^2}{4 \sqrt{I_{kj}}} \sum_{k=1}^K \frac{\lambda_k}{\sqrt{\beta_k}} \right),
 \end{aligned} \tag{5.34}$$

where  $z$  is equal to the multiplication of the largest transmit power in the  $k^{\text{th}}$ -tier and  $-\alpha_k^{\text{th}}$  power of the distance which is the same as the cell height ( $z = P_{\text{tk}} d_{\text{Cell}}^{-\alpha_k}$ ). With this approach, the assumption of considering only one outdoor interferer made in Chapter 3 and Chapter 4 can be fully justified. The interference comes from the outdoor BSs only and thus  $z$  should be set to the transmit power of BS multiplied by  $500^{-4}$  and the closest interferer except for the strongest one considered is at least one cell radius (500 m) away. Fig. 5.3 illustrates the received interference power comparison between the closest MBS and all other BSs corresponding to different setting of MBS transmit power. It can be seen that the discrepancy between these two different interference powers is roughly at a ratio of  $1.4 \times 10^4$ . Therefore, it is reasonable to ignore the other interference effect in the study of interference avoidance and optimal deployment of indoor FAPs.

## 5.4 Conclusions

General models for the multi-cell SINR, average user data rate and interference statistics using stochastic geometry have been derived by incorporating the latest existence literature. Under the assumption of Rayleigh fading, the resulting expressions for the downlink SINR CDF (equivalent to the outage probability), the ergodic user data rate and the aggregate interference distribution involve quickly computable integrals, and in some practical special cases can be simplified to common integrals (e.g., error or complementary error function) or even to simple

## 5. HETEROGENEOUS NETWORK: CAPACITY, COVERAGE AND INTERFERENCE PERFORMANCE CHARACTERISATION

---

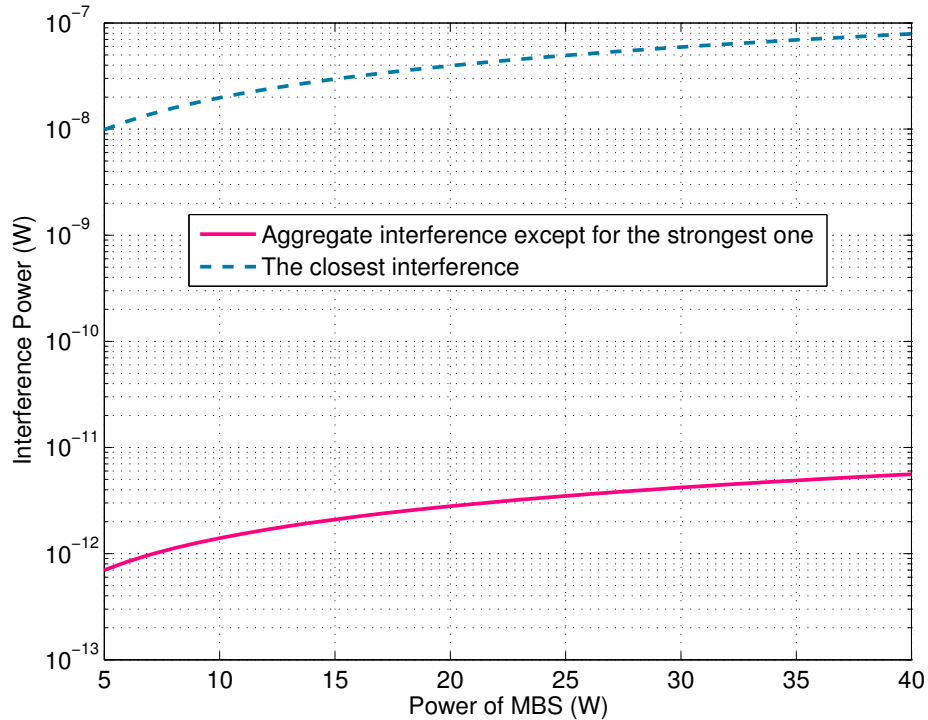


Figure 5.3: Interference power comparison between the strongest outdoor BS and all the remaining cells vs. different transmit power of BS

closed-form expressions. The SPPP model is as accurate as the traditional grid model and in addition to being more tractable, the SPPP model may better capture the increasingly opportunistic and ever-increasingly dense placement of BSs with variable cell radii in future LTE and LTE-Advanced networks.



## Chapter 6

# Energy Efficiency in Heterogeneous Network: Outdoor-Indoor Coordination

The first part of the study in this chapter will demonstrate that without any other interfaces, the mutual interference between indoor and outdoor networks significantly erodes the spectral efficiency of each other in a closed access heterogeneous network. The outdoor-indoor interference problem is then tackled by increasing the penetration loss of the outdoor-indoor wall boundary. The second part of the investigation considers the usage of a controllable interface that acts as a dynamic barrier between the outdoor and indoor networks to mitigate the interference. The interfaces comprise a frequency-selective-surface (FSS) which is a band-stop filter. This yielded significantly improved throughput and energy efficiency gains. However, effectively separating the outdoor and indoor networks means that they are unable to share radio resources during periods of asymmetric loading. In the event that an indoor FAP is overloaded and the outdoor MBS is under-loaded, it may prove beneficial to remove the FSS. In doing so, indoor users can be offloaded to the outdoor MBS (or vice versa), but mutual interference is increased. The trade-off between interference mitigation and outdoor-indoor resource sharing is analysed. The analysis is conducted by using both a theoretical stochastic geometry analysis derived in the previous chapter and multi-cell-multi-user simulation results, which serves to jointly address the long-standing problems of spectrum and energy efficiencies.

## 6.1 Introduction

The exponential growth in mobile data demand has a significant caveat. More than 70% of the mobile traffic is demanded by indoor users, where the coverage by outdoor cells is typically poor. This is primarily due to the fact that outdoor MBSs are planned to maximise outdoor coverage. Furthermore, the insufficient coverage for the MBSs leads to the appearance of indoor dead zones and the challenging indoor channel propagation environment makes accurate network planning difficult and expensive [16, 124, 125].

In order to accommodate for the rapid growth of indoor cellular traffic, mobile operators have proposed to deploy low-powered small cells such as FAPs, as an integrated indoor-outdoor solution for the ever increasing appetite of high data-rate wireless applications. The challenge in the two-tier network consisting of a MBS network underlaid with FAPs is how to mitigate the inter-tier interference, which hinders the indoor user communication, from the outdoor network, and vice versa. Existing proposals on centralised interference management are not feasible for the random deployed FAPs which are installed and controlled by the end users [95]. The work integrates the FSS with a two-tier closed access network to mitigate the inter-tier interference, and quantify the spectral efficiency and the transmission and deployment related energy savings. The FSS has been proposed as a method to reduce the power of a signal passing through it [126], typically for security and interference reduction purposes [127]. Their design is relatively straightforward, consisting of repeated manufactured patterns on a film that can be as thin as paper. When femtocells are configured as closed access, each FAP is only accessible by its own users. When they are configured as open access, a FAP could be accessed by both its users and all co-frequency macro-cell users. The remaining of this piece of work will only concern the closed access unless stated otherwise.

### 6.1.1 Related Work

In order to mitigate the mutual interference between cells, existing research has focused on coordinated transmission and scheduling techniques [73, 128]. The emphasis from network operators is that the coordinated solutions need to be

distributed and coordination needs to be localised to a small group of cells. Nonetheless, existing research on self-organising-networks (SONs) largely requires the exchange of instantaneous or statistical CSI between cells [129]. The exchange is largely conducted on the control interface between the concerned cells [130]. However, there is a lack of willingness for operators to implement control interfaces between outdoor and indoor cells due to complexity. Furthermore, the closed subscriber group (CSG) nature of many indoor cells increases the complexity of inter-cell coordination. In addition, the difficulty of mitigating the inter-tier interference has initiated research on different interference management schemes for two-tier networks, which encompasses multiple-antennas [131–133], power control [40,134,135], cognitive radio, [136,137], adaptive FAP access scheme [138–140] and spectrum allocation [141–144]. In terms of the intra-tier and inter-cell interference analysis, the performance of two-tier networks using stochastic geometry has been reviewed in the last chapter. It needs to be emphasised once again that the advantage of having the MBSs and FAPs modelled as an SPPP is that its throughput and outage performance is mathematically tractable yet accurate compared to the traditional distribution modelled by lattices or a hexagonal layout which is regular, well-planned and centralised.

### 6.1.2 Contributions

In this study, a tractable theoretical two-tier network framework with wall and FSS loss is presented. The body of investigation is conducted by extending a mathematically tractable SPPP framework of a two-tier network for closed access to include wall and FSS loss and the theoretical energy reduction gain. The throughput benefit of FSS on the outdoor-indoor cellular network, the potential transmission energy saving compared to the reference network without FSS deployment and the total energy efficiency compared to the reference network of deploying more non-co-channel indoor FAPs to improve the mean user throughput have been intensively examined by a multi-cell-multi-user simulator reinforced by the extended analytical and tractable framework provided by SPPP. The trade-off between outdoor interference to the indoor users and off-loading indoor traffic to outdoor MBS with the resulting total energy saving have been well balanced

and captured.

## 6.2 System Setup

### 6.2.1 Network Topology

The investigation considers two popular forms of cellular network topology, as shown in Fig. 6.1 and Fig. 6.2:

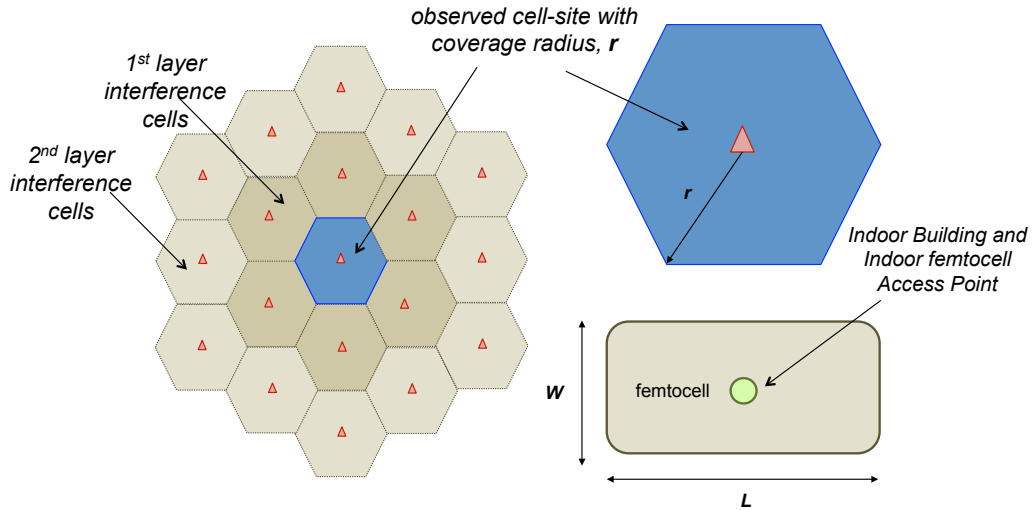


Figure 6.1: Network topology uniform hexagonal outdoor and indoor cell-site model

- **Uniform Cell Deployment:** the outdoor MBSs are deployed in a conventional hexagonal grid [145] and the indoor femtocells are deployed randomly within each outdoor cell. This is shown in Fig. 6.1. The rationale for the conventional uniform hexagonal deployment of outdoor cells is that its regular geometry offers the best network capacity performance and can be seen as an upper-bound.
- **Irregular Cell Deployment:** both the outdoor MBSs and the indoor FAPs follow an SPPP distribution with different intensities. This is shown in Fig. 6.2. Two different types of BSs are randomly placed on a 2-D Euclidean plane according to the aforementioned independent SPPs. The space is then fully tessellated following the maximum power connectivity

6. ENERGY EFFICIENCY IN HETEROGENEOUS NETWORK:  
OUTDOOR-INDOOR COORDINATION

---

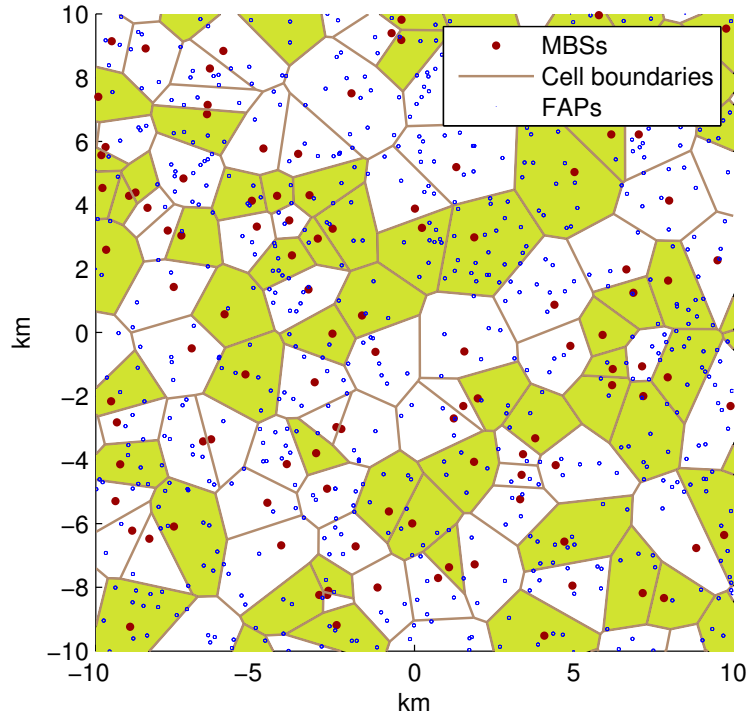


Figure 6.2: Network topology of non-uniform SPPP two-tier network model in an  $20 \text{ km} \times 20 \text{ km}$  area

model when fading is ignored. The rationale for the irregular random deployment is that in reality cell-site location is non-uniform and is based on site rental cost and the local propagation environment. While this SPPP model of a two-tier network may lead to a FAP being unacceptably close to a MBS, the results thus can be seen as a lower-bound of the network capacity.

For the uniform cell deployment, the performance statistics are taken from the central cell-site and two-tiers of cellular interference is considered to accurately reflect the interference-limited network performance [145]. Each cell has a coverage radius  $\mathbf{r}$  and an inter-cell-site distance of  $\sqrt{3}\mathbf{r}$  for one-sector MBSs. The indoor network is a single room with length  $\mathcal{L}$  and width  $\mathcal{W}$ , covered by a single femtocell in the middle of the room. For the irregular cell deployment, a single user is considered and a large sample of random cell distributions are considered

from an SPPP. The cell density is  $\lambda$ , which is inversely proportional to the square of the coverage radius:  $\lambda \propto \frac{1}{r^2}$ .

The system considered is still the LTE-OFDMA system. The standard deployment for LTE is to deploy all cells on the same frequency, which means that all cells in any tier are interfering with each other. The SPPP notations and the associated random variables are adopted from Section 5.2 in Chapter 5 by setting the number of tiers  $K = 2$ . In a realistic wireless system, the throughput is governed by the received channel quality, which determines the amount of data that can be decoded successfully at the receiver. For an increasing channel quality, the transmitter is able to transmit higher order modulation and coding schemes, achieving a greater throughput per radio resource. In terms of modelling, the spectral efficiency of the system is determined by either employing AMC schemes for simulation results in Table 2.1 and adjusted Shannon expression for theoretical framework (Eq. (5.22)), which is an upper-bound capacity performance function.

The study consider both mean and edge user throughput. The edge user throughput is defined as the minimum user throughput that 95% of the users can achieve. Both metrics are useful in the sense that often the mean yields an indication of how efficient the network resources are being utilised, whereas the ratio between edge and mean throughput indicates the fairness in QoS received [146]. The ratio in this thesis is defined as the **fairness index**.

### 6.2.2 Frequency-Selective-Surfaces

FSS technology is an RF technology and that the filtering is operating in the pass band. FSS is traditionally employed in radars and satellite communication antennas, but more recently, they have been applied to indoor environments to block certain carrier bands for security and interference reduction reasons.

A typical square-loop FSS design is shown in Fig. 6.3 along with the frequency response. Typically, a band-stop FSS will have the following key electro-magnetic characteristics that affect the system level performance:

- **Stop-Band:** The frequency band at which attenuation takes place when the FSS is in the active state. In our investigation, this is the 1.9–2.6 GHz band, which covers most of the LTE, 802.11n Wi-Fi and HSPA bands.

## 6. ENERGY EFFICIENCY IN HETEROGENEOUS NETWORK: OUTDOOR-INDOOR COORDINATION

---

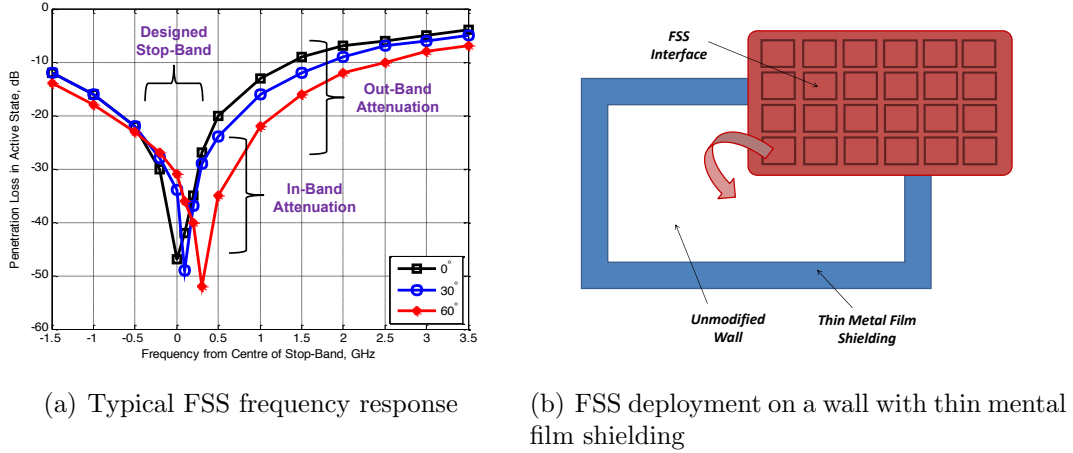


Figure 6.3: Typical frequency response and deployment of Frequency-Selective-Surface (FSS)

Typically it is difficult to make very narrow or very wide-band FSS due to the physical structure of the pattern.

- ***In-Band and Out-Band Attenuation***: The in-band attenuation is the amount of signal power attenuation achieved over the ***stop-band*** region. Typically a value of 25–50 dB can be achieved. The out-band attenuation is the amount of signal power attenuation achieved in other spectrum regions, which typically is 5–25 dB.
- ***Incidence Angle Tolerance***: The frequency response of the FSS typically varies with the incidence angle of the incoming signal. A tolerance of  $\pm 60^\circ$  is generally achievable.
- ***Insertion Loss***: There is generally an insertion loss inherent when deploying the FSS, which is the loss experienced when the FSS is in the off-state. When the FSS is in the off-state, it is transparent with typically 2–5 dB insertion loss. The off-state is also called the in-active state in this thesis. On the other hand, the on-state is therefore the active state which is used in the numerical results section.

The typical material costs of the FSS are very low.

Table 6.1: Modeling Parameters [37]

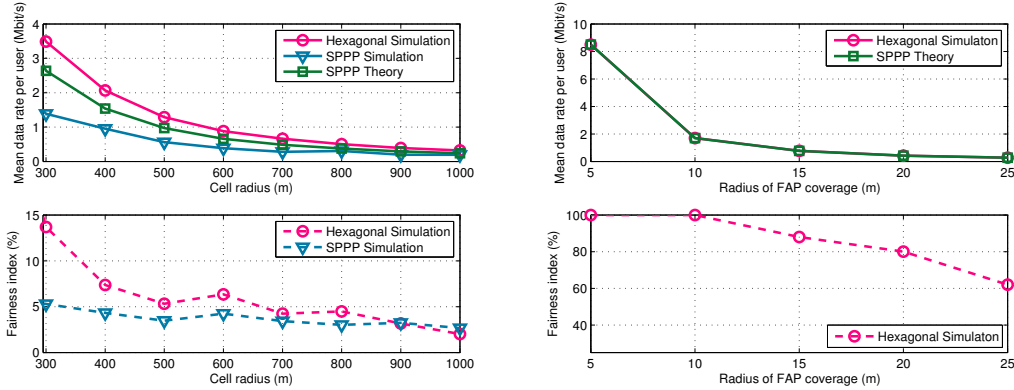
| Parameter                    | Symbol                 | Value                       |
|------------------------------|------------------------|-----------------------------|
| Operating frequency          | $f$                    | 2.13 MHz                    |
| Bandwidth for macro-cell     |                        | 20 MHz                      |
| Bandwidth for femtocell      |                        | 5 MHz                       |
| Macro-cell transmit power    | $P_{\text{MBS}}$       | 20 W, 40 W                  |
| Femtocell transmit power     | $P_{\text{FAP}}$       | 0.1 W                       |
| Femtocell over-head power    |                        | 5.2 W                       |
| Outdoor cell distribution    |                        | Uniform Hex. or SPPP        |
| Outdoor cell density         | $\lambda_{\text{MBS}}$ | 0.4–4 per km <sup>2</sup>   |
| Indoor femtocell density     | $\lambda_{\text{FAP}}$ | $10\lambda_{\text{MBS}}$    |
| Outdoor cell coverage radius | $\mathbf{r}$           | 300–1000 m                  |
| User distribution            |                        | SPPP and Uniform            |
| Outdoor user density         |                        | 30 per km <sup>2</sup>      |
| Indoor user density          |                        | 0.1 per m <sup>2</sup>      |
| Path loss exponent           | $\alpha$               | 4                           |
| AWGN power spectral density  | $N_0$                  | $4 \times 10^{-21}$ W/Hz    |
| Scheduler                    |                        | Round Robin                 |
| Adaptive modulation scheme   |                        | Look-up tables (Table. 2.1) |
| External wall loss           | $L_{\text{wall}}$      | 5 dB, 10 dB                 |
| FSS band-stop frequency      | $f_{\text{FSS}}$       | 1.9–2.7 GHz                 |
| FSS in-band attenuation      | $L_{\text{FSS}}$       | 20 dB                       |
| FSS insertion loss           |                        | 3–5 dB                      |

### 6.3 Baseline Performance of the Two-tier Closed-access Heterogeneous Network

The thesis now examines the baseline performance of a two-tier closed-access heterogeneous network without FSS. Conventionally, indoor cellular users are served by outdoor cells whose signal has to suffer the high penetration losses of building walls (typically 10 dB). The deployment of indoor femtocells significantly improves indoor capacity and alleviates the available radio resources for outdoor cells. However, the indoor cells cause additional interference to outdoor regions close to the indoor deployment location. The detailed simulation parameters can be found in Table 6.1.



## 6. ENERGY EFFICIENCY IN HETEROGENEOUS NETWORK: OUTDOOR-INDOOR COORDINATION



(a) Outdoor one-tier baseline results without indoor interference (b) Indoor one-tier baseline results without outdoor interference

Figure 6.4: Mean data rate per user and fairness index results for: 6.4(a) one-tier outdoor network, 6.4(b) one-tier indoor network.

### 6.3.1 Performance of Mean Data Rate per User in the One-Tier Network

The results in Fig. 6.4(a) and Fig. 6.4(b) show the performance of the isolated one-tier outdoor and one-tier indoor networks respectively. As the cell coverage decreases, each cell has proportionally fewer users, yielding a greater number of radio resources per user. Therefore, the mean throughput per user increases. The theoretical macro-cell spectral efficiency is 0.92 bit/s/Hz (using Eq. (5.18)) and the theoretical user throughput is obtained from the multiplication of the theoretical macro-cell spectral efficiency and the number of resource blocks per user. This performance can be regarded as an upper-bound to the two-tier network performance because by integrating the indoor and outdoor networks, the mutual interference will degrade their isolated performances.

The curves of mean user throughput in Fig. 6.4(a) exhibit the same basic shape and as one would expect that a regular hexagonal simulation provides an upper-bound result and the SPPP model simulation offers a lower-bound result. The SPPP theoretical results serves as a verification of the SPPP simulation results. The difference between the results of SPPP simulation and theory is due to the perfect Shannon's equation being applied to the analytical model while the adaptive modulation and coding scheme being used in the simulator. The

6. ENERGY EFFICIENCY IN HETEROGENEOUS NETWORK:  
OUTDOOR-INDOOR COORDINATION

---

results in Fig. 6.4(b) is obtained from one single room without any interference known as a noise limited network. The theoretical results for SINR higher than the maximum value (3.55 bit/s/Hz) in the look-up table (Table 2.1) of the MCS have been backed-off to the same level as that in the look-up table. The fairness index decreases as the number of users increases for both outdoor and indoor network.

### 6.3.2 Performance of Mean Data Rate per User in the Two-Tier Network without FSS

The results in Fig. 6.5(a) and Fig. 6.5(b) show the performance of the integrated two-tier closed access network. Whilst the trends are similar to those found in the isolated one-tier results, the performance has been degraded due to their mutual interference coupling. The theoretical macro-cell spectral efficiency reduces to 0.80 bit/s/Hz calculated using Eq. (6.1)

$$\begin{aligned}
 C_{\text{Macro}}^{\text{NoFSS}}(4)|_{\sigma^2=0} &= B_{\text{eff}} \int_0^{+\infty} \left[ 1 + \sum_{k=\text{Macro}}^{\text{FAP}} \frac{\lambda_k}{\lambda_{\text{Macro}}} \sqrt{\frac{P_{\text{tk}}}{P_{\text{tMacro}}}} \mathcal{A}(\zeta, 4) \right]^{-1} d\zeta, \\
 &= B_{\text{eff}} \int_0^{+\infty} \left[ 1 + \sum_{k=\text{Macro}}^{\text{FAP}} \frac{\lambda_k}{\lambda_{\text{Macro}}} \sqrt{\frac{P_{\text{tk}}}{P_{\text{tMacro}}}} \sqrt{\gamma_{\text{eff}}(2^\zeta - 1)} \arctan \sqrt{\gamma_{\text{eff}}(2^\zeta - 1)} \right]^{-1} d\zeta, \\
 &= 0.80 \text{ bit/s/Hz},
 \end{aligned} \tag{6.1}$$

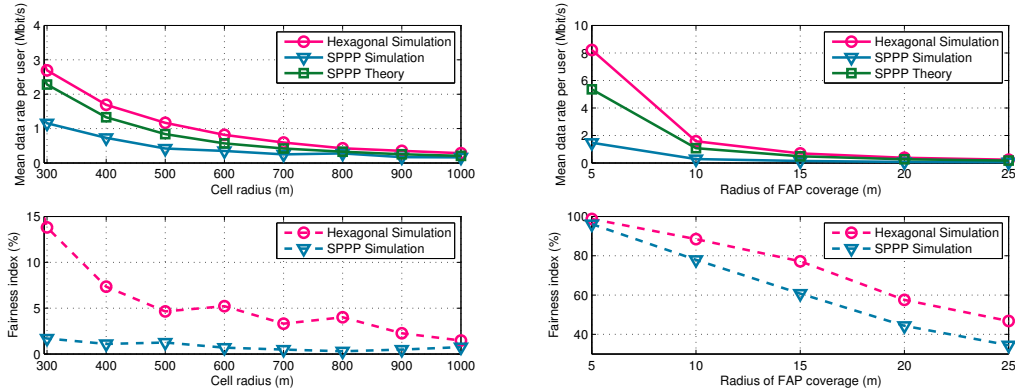
where the power ratio of MBS to FAP is set to  $200 \times 10^{\frac{L_{\text{wall}}}{10}}$ , and the theoretical FAP spectral efficiency is 2.15 bit/s/Hz computed using Eq. (5.25)

## 6. ENERGY EFFICIENCY IN HETEROGENEOUS NETWORK: OUTDOOR-INDOOR COORDINATION

---

$$\begin{aligned}
C_{\text{FAP}}^{\text{NoFSS}}(4)|_{\sigma^2=0} &= B_{\text{eff}} \int_0^{+\infty} \left[ 1 + \sum_{k=\text{Macro}}^{\text{FAP}} \frac{\lambda_k}{\lambda_{\text{FAP}}} \sqrt{\frac{P_{\text{tk}}}{P_{\text{tFAP}}}} \mathcal{A}(\Delta\zeta, 4) \right]^{-1} d\zeta, \\
&= B_{\text{eff}} \int_0^{+\infty} \left[ 1 + \sum_{k=\text{Macro}}^{\text{FAP}} \frac{\lambda_k}{\lambda_{\text{FAP}}} \sqrt{\frac{P_{\text{tk}}}{P_{\text{tFAP}}}} \sqrt{\gamma_{\text{eff}}(2^{\Delta\zeta} - 1)} \arctan \sqrt{\gamma_{\text{eff}}(2^{\Delta\zeta} - 1)} \right]^{-1} d\zeta, \\
&= 2.15 \text{ bit/s/Hz},
\end{aligned} \tag{6.2}$$

where the factor of  $\Delta = 10^{-\frac{2L_{\text{wall}}}{10}}$  is introduced for the compensation for the home FAP which has been affected by the adjusted wall loss in the SINR expression. The theoretical user throughputs are calculated in the same way as the one-tier scenario.



(a) Outdoor two-tier baseline results with indoor interference (b) Indoor two-tier baseline results with outdoor interference

Figure 6.5: Mean data rate per user and fairness index results for: 6.5(a) two-tier outdoor network, 6.5(b) two-tier indoor network.

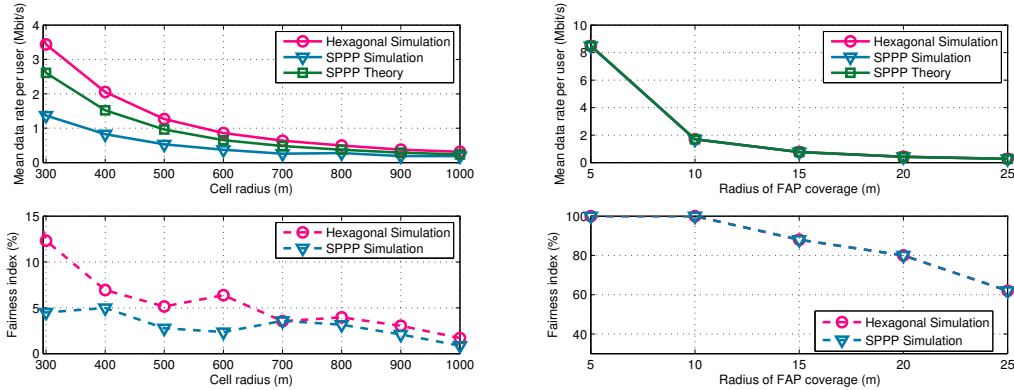
## 6.4 Integrated Performance with FSS

In this section, the similar sets of results will be illustrated while the FSS attenuation is switched on.

## 6. ENERGY EFFICIENCY IN HETEROGENEOUS NETWORK: OUTDOOR-INDOOR COORDINATION

### 6.4.1 Throughput Performance

The results in Fig. 6.6(a) and Fig. 6.6(b) show the performance of the integrated two-tier outdoor and two-tier indoor networks respectively. The theoretical macro-cell spectral efficiency reverts to 0.91 bit/s/Hz (using Eq. (6.1) and setting the power ratio of MBS to FAP to  $200 \times 10^{\frac{L_{\text{wall}} + L_{\text{FSS}}}{10}}$ ) gives theoretical FAP spectral efficiency of 7.54 bit/s/Hz (using Eq. (6.2) and setting  $\Delta = 10^{-\frac{2L_{\text{wall}} + L_{\text{FSS}}}{10}}$ ). The theoretical spectral efficiency for the indoor network is far too optimistic due to Shannon's Equation and is capped to the highest value (3.55 bit/s/Hz) that the adaptive modulation and coding scheme can provide for illustrational comparison. Whilst the trends are similar to those found in the results for the one tier network, the performance has returned to that of the isolated one-tier networks, which can be regarded as optimal. This is because the FSS has eliminated the mutual interference between the outdoor and indoor networks. The results exhibit that by deploying FSS interfaces, an improvement of up to 1.3 fold in mean throughput and 4.6 fold in throughput fairness for outdoor users is achieved while an enhancement of 1.2 fold in mean throughput and 2 fold in throughput fairness for indoor users can be obtained.



(a) Outdoor two-tier baseline results with outdoor interference and FSS (b) Indoor two-tier baseline results with outdoor interference and FSS

Figure 6.6: Mean data rate per user and fairness index results for: 6.6(a) outdoor network with FSS, 6.6(b) indoor network with FSS in a two-tier heterogeneous network

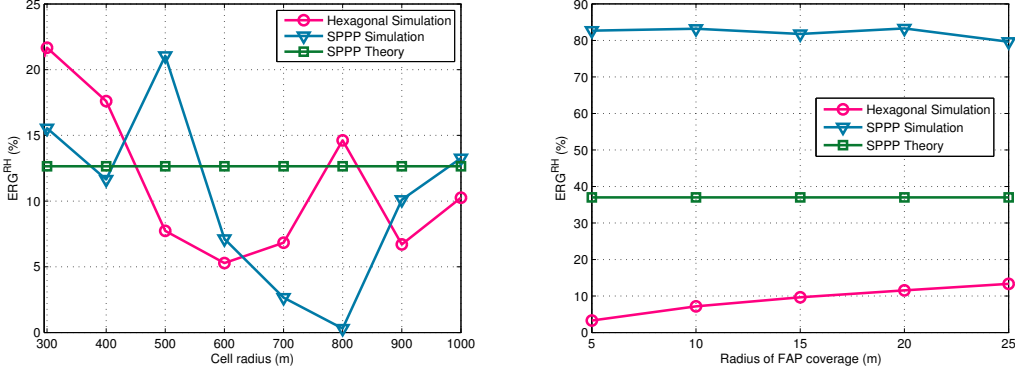
### 6.4.2 Energy Reduction Results

The radio-head  $ERG^{RH}$  results for both the outdoor two-tier network and the indoor two-tier network are illustrated in Fig. 6.7(a) and Fig. 6.7(b), respectively. The test network is the one aided by the FSS while the reference network is the one without the introduction of the FSS. All the results are obtained from Eq. (2.28). As the radio-head powers for the MBS and FAP remain unchanged, the  $ERG^{RH}$  is therefore proportional to the ratio of the network throughput in the test network to the throughput in the reference network. This ratio fluctuates in Fig. 6.7(a) as the cell radius varies in the simulation due to the different fading and shadowing experienced in each transmission time interval whereas the  $ERG^{RH}$  is fixed for SPPP theoretical model since the spectral efficiency is independent of the intensity. It can be noted from Fig. 6.7(a) that the  $ERG^{RH}$  is 12.5% for the theoretical model and the simulation results provide an average  $ERG^{RH}$  of 10% and up to 22% for the outdoor network.

For the indoor network, Fig. 6.7(b) shows that the  $ERG^{RH}$  is 37% and 82% for the theoretical and simulated SPPP models, respectively. The hexagonal simulation results offer an average  $ERG^{RH}$  of 9% and up to 13%. The radio-head ERG results for simulated and theoretical SPPP are much greater than the results for an hexagonal model. This is because the throughput in the test network is almost same for the both hexagonal and SPPP models illustrated in Fig. 6.6(b) while the throughput in the reference network for SPPP is a lower-bound and for hexagonal layout is an upper-bound shown in Fig. 6.5(b). For the same test network, the lower-bound of mean throughput in reference network leads to an upper-bound in energy saving and the upper-bound of mean throughput in reference network results in a lower-bound in energy saving. The operational ERG is not studied in this section as the number of MBSs or FAPs does not change during this evaluation and thus there would not be too much gain in  $ERG^{OP}$  which is basically determined by the over-head power of base stations.

## 6. ENERGY EFFICIENCY IN HETEROGENEOUS NETWORK: OUTDOOR-INDOOR COORDINATION

---



(a) Outdoor two-tier ERG<sup>RH</sup> results with indoor interference (b) Indoor two-tier ERG<sup>RH</sup> results with outdoor interference

Figure 6.7: ERG<sup>RH</sup> comparison between the baseline without FSS and the test network with FSS: 6.7(a) Outdoor two-tier ERG<sup>RH</sup> results with indoor interference] and 6.7(b) Indoor two-tier ERG<sup>RH</sup> results with outdoor interference

### 6.5 Offloading Indoor Users to Outdoor Macro-cell Base Station

The study has covered the evaluation of system throughput and the ERG<sup>RH</sup> in the case when the FSS is active for both outdoor and indoor users. It has been shown that the FSS effectively shields the mutual interference for all the users. In this section, the investigation of the ERG<sup>OP</sup> performance for the indoor two-tier network is presented for the case when the FSS is inactive due to the demand of serving more indoor users which will be offloaded to the available resource blocks provided by the MBS. By switching off the FSS, the indoor system performance will incur a considerable degradation and thus can serve fewer users for a targeted mean user data rate. The subsequent section will illustrate how much traffic needs to be offloaded to the outdoor MBS and how large a percentage of the demanded resource blocks are taken in the total available number of resource blocks. The ERG<sup>OP</sup> performance will be evaluated in comparison between the baseline scenario in which more non-co-frequency FAPs will be deployed (up to 4) when the FSS remains active and the proposed scenario in which an unsupported number of indoor users will be offloaded to the nearest MBS while keeping the

targeted mean user data rate unchanged when the FSS is inactive. The trade-off of this proposed soft FSS switching between interference mitigation and open access to the outdoor MBS for indoor users is also investigated.

### 6.5.1 Hexagonal Model

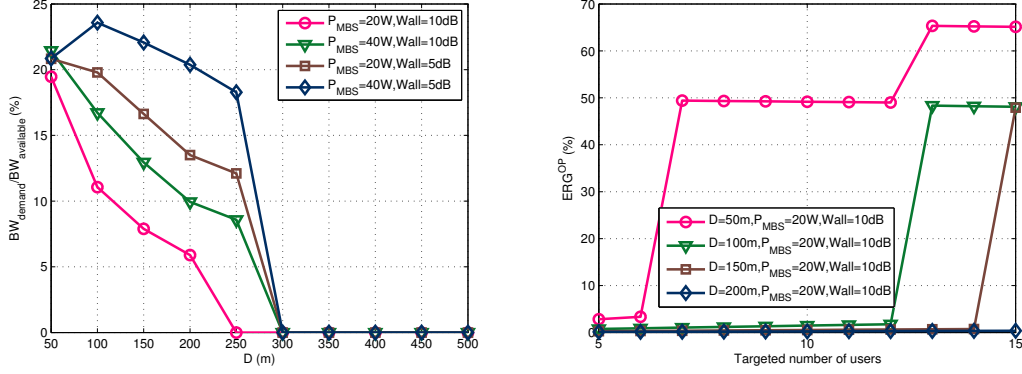
Fig. 6.8(a) shows that the required percentage of resource blocks needed from the MBS is up to 25% for different configuration of MBS transmit power and external wall loss (shown as Wall in the legend on the plots). It can also be seen that there is no need to offload any indoor users when the distance  $D$  from the MBS to the FAP is greater than or equal to 300 m when the indoor network turns into a noise limited network due to not much interference caused from the MBSs. The four curves roughly exhibit the same trend that the percentage reduces as  $D$  increases (i.e. the effect of mutual interference diminishes).

The operational ERG versus number of indoor users is depicted in Fig. 6.8(b). In an interference limited scenario when  $D$  is not greater than 200 m, an ERG of up to 65% can be achieved compared with placing more indoor FAPs. There is almost no operational ERG in a noise limited scenario when  $D$  is greater than 200 m as the over-head power dominates the ERG performance though a radio-head ERG is obtained. Due to this power characteristic, a huge operational ERG can only be expected by means of reducing the number of deployed FAPs. This is to say, by deploying more FAPs, the  $\text{ERG}^{\text{OP}}$  will experience a substantial jump from the previous point.

### 6.5.2 SPPP Model

In Fig. 6.9(a), the horizontal black line without any markers indicates the FSS switching point. It represents the most number of resource blocks that the outside MBS can offer. The required percentage of resource blocks, plotted with markers on the four other curves below the switching point line, can be potentially met. The dynamic FSS should always be active (on-state) when the curves exceed the switching point line corresponding to the scenario in which the outdoor MBS is incapable of supporting the number of resource blocks that the FAP needs. As mentioned previously, the throughput result of the SPPP model can be regarded

## 6. ENERGY EFFICIENCY IN HETEROGENEOUS NETWORK: OUTDOOR-INDOOR COORDINATION



(a) Required percentage of resource blocks from MBS versus the distance from the MBS indoor users to the FAP (b) ERG<sup>OP</sup> results versus targeted number of

Figure 6.8: Required percentage of resource blocks from MBS versus the distance from the MBS to the FAP and ERG<sup>OP</sup> results versus targeted number of indoor users in hexagonal model

as a lower bound since the base stations will in some cases be located very close together. Based on this lower bound throughput, more resource from the outside MBS may be required, hence the percentage can be seen as an upper bound which on average is around 80%. The actual deployment of the two-tier network will require some percentage between this upper bound and the lower bound of 25% obtained from the regular hexagonal model.

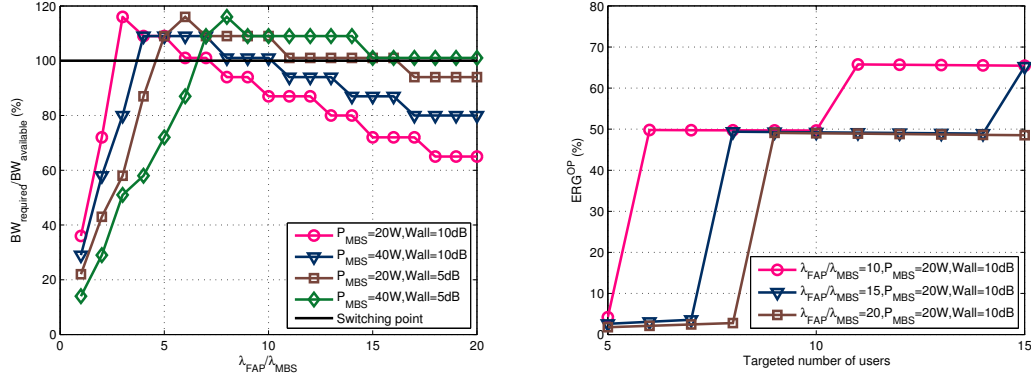
The operational ERG versus the targeted number of indoor users is depicted in Fig. 6.9(b). An ERG of up to 65% is achieved compared with deploying more indoor FAPs. All curves exhibit a similar trend to those in the hexagonal model shown in Fig. 6.8(b). The difference arises because the SPPP approach offers an upper bound on the ERG performance as it can be seen that for a given targeted number of users, the required number of extra FAPs is always never less than that for the hexagonal model.

## 6.6 Conclusions

This chapter has attempted to address the long-standing problems of jointly optimising spectrum and energy efficiencies for a radio access network. A novel



## 6. ENERGY EFFICIENCY IN HETEROGENEOUS NETWORK: OUTDOOR-INDOOR COORDINATION



(a) Required percentage of resource blocks from MBS versus the ratio of FAP intensity indoor users to MBS intensity (b)  $ERG^{OP}$  results versus targeted number of indoor users in SPPP model

Figure 6.9: Required percentage of resource blocks from MBS versus the ratio of FAP intensity to MBS intensity and  $ERG^{OP}$  results versus targeted number of indoor users in SPPP model

approach of balancing interference mitigation and off-loading users using a controllable interface comprising of a FSS, which acts as a dynamic signal barrier between the outdoor and indoor networks has been investigated. The theoretical and matching simulation results have demonstrated that without any FSS interfaces, the mutual interference between indoor and outdoor networks erodes the capacity of each other significantly. An improvement of up to 1.3 fold in mean throughput, 4.6 fold in fairness index for outdoor users and 1.2 fold in mean throughput, 2 fold in fairness index for indoor users can be achieved. It has also shown that when some of the indoor traffic was off-loaded to the outdoor network by switching off the FSS interface to maintain the QoS of the remaining indoor users compared with the reference scenario of deploying more indoor femtocells in the traditional way, the indoor operational energy reduction gain can range from no gain for the noise limited network and up to 65% in cases where outdoor interference is the limiting factor for indoor users.

# Chapter 7

## Conclusions and Future Work

### 7.1 Conclusions

The thesis has investigated the capacity and energy performance for Wi-Fi technology and mobile cellular heterogeneous network consisting of outdoor macro-cell basestations (BSs) and indoor home (femtocell access points) FAPs. It has addressed the question of whether home FAPs or Wi-Fi APs are more energy- and spectral-efficient for a given quality-of-service (QoS). The thesis then presented novel approaches to further reduce the energy consumption by providing a higher network capacity or deploying less access points with the aid of interference avoidance and dynamic optimal placement algorithms. Throughout the analysis, a co-channel LTE multi-user and multi-cell simulator has been developed to evaluate the system-level performance of the Orthogonal Frequency Division Multiple Access (OFDMA) based cellular networks. Aside from that, an extension of the emerging abstraction model for cellular heterogeneous networks has also been provided to reinforce the simulation results or simply produce certain results that require considerable simulation effort before. Finally, the analysis of a trade-off between an interference mitigation technique for indoor home network and outdoor-indoor resource sharing has been explored and the optimal solution has been provided for different settings of the network.

Based on the analyses and results presented throughout this thesis, the detailed descriptions of contributions are illustrated below in different themes.

### 7.1.1 Wi-Fi or Femtocells

This body of investigation has examined the relative merits of LTE and 802.11n Wi-Fi radio access technologies (RATs), in order to establish a baseline system-level performance. It was found that LTE-femtocells best suit small home networks, providing a high level of spectral- and energy-efficiency. Results indicate that one FAP is always more energy efficient than one 802.11n AP for both Single Input, Single Output (SISO) and Multiple Input, Multiple Output (MIMO) antenna configurations irrespective of whether there is outdoor interference or not. However, the bandwidth availability of 802.11n allows greater system-level throughput to be achieved for multi-AP networks, suitable for enterprises. A simulated novel trade-off between capacity and energy consumption has been presented for indoor networks, which serves as a useful guidance for deployment. It can be concluded that deploying one FAP is always more spectral and energy efficient than one 802.11n Wi-Fi AP (saves 4.44% operational energy); Deploying up to 3 multiple 802.11n APs is always more energy efficient (21.80% operational energy saving) than deploying multiple FAPs within the same room in conventional scenario.

### 7.1.2 Interference Avoidance

This study has applied an alternative form of hard frequency reuse method to an indoor LTE-Femtocell network, which mitigates the effects of interference through a sequential game play between FAPs in the E-UTRAN based on the offered load presented to the individual FAP. The results have shown that up to 12% in radio-head energy and 3% in operational energy can be saved by consuming less than half the radio-head power while maintaining the user offered load unchanged. Since the operational energy saving directly links to the number of FAPs deployed, the current 3% saving without reducing the number of FAPs is good enough considering there will be more and more small cells deployed in the next 5 years.

### 7.1.3 Optimal Indoor FAPs Deployment

Given the large number of propagation variables in indoor buildings and its relation to the outdoor cellular network, this work has provided a best practice in optimising FAP deployment with very little Signal to Interference-plus-Noise Ratio (SINR) degradation for outdoor users. In the first part of this investigation, this thesis has optimised one indoor FAP position with the aim of achieving the highest mean network throughput in the presence of co-channel interference from a dominant source (either a micro-cell or a FAP in an adjacent room). In contrast with previous research, the analytical approach is corroborated by means of a Monte Carlo simulation which encapsulates sub-carrier level interference and user mobility modelling. The novel contribution is the simulation results and the proposed theoretical framework that reinforces the key deployment solutions. Moreover, for a given building size, the trade-off between increased user QoS and power consumption, as well as the capacity saturation points are demonstrated in the second part of the study. Finally, it is shown by simulation that the key results hold for a generic building with multiple rooms on multiple floors with an outdoor interference source. The combined results of the three scenarios have lead to a general low energy indoor deployment rule.

The key conclusions besides those given in the study of Wi-Fi or Femtoecells are as follows:

- For buildings with more than one room, no FAPs should be deployed in the same room of a building;
- In the presence of a strong outdoor interference source (i.e., from a micro-cell), the location of some of the co-frequency FAPs, should be placed near the wall nearest the outdoor interference source to counter-act the high level of indoor interference.

The energy reductions for several key comparisons are as follows:

- Optimising placement of a single FAP in a single room saves 5% operational energy;
- Optimising placement of multiple FAPs in a multi-room building saves average 12% operational energy.

In general, improving the location of the FAPs, whilst keeping their number the

same can improve the RAN throughput by 33%. Whilst, improving the location of the FAPs and reducing the number of FAPs can save 40% operational energy.

### 7.1.4 Extending Analytical Heterogeneous Network Model with Stochastic Geometry

In this theoretical framework, a tractable model for the multi-cell SINR, average user data rate and interference statistics using stochastic geometry have been derived by incorporating the latest literature. Under the assumption of Rayleigh fading, the resulting expressions for the downlink SINR Cumulative Distribution Function (CDF) (equivalent to the outage probability), the ergodic user data rate and the aggregate interference distribution involve quickly computable integrals, and in some practical special cases can be simplified to common integrals (e.g., error or complementary error function) or even to simple closed-form expressions. This fundamental portfolio has provided an approach of double verification for future simulation generated results. It should be noted that the result of the statistics of aggregate interference has made it possible to analytically justify the reason why only one dominant outdoor interference considered in the previous chapter is sufficient from a certain distance between the interference and the observed indoor FAP.

### 7.1.5 Interference Mitigation via FSS and Indoor-outdoor Interactions Evaluation

In the final work of this thesis, it has first demonstrated that without any other interfaces, the mutual interference between indoor and outdoor networks erodes significantly the spectral efficiency of each other in a closed access heterogeneous network. The outdoor-indoor interference problem is then tackled by increasing the penetration loss of the outdoor-indoor wall boundary via the usage of a controllable interface, namely, a frequency-selective-surface (FSS). This yielded significantly improved mean throughput (1.3 fold for outdoor users and 1.2 fold for indoor users) and energy efficiency gains. However, effectively separating the

outdoor and indoor networks means that they are unable to share radio resources during periods of asymmetric loading. In the event that an indoor FAP is overloaded and the outdoor MBS is under-loaded, it has been proved that indoor users can be offloaded to the outdoor MBS (or vice versa) to achieve a higher network capacity as a whole although mutual interference is increased. The trade-off between interference mitigation and outdoor-indoor resource sharing has been analysed. The study jointly addressed the long-standing problems of spectrum and energy efficiencies. It has shown that by switching off the FSS interface to maintain the QoS of the remaining indoor users compared with the reference scenario of deploying more indoor femtocells in the traditional way, the indoor operational energy reduction gain can range from no gain for the noise limited network and up to 65% for the interference-limited network, respectively.

## 7.2 Future Works

One of the most interesting extension of this thesis is to see the performance from integrated solution that combines the approaches of interference avoidance, optimal placement and the dynamic control of FSS and switch-over between indoor and outdoor interaction. In addition to that, there are some other techniques worth exploring to gain a much wider insight on the topic of energy efficient networks.

### 7.2.1 Traffic Aware and QoS Constrained Sleep Mode Mechanisms

This investigation can evaluate the potential operational cost and energy savings that can arise from implementing a sleep mode mechanism. Two questions need to be considered before a sleep signal can be triggered. First, if a cell is switched off (sleep), what is the new coverage and capacity pattern of the network? Second, when does a cell decide to sleep or stay active? The theoretical framework devised in this thesis can help to derive the network coverage as a function of a certain sleep mode threshold in a realistic network. By using an empirical traffic load

and achievable capacity formula, the associated energy-cost consumption model can also be attained. The objective of the proposed work is to maximise the energy savings, whilst satisfying the performance both in terms of the achievable throughput and user coverage.

### 7.2.2 Migration to Extremely High Frequencies

There is debate regarding whether increasing the transmission frequency to the high GHz micro-wave spectrum will be beneficial in terms of energy consumption. The benefits include a significantly greater availability of unlicensed spectrum (up to 40 fold). However, the concern is that the propagation characteristics at high frequencies will limit the wireless application to very short ranges (personal space). The study can show how high in frequency the current cellular network and Wi-Fi outdoor network can migrate up to, respectively. The potential benefit of this analysis is that knowledge of the governing trade-offs allows the radio planner to better understand the relative spectral and energy benefits and pitfalls of migrating to higher transmission frequencies.

### 7.2.3 D2D Communications

The challenge of reliably communicating data from one device to another has been the underpinning motivation for communications research. There is a strong business case for growth of the wireless capacity to match the ever increasing data demand. Given the proliferation of cellular communication devices, it makes sense to consider new protocols within the framework of a cellular network or at least in co-existence to reduce the burden of current BSs both in delivering information bits and excessive power consumption. Device-to-device (D2D) communication is one of the best candidates to fulfil the commitment. The proposed work can devise a dynamic algorithm that optimally selects the transmission band and D2D routing path strategy based on the conventional cellular outage constraint using a combination of Monte-Carlo simulations and stochastic geometry. The expected interference from regular cellular users and other D2D transmissions and the overall routing distance will be of importance. The algorithm could be

## *7. CONCLUSIONS AND FUTURE WORK*

---

used to estimate the expected outage probability of the D2D channel and the impact it has on conventional cellular channels. The benefit of this algorithm is that a serving BS is able to make decisions that balance the performance of both regular cellular users and D2D users to achieve a desired energy savings.



# Appendix A

## Appendix

### A.1 Copyright permissions

The permission for reusing the published works in both print and electronic versions of this thesis have been duly acquired from the publishers and attached herein.



**Title:** Energy Efficiency Evaluation of SISO and MIMO between LTE-Femtocells and 802.11n Networks

Logged in as:  
Siyi Wang

LOGOUT

**Conference Proceedings:** Energy Efficiency Evaluation of SISO and MIMO between LTE-Femtocells and 802.11n Networks

**Author:** Siyi Wang; Weisi Guo; O'Farrell, T.

**Publisher:** IEEE

**Date:** 6-9 May 2012

Copyright © 2012, IEEE

## Thesis / Dissertation Reuse

**The IEEE does not require individuals working on a thesis to obtain a formal reuse license, however, you may print out this statement to be used as a permission grant:**

*Requirements to be followed when using any portion (e.g., figure, graph, table, or textual material) of an IEEE copyrighted paper in a thesis:*

- 1) In the case of textual material (e.g., using short quotes or referring to the work within these papers) users must give full credit to the original source (author, paper, publication) followed by the IEEE copyright line © 2011 IEEE.
- 2) In the case of illustrations or tabular material, we require that the copyright line © [Year of original publication] IEEE appear prominently with each reprinted figure and/or table.
- 3) If a substantial portion of the original paper is to be used, and if you are not the senior author, also obtain the senior author's approval.

*Requirements to be followed when using an entire IEEE copyrighted paper in a thesis:*

- 1) The following IEEE copyright/ credit notice should be placed prominently in the references: © [year of original publication] IEEE. Reprinted, with permission, from [author names, paper title, IEEE publication title, and month/year of publication]
- 2) Only the accepted version of an IEEE copyrighted paper can be used when posting the paper or your thesis on-line.
- 3) In placing the thesis on the author's university website, please display the following message in a prominent place on the website: In reference to IEEE copyrighted material which is used with permission in this thesis, the IEEE does not endorse any of [university/educational entity's name goes here]'s products or services. Internal or personal use of this material is permitted. If interested in reprinting/republishing IEEE copyrighted material for advertising or promotional purposes or for creating new collective works for resale or redistribution, please go to [http://www.ieee.org/publications\\_standards/publications/rights/rights\\_link.html](http://www.ieee.org/publications_standards/publications/rights/rights_link.html) to learn how to obtain a License from RightsLink.

If applicable, University Microfilms and/or ProQuest Library, or the Archives of Canada may supply single copies of the dissertation.

BACK

CLOSE WINDOW



**Title:** Energy Efficiency and Spectral Efficiency Trade-Off of a Novel Interference Avoidance Approach for LTE-Femtocell Networks

Logged in as:  
Siyi Wang

LOGOUT

**Conference Proceedings:** Energy Efficiency and Spectral Efficiency Trade-Off of a Novel Interference Avoidance Approach for LTE-Femtocell Networks

**Author:** Siyi Wang; Turyagyenda, C.; O'Farrell, T.

**Publisher:** IEEE

**Date:** 6-9 May 2012

Copyright © 2012, IEEE

## Thesis / Dissertation Reuse

**The IEEE does not require individuals working on a thesis to obtain a formal reuse license, however, you may print out this statement to be used as a permission grant:**

*Requirements to be followed when using any portion (e.g., figure, graph, table, or textual material) of an IEEE copyrighted paper in a thesis:*

- 1) In the case of textual material (e.g., using short quotes or referring to the work within these papers) users must give full credit to the original source (author, paper, publication) followed by the IEEE copyright line © 2011 IEEE.
- 2) In the case of illustrations or tabular material, we require that the copyright line © [Year of original publication] IEEE appear prominently with each reprinted figure and/or table.
- 3) If a substantial portion of the original paper is to be used, and if you are not the senior author, also obtain the senior author's approval.

*Requirements to be followed when using an entire IEEE copyrighted paper in a thesis:*

- 1) The following IEEE copyright/ credit notice should be placed prominently in the references: © [year of original publication] IEEE. Reprinted, with permission, from [author names, paper title, IEEE publication title, and month/year of publication]
- 2) Only the accepted version of an IEEE copyrighted paper can be used when posting the paper or your thesis on-line.
- 3) In placing the thesis on the author's university website, please display the following message in a prominent place on the website: In reference to IEEE copyrighted material which is used with permission in this thesis, the IEEE does not endorse any of [university/educational entity's name goes here]'s products or services. Internal or personal use of this material is permitted. If interested in reprinting/republishing IEEE copyrighted material for advertising or promotional purposes or for creating new collective works for resale or redistribution, please go to [http://www.ieee.org/publications\\_standards/publications/rights/rights\\_link.html](http://www.ieee.org/publications_standards/publications/rights/rights_link.html) to learn how to obtain a License from RightsLink.

If applicable, University Microfilms and/or ProQuest Library, or the Archives of Canada may supply single copies of the dissertation.

BACK

CLOSE WINDOW



**Title:** Optimising Femtocell Placement in an Interference Limited Network: Theory and Simulation

Logged in as:  
Siyi Wang

LOGOUT

**Conference Proceedings:** Optimising Femtocell Placement in an Interference Limited Network: Theory and Simulation

**Author:** Siyi Wang; Weisi Guo; O'Farrell, T.

**Publisher:** IEEE

**Date:** 3-6 Sept. 2012

Copyright © 2012, IEEE

## Thesis / Dissertation Reuse

**The IEEE does not require individuals working on a thesis to obtain a formal reuse license, however, you may print out this statement to be used as a permission grant:**

*Requirements to be followed when using any portion (e.g., figure, graph, table, or textual material) of an IEEE copyrighted paper in a thesis:*

- 1) In the case of textual material (e.g., using short quotes or referring to the work within these papers) users must give full credit to the original source (author, paper, publication) followed by the IEEE copyright line © 2011 IEEE.
- 2) In the case of illustrations or tabular material, we require that the copyright line © [Year of original publication] IEEE appear prominently with each reprinted figure and/or table.
- 3) If a substantial portion of the original paper is to be used, and if you are not the senior author, also obtain the senior author's approval.

*Requirements to be followed when using an entire IEEE copyrighted paper in a thesis:*

- 1) The following IEEE copyright/ credit notice should be placed prominently in the references: © [year of original publication] IEEE. Reprinted, with permission, from [author names, paper title, IEEE publication title, and month/year of publication]
- 2) Only the accepted version of an IEEE copyrighted paper can be used when posting the paper or your thesis on-line.
- 3) In placing the thesis on the author's university website, please display the following message in a prominent place on the website: In reference to IEEE copyrighted material which is used with permission in this thesis, the IEEE does not endorse any of [university/educational entity's name goes here]'s products or services. Internal or personal use of this material is permitted. If interested in reprinting/republishing IEEE copyrighted material for advertising or promotional purposes or for creating new collective works for resale or redistribution, please go to [http://www.ieee.org/publications\\_standards/publications/rights/rights\\_link.html](http://www.ieee.org/publications_standards/publications/rights/rights_link.html) to learn how to obtain a License from RightsLink.

If applicable, University Microfilms and/or ProQuest Library, or the Archives of Canada may supply single copies of the dissertation.

BACK

CLOSE WINDOW

**SPRINGER LICENSE  
TERMS AND CONDITIONS**

Jul 08, 2013

---

---

This is a License Agreement between Siyi Wabg ("You") and Springer ("Springer") provided by Copyright Clearance Center ("CCC"). The license consists of your order details, the terms and conditions provided by Springer, and the payment terms and conditions.

**All payments must be made in full to CCC. For payment instructions, please see information listed at the bottom of this form.**

|                                     |  |
|-------------------------------------|--|
| License Number                      | 3184561190192  |
| License date                        | Jul 08, 2013   |
| Licensed content publisher          | Springer   |
| Licensed content publication        | EURASIP Journal on Wireless Communications and Networking                |
| Licensed content title              | Low energy indoor network: deployment optimisation                       |
| Licensed content author             | Siyi Wang  |
| Licensed content date               | Jan 1, 2012  |
| Volume number                       | 2012   |
| Issue number                        | 1  |
| Type of Use                         | Thesis/Dissertation  |
| Portion                             | Full text  |
| Number of copies                    | 1  |
| Author of this Springer article     | Yes and you are the sole author of the new work                          |
| Order reference number              |  |
| Title of your thesis / dissertation | An Investigation of Energy Efficiency in Heterogeneous Wireless Networks |
| Expected completion date            | Jul 2013   |
| Estimated size(pages)               | 150  |
| Total                               | 0.00 USD   |

**Terms and Conditions**

**Introduction**

The publisher for this copyrighted material is Springer Science + Business Media. By clicking "accept" in connection with completing this licensing transaction, you agree that the following terms and conditions apply to this transaction (along with the Billing and Payment terms and conditions established by Copyright Clearance Center, Inc. ("CCC"), at the time that you opened your Rightslink account and that are available at any time at <http://myaccount.copyright.com>).

**Limited License**

With reference to your request to reprint in your thesis material on which Springer Science and Business Media control the copyright, permission is granted, free of charge, for the use indicated in your enquiry.

Licenses are for one-time use only with a maximum distribution equal to the number that you identified in the licensing process.

This License includes use in an electronic form, provided its password protected or on the university's intranet or repository, including UMI (according to the definition at the Sherpa website: <http://www.sherpa.ac.uk/romeo/>). For any other electronic use, please contact Springer at ([permissions.dordrecht@springer.com](mailto:permissions.dordrecht@springer.com) or [permissions.heidelberg@springer.com](mailto:permissions.heidelberg@springer.com)).

The material can only be used for the purpose of defending your thesis, and with a maximum of 100 extra copies in paper.

Although Springer holds copyright to the material and is entitled to negotiate on rights, this license is only valid, subject to a courtesy information to the author (address is given with the article/chapter) and provided it concerns original material which does not carry references to other sources (if material in question appears with credit to another source, authorization from that source is required as well).

Permission free of charge on this occasion does not prejudice any rights we might have to charge for reproduction of our copyrighted material in the future.

#### Altering/Modifying Material: Not Permitted

You may not alter or modify the material in any manner. Abbreviations, additions, deletions and/or any other alterations shall be made only with prior written authorization of the author(s) and/or Springer Science + Business Media. (Please contact Springer at ([permissions.dordrecht@springer.com](mailto:permissions.dordrecht@springer.com) or [permissions.heidelberg@springer.com](mailto:permissions.heidelberg@springer.com)))

#### Reservation of Rights

Springer Science + Business Media reserves all rights not specifically granted in the combination of (i) the license details provided by you and accepted in the course of this licensing transaction, (ii) these terms and conditions and (iii) CCC's Billing and Payment terms and conditions.

#### Copyright Notice:Disclaimer

You must include the following copyright and permission notice in connection with any reproduction of the licensed material: "Springer and the original publisher /journal title, volume, year of publication, page, chapter/article title, name(s) of author(s), figure number(s), original copyright notice) is given to the publication in which the material was originally published, by adding; with kind permission from Springer Science and Business Media"

#### Warranties: None

Example 1: Springer Science + Business Media makes no representations or warranties with respect to the licensed material.

Example 2: Springer Science + Business Media makes no representations or warranties with respect to the licensed material and adopts on its own behalf the limitations and disclaimers established by CCC on its behalf in its Billing and Payment terms and conditions for this licensing transaction.

#### Indemnity

You hereby indemnify and agree to hold harmless Springer Science + Business Media and CCC, and their respective officers, directors, employees and agents, from and against any and all claims arising out of your use of the licensed material other than as specifically authorized pursuant to this license.

#### No Transfer of License

This license is personal to you and may not be sublicensed, assigned, or transferred by you to any other person without Springer Science + Business Media's written permission.

#### No Amendment Except in Writing

This license may not be amended except in a writing signed by both parties (or, in the case of Springer Science + Business Media, by CCC on Springer Science + Business Media's behalf).

#### Objection to Contrary Terms

Springer Science + Business Media hereby objects to any terms contained in any purchase order, acknowledgment, check endorsement or other writing prepared by you, which terms are inconsistent with these terms and conditions or CCC's Billing and Payment terms and conditions. These terms and conditions, together with CCC's Billing and Payment terms and conditions (which are incorporated herein), comprise the entire agreement between you and Springer Science + Business Media (and CCC) concerning this licensing transaction. In the event of any conflict between your obligations established by these terms and conditions and those established by CCC's Billing and Payment terms and conditions, these terms and conditions shall control.

#### Jurisdiction

All disputes that may arise in connection with this present License, or the breach thereof, shall be settled exclusively by arbitration, to be held in The Netherlands, in accordance with Dutch law, and to be conducted under the Rules of the 'Netherlands Arbitrage Instituut' (Netherlands Institute of Arbitration). **OR:**

**All disputes that may arise in connection with this present License, or the breach thereof, shall be settled exclusively by arbitration, to be held in the Federal Republic of Germany, in accordance with German law.**

#### Other terms and conditions:

v1.3

**If you would like to pay for this license now, please remit this license along with your payment made payable to "COPYRIGHT CLEARANCE CENTER" otherwise you will be invoiced within 48 hours of the license date. Payment should be in the form of a check or money order referencing your account number and this invoice number RLNK501061221.**

**Once you receive your invoice for this order, you may pay your invoice by credit card. Please follow instructions provided at that time.**

#### Make Payment To:

**Copyright Clearance Center  
Dept 001  
P.O. Box 843006  
Boston, MA 02284-3006**

**For suggestions or comments regarding this order, contact RightsLink Customer Support: [customercare@copyright.com](mailto:customercare@copyright.com) or +1-877-622-5543 (toll free in the US) or +1-978-646-2777.**

**Gratis licenses (referencing \$0 in the Total field) are free. Please retain this printable license for your reference. No payment is required.**

---

---



**Title:** Automated small-cell deployment for heterogeneous cellular networks

**Author:** Weisi Guo; Siyi Wang; Xiaoli Chu; Jie Zhang; Jiming Chen; Hui Song

**Publication:** IEEE Communications Magazine

**Publisher:** IEEE

**Date:** May 2013

Copyright © 2013, IEEE

Logged in as:  
Siyi Wang

LOGOUT

## Thesis / Dissertation Reuse

**The IEEE does not require individuals working on a thesis to obtain a formal reuse license, however, you may print out this statement to be used as a permission grant:**

*Requirements to be followed when using any portion (e.g., figure, graph, table, or textual material) of an IEEE copyrighted paper in a thesis:*

- 1) In the case of textual material (e.g., using short quotes or referring to the work within these papers) users must give full credit to the original source (author, paper, publication) followed by the IEEE copyright line © 2011 IEEE.
- 2) In the case of illustrations or tabular material, we require that the copyright line © [Year of original publication] IEEE appear prominently with each reprinted figure and/or table.
- 3) If a substantial portion of the original paper is to be used, and if you are not the senior author, also obtain the senior author's approval.

*Requirements to be followed when using an entire IEEE copyrighted paper in a thesis:*

- 1) The following IEEE copyright/ credit notice should be placed prominently in the references: © [year of original publication] IEEE. Reprinted, with permission, from [author names, paper title, IEEE publication title, and month/year of publication]
- 2) Only the accepted version of an IEEE copyrighted paper can be used when posting the paper or your thesis on-line.
- 3) In placing the thesis on the author's university website, please display the following message in a prominent place on the website: In reference to IEEE copyrighted material which is used with permission in this thesis, the IEEE does not endorse any of [university/educational entity's name goes here]'s products or services. Internal or personal use of this material is permitted. If interested in reprinting/republishing IEEE copyrighted material for advertising or promotional purposes or for creating new collective works for resale or redistribution, please go to [http://www.ieee.org/publications\\_standards/publications/rights/rights\\_link.html](http://www.ieee.org/publications_standards/publications/rights/rights_link.html) to learn how to obtain a License from RightsLink.

If applicable, University Microfilms and/or ProQuest Library, or the Archives of Canada may supply single copies of the dissertation.

BACK

CLOSE WINDOW





**Title:** Two-tier Cellular Networks with Frequency Selective Surface  
**Conference Proceedings:** Two-tier Cellular Networks with Frequency Selective Surface  
**Author:** Siyi Wang; Weisi Guo; O'Farrell, T.  
**Publisher:** IEEE  
**Date:** 25-27 June 2012  
Copyright © 2012, IEEE

Logged in as:  
Siyi Wang

LOGOUT

## Thesis / Dissertation Reuse

**The IEEE does not require individuals working on a thesis to obtain a formal reuse license, however, you may print out this statement to be used as a permission grant:**

*Requirements to be followed when using any portion (e.g., figure, graph, table, or textual material) of an IEEE copyrighted paper in a thesis:*

- 1) In the case of textual material (e.g., using short quotes or referring to the work within these papers) users must give full credit to the original source (author, paper, publication) followed by the IEEE copyright line © 2011 IEEE.
- 2) In the case of illustrations or tabular material, we require that the copyright line © [Year of original publication] IEEE appear prominently with each reprinted figure and/or table.
- 3) If a substantial portion of the original paper is to be used, and if you are not the senior author, also obtain the senior author's approval.

*Requirements to be followed when using an entire IEEE copyrighted paper in a thesis:*

- 1) The following IEEE copyright/ credit notice should be placed prominently in the references: © [year of original publication] IEEE. Reprinted, with permission, from [author names, paper title, IEEE publication title, and month/year of publication]
- 2) Only the accepted version of an IEEE copyrighted paper can be used when posting the paper or your thesis on-line.
- 3) In placing the thesis on the author's university website, please display the following message in a prominent place on the website: In reference to IEEE copyrighted material which is used with permission in this thesis, the IEEE does not endorse any of [university/educational entity's name goes here]'s products or services. Internal or personal use of this material is permitted. If interested in reprinting/republishing IEEE copyrighted material for advertising or promotional purposes or for creating new collective works for resale or redistribution, please go to [http://www.ieee.org/publications\\_standards/publications/rights/rights\\_link.html](http://www.ieee.org/publications_standards/publications/rights/rights_link.html) to learn how to obtain a License from RightsLink.

If applicable, University Microfilms and/or ProQuest Library, or the Archives of Canada may supply single copies of the dissertation.

BACK

CLOSE WINDOW

# References

- [1] W. Guo, S. Wang, and T. O'Farrell, "Environmental and Economically Sustainable Cellular Networks," *Journal of Green Engineering*, vol. 2, no. 3, pp. 273–283, 2012. [Online]. Available: [http://riverpublishers.com/journal/journal\\_articles/download\\_file.php?file=RP\\_Journal\\_1904-4720\\_235.pdf](http://riverpublishers.com/journal/journal_articles/download_file.php?file=RP_Journal_1904-4720_235.pdf) xxxi, 2
- [2] M.-S. David, M. Jose F, C.-P. n. Jorge, C. Daniel, G. Salvador, C. Narcís, and Others, "On the way towards fourth-generation mobile: 3GPP LTE and LTE-advanced," *EURASIP Journal on Wireless Communications and Networking*, vol. 2009, 2009. 1
- [3] D. Raychaudhuri and N. B. Mandayam, "Frontiers of wireless and mobile communications," *Proceedings of the IEEE*, vol. 100, no. 4, pp. 824–840, 2012. 1
- [4] P. Rinaldi and G. M. Veca, "The hydrogen for base radio stations," in *29<sup>th</sup> International Telecommunications Energy Conference (INTELEC)*, 2007, pp. 288–292. 2
- [5] G. Fettweis and E. Zimmermann, "ICT energy consumption-trends and challenges," in *Proceedings of the 11<sup>th</sup> International Symposium on Wireless Personal Multimedia Communications*, vol. 2, no. 4, 2008, p. 6. 2
- [6] A. Fehske, G. Fettweis, J. Malmudin, and G. Biczok, "The global footprint of mobile communications: The ecological and economic perspective," *IEEE Communications Magazine*, vol. 49, no. 8, pp. 55–62, 2011. 2

- [7] Vodafone, “Sustainability report 2011,” Tech. Rep. March, 2011. 3
- [8] J. G. Andrews, H. Claussen, M. Dohler, S. Rangan, and M. C. Reed, “Femtocells: Past, present, and future,” *IEEE Journal on Selected Areas in Communications*, vol. 30, no. 3, pp. 497–508, 2012. 3, 81
- [9] S. Wang, W. Guo, and T. O’Farrell, “Energy Efficiency Evaluation of SISO and MIMO between LTE-Femtocells and 802.11n Networks,” in *2012 IEEE 75th Vehicular Technology Conference (VTC Spring)*, May 2012, pp. 1–5. [Online]. Available: <http://ieeexplore.ieee.org/lpdocs/epic03/wrapper.htm?arnumber=6240229> 3
- [10] S. Wang, C. Turyagyenda, and T. O’Farrell, “Energy Efficiency and Spectral Efficiency Trade-Off of a Novel Interference Avoidance Approach for LTE-Femtocell Networks,” in *2012 IEEE 75th Vehicular Technology Conference (VTC Spring)*, May 2012, pp. 1–5. [Online]. Available: <http://ieeexplore.ieee.org/lpdocs/epic03/wrapper.htm?arnumber=6240230> 4, 47
- [11] S. Wang, W. Guo, and T. O’Farrell, “Optimising Femtocell Placement in an Interference Limited Network: Theory and Simulation,” in *2012 IEEE Vehicular Technology Conference (VTC Fall)*, Sep. 2012, pp. 1–6. [Online]. Available: <http://ieeexplore.ieee.org/lpdocs/epic03/wrapper.htm?arnumber=6399231> 4
- [12] —, “Low energy indoor network: deployment optimisation,” *EURASIP Journal on Wireless Communications and Networking*, vol. 2012, no. 1, p. 193, 2012. [Online]. Available: <http://jwcn.eurasipjournals.com/content/2012/1/193> 4
- [13] W. Guo and S. Wang, “Interference-Aware Self-Deploying Femto-Cell,” *IEEE Wireless Communications Letters*, vol. 1, no. 6, pp. 609–612, Dec. 2012. [Online]. Available: <http://ieeexplore.ieee.org/lpdocs/epic03/wrapper.htm?arnumber=6308771> 4
- [14] W. Guo, S. Wang, X. Chu, J. Zhang, J. Chen, and H. Song, “Automated small-cell deployment for heterogeneous cellular networks,”

- IEEE Communications Magazine*, vol. 51, no. 5, pp. 46–53, May 2013. [Online]. Available: <http://ieeexplore.ieee.org/lpdocs/epic03/wrapper.htm?arnumber=6515046> 4, 73
- [15] S. Wang, W. Guo, and T. O'Farrell, "Two-tier Cellular Networks with Frequency Selective Surface," in *2012 IEEE 14th International Conference on High Performance Computing and Communication & 2012 IEEE 9th International Conference on Embedded Software and Systems*, Jun. 2012, pp. 740–747. [Online]. Available: <http://ieeexplore.ieee.org/stamp/stamp.jsp?arnumber=6332243> 5
- [16] V. Chandrasekhar, J. Andrews, and A. Gatherer, "Femtocell networks: a survey," *IEEE Communications Magazine*, vol. 46, no. 9, pp. 59–67, 2008. 6, 104
- [17] S. F. Hasan, N. H. Siddique, and S. Chakraborty, "Femtocell versus WiFi-A survey and comparison of architecture and performance," in *1st International Conference on, Wireless Communication, Vehicular Technology, Information Theory and Aerospace & Electronic Systems Technology, 2009. Wireless VITAE 2009. Aalborg, Denmark, 2009*, pp. 916–920. 7
- [18] H. Claussen, "Performance of macro-and co-channel femtocells in a hierarchical cell structure," in *IEEE 18th International Symposium on Personal, Indoor and Mobile Radio Communications (PIMRC), 2007*, pp. 1–5. 7
- [19] M. Z. Chowdhury, W. Ryu, E. Rhee, and Y. M. Jang, "Handover between macrocell and femtocell for UMTS based networks," in *11th International Conference on Advanced Communication Technology, 2009. ICACT 2009.*, vol. 1, 2009, pp. 237–241. 7
- [20] 3GPP, "Requirements for Evolved UTRA (E-UTRA) and Evolved UTRAN (E-UTRAN)," 3rd Generation Partnership Project, Tech. Rep. TR 25.913 V9.0.0, 2009. 8
- [21] "IEEE 802.11-2007: Wireless LAN Medium Access Control (MAC) and Physical Layer (PHY) specifications." 8

- [22] 3GPP, “Physical layer aspects for Evolved Universal Terrestrial Radio Access (UTRA),” 3rd Generation Partnership Project, Tech. Rep. TR 25.814 V7.1.0, 2006. [11](#)
- [23] —, “Physical channels and modulation,” 3rd Generation Partnership Project, Tech. Rep. TS 36.211 V8.8.0 Release 8, 2009. [11](#)
- [24] S. R. Saunders, S. Carlaw, A. Giustina, R. R. Bhat, and R. Siegberg, *Femtocells: Opportunities and Challenges for Business and Technology*. Wiley, 2009. [13](#)
- [25] C. Mehlführer, M. Wrulich, J. C. Ikuno, D. Bosanska, and M. Rupp, “Simulating the Long Term Evolution physical layer,” in *Proc. of the 17th European Signal Processing Conference (EUSIPCO 2009), Glasgow, Scotland, 2009*, pp. 1471–1478. [19](#), [58](#)
- [26] P. Kyösti, J. Meinilä, L. Hentilä, X. Zhao, T. Jämsä, C. Schneider, M. Narandzic, M. Milojevic, A. Hong, J. Ylitalo, and Others, “WINNER II channel models (d1. 1.2 v1. 1),” *no. IST-4-027756 WINNER II, D*, vol. 1. [19](#), [33](#), [44](#), [58](#), [84](#)
- [27] G. Bianchi, “Performance Analysis of the IEEE 802.11 Distributed Coordination function,” *IEEE Journal on selected areas in communications*, vol. 18, no. 3, pp. 535–547, 2000. [25](#)
- [28] Y. C. Tay and K. C. Chua, “A capacity analysis for the IEEE 802.11 MAC protocol,” *Wireless networks*, vol. 7, no. 2, pp. 159–171, 2001. [25](#)
- [29] Y. Lin and V. W. S. Wong, “WSN01-1: frame aggregation and optimal frame size adaptation for IEEE 802.11n WLANs,” in *IEEE Global Telecommunications Conference, 2006. GLOBECOM’06, 2007*, pp. 1–6. [25](#)
- [30] EARTH, “Energy efficiency analysis of the reference systems, areas of improvements and target breakdown,” Energy Aware Radio and neTwork tecHnologies, Tech. Rep. Deliverable D2.3, Dec. 2010. [29](#), [33](#)

- [31] B. Badic, T. O'Farrell, P. Loskot, and J. He, "Energy efficient radio access architectures for green radio: large versus small cell size deployment," in *IEEE 70th Vehicular Technology Conference Fall (VTC 2009-Fall)*, 2009, 2010, pp. 1–5. [29](#)
- [32] J. He and T. O'Farrell, "Book of assumptions," Mobile VCE, Tech. Rep. v2.0, Sep. 2012. [30](#)
- [33] A. B. Carleial, "A case where interference does not reduce capacity," *IEEE Transactions on Information Theory*, vol. 21, p. 569, 1975. [41](#)
- [34] J. G. Andrews, "Interference cancellation for cellular systems: A contemporary overview," *IEEE Wireless Communications*, vol. 12, no. 2, pp. 19–29, 2005. [41](#)
- [35] C. Esli, M. Koca, and H. Deliç, "Iterative joint tone-interference cancellation and decoding for MIMO-OFDM," *IEEE Transactions on Vehicular Technology*, vol. 57, no. 5, pp. 2843–2855, 2008. [41](#)
- [36] W. Webb, *Wireless communications: The future*. John Wiley, 2007. [41](#)
- [37] 3GPP, "Further advancements for E-UTRA physical layer aspects (Release 9)," 3rd Generation Partnership Project, Tech. Rep. TR 36.814 V9.0.0, Mar. 2010. [42](#), [110](#)
- [38] S. Al-Rubaye, A. Al-Dulaimi, and J. Cosmas, "Cognitive Femtocell," *IEEE Vehicular Technology Magazine*, vol. 6, no. 1, pp. 44–51, 2011. [42](#)
- [39] S. Park, W. Seo, S. Choi, and D. Hong, "A Beamforming Codebook Restriction for Cross-Tier Interference Coordination in Two-tier Femtocell Networks," *IEEE Transactions on Vehicular Technology*, no. 99, pp. 1651–1663, 2011. [42](#)
- [40] V. Chandrasekhar, J. G. Andrews, T. Muharemovic, Z. Shen, and A. Gatherer, "Power control in two-tier femtocell networks," *IEEE Transactions on Wireless Communications*, vol. 8, no. 8, pp. 4316–4328, 2009. [42](#), [105](#)

- [41] H. S. Jo, C. Mun, J. Moon, and J. G. Yook, "Interference mitigation using uplink power control for two-tier femtocell networks," *IEEE Transactions on Wireless Communications*, vol. 8, no. 10, pp. 4906–4910, 2009. [42](#)
- [42] V. Chandrasekhar and J. Andrews, "Uplink capacity and interference avoidance for two-tier femtocell networks," *IEEE Transactions on Wireless Communications*, vol. 8, no. 7, pp. 3498–3509, 2009. [42](#)
- [43] D. Fagen, P. A. Vicharelli, and J. Weitzen, "Automated wireless coverage optimization with controlled overlap," *IEEE Transactions on Vehicular Technology*, vol. 57, no. 4, pp. 2395–2403, 2008. [42](#)
- [44] I. Ashraf, H. Claussen, and L. T. W. Ho, "Distributed radio coverage optimization in enterprise femtocell networks," in *IEEE International Conference on Communications (ICC), 2010, Cape Town, South Africa*, pp. 1–6. [42](#)
- [45] K. W. Sung, H. Haas, and S. McLaughlin, "A semianalytical PDF of downlink SINR for femtocell networks," *EURASIP Journal on Wireless Communications and Networking*, vol. 2010, p. 5, 2010. [42](#)
- [46] J. Lee, S. Bae, Y. Kwon, and M. Chung, "Interference Analysis for Femtocell Deployment in OFDMA Systems Based on Fractional Frequency Reuse," *IEEE Communications Letters*, no. 99, pp. 1–3. [42](#)
- [47] M. Necker, "Interference coordination in cellular OFDMA networks," *IEEE Network*, vol. 22, no. 6, pp. 12–19, 2008. [43](#)
- [48] R. Y. Chang, Z. Tao, J. Zhang, and C.-C. Kuo, "A graph approach to dynamic fractional frequency reuse (FFR) in multi-cell OFDMA networks," in *IEEE International Conference on Communications, 2009. ICC'09, 2009*, pp. 1–6. [43](#)
- [49] S. H. Ali and V. C. M. Leung, "Dynamic frequency allocation in fractional frequency reused OFDMA networks," *IEEE Transactions on Wireless Communications*, vol. 8, no. 8, pp. 4286–4295, 2009. [43](#)

- [50] R. Kwan, C. Leung, and J. Zhang, "Multiuser scheduling on the downlink of an LTE cellular system," *Research Letters in Communications*, vol. 2008, p. 3, 2008. [43](#)
- [51] C. Turyagyenda, T. O'Farrell, and W. Guo, "Energy efficient coordinated radio resource management: a two player sequential game modelling for the long-term evolution downlink," *IET Communications*, vol. 6, no. 14, pp. 2239–2249, 2012. [47](#)
- [52] D. Stamatelos and A. Ephremides, "Spectral efficiency and optimal base placement for indoor wireless networks," *IEEE Journal on Selected Areas in Communications*, vol. 14, no. 4, pp. 651–661, 1996. [55](#)
- [53] R. C. Rodrigues, G. R. Mateus, and A. A. F. Loureiro, "Optimal base station placement and fixed channel assignment applied to wireless local area network projects," in *IEEE International Conference on Networks, 1999.(ICON'99) Proceedings*, 1999, pp. 186–192. [55](#)
- [54] A. V. Pais, K. W. Sowerby, and M. J. Neve, "Implications of power control and successive interference cancellation on indoor DS-CDMA system deployment and performance," *IEEE Communications Letters*, vol. 9, no. 3, pp. 204–206, 2005. [55](#)
- [55] A. Eisenblatter, H.-F. Geerdes, and I. Siomina, "Integrated access point placement and channel assignment for wireless LANs in an indoor office environment," in *IEEE International Symposium on a World of Wireless, Mobile and Multimedia Networks, (WoWMoM) 2007.*, 2007, pp. 1–10. [55](#)
- [56] J. Liu, Q. Chen, and H. D. Sherali, "Algorithm design for femtocell base station placement in commercial building environments," in *Proceedings IEEE INFOCOM, 2012*, 2012, pp. 2951–2955. [55](#)
- [57] J. Liu, T. Kou, Q. Chen, and H. D. Sherali, "Femtocell base station deployment in commercial buildings: A global optimization approach," *IEEE Journal on Selected Areas in Communications*, vol. 30, no. 3, pp. 652–663, 2012. [55](#)



- [58] W. Guo, C. Turyagyenda, H. Hamdoun, S. Wang, P. Loskot, and T. O’Farrell, “Towards a low energy LTE cellular network: Architectures,” in *Proceedings of the 19th European Signal Processing Conference*, 2011, pp. 879–883. [Online]. Available: <http://www.eurasip.org/Proceedings/Eusipco/Eusipco2011/papers/1569422763.pdf> 57
- [59] W. Guo and T. O’Farrell, “Relay Deployment in Cellular Networks: Planning and Optimization,” *IEEE Journal on Selected Areas in Communications*, vol. 31, no. 8, pp. 1597–1606. 58
- [60] K. S. Gilhousen, I. M. Jacobs, R. Padovani, A. J. Viterbi, J. LA Weaver, and C. E. Wheatley III, “On the capacity of a cellular CDMA system,” *IEEE Transactions on Vehicular Technology*, vol. 40, no. 2, pp. 303–312, 1991. 80, 82
- [61] J. G. Andrews, R. K. Ganti, M. Haenggi, N. Jindal, and S. Weber, “A primer on spatial modeling and analysis in wireless networks,” *IEEE Communications Magazine*, vol. 48, no. 11, pp. 156–163, 2010. 80
- [62] F. Baccelli, M. Klein, M. Lebourges, and S. Zuyev, “Stochastic geometry and architecture of communication networks,” *Telecommunication Systems*, vol. 7, no. 1-3, pp. 209–227, 1997. 80
- [63] A. Rabbachin, T. Q. S. Quek, H. Shin, and M. Z. Win, “Cognitive network interference,” *IEEE Journal on Selected Areas in Communications*, vol. 29, no. 2, pp. 480–493, 2011. 81
- [64] S. Landström, A. Furuskär, K. Johansson, L. Falconetti, and F. Kronstedt, “Heterogeneous networks—increasing cellular capacity,” *The data boom: opportunities and challenges*, p. 4, 2011. 81
- [65] R. W. Heath and M. Kountouris, “Modeling heterogeneous network interference,” in *Information Theory and Applications Workshop (ITA), 2012*, 2012, pp. 17–22. 81

- [66] A. D. Wyner, "Shannon-theoretic approach to a Gaussian cellular multiple-access channel," *IEEE Transactions on Information Theory*, vol. 40, no. 6, pp. 1713–1727, 1994. [81](#)
- [67] S. Shamai and A. D. Wyner, "Information-theoretic considerations for symmetric, cellular, multiple-access fading channels. I," *IEEE Transactions on Information Theory*, vol. 43, no. 6, pp. 1877–1894, 1997. [81](#)
- [68] O. Somekh and S. Shamai, "Shannon-theoretic approach to a Gaussian cellular multiple-access channel with fading," *IEEE Transactions on Information Theory*, vol. 46, no. 4, pp. 1401–1425, 2000. [81](#)
- [69] O. Somekh, B. M. Zaidel, and S. Shamai, "Sum rate characterization of joint multiple cell-site processing," *IEEE Transactions on Information Theory*, vol. 53, no. 12, pp. 4473–4497, 2007. [81](#)
- [70] J. Sheng, T. David NC, S. Joseph B, H. Jilei, S. John E, P. Roberto, and Others, "Multicell downlink capacity with coordinated processing," *EURASIP Journal on Wireless Communications and Networking*, vol. 2008, 2008. [81](#)
- [71] O. Simeone, O. Somekh, H. V. Poor, and S. Shamai, "Local base station cooperation via finite-capacity links for the uplink of linear cellular networks," *IEEE Transactions on Information Theory*, vol. 55, no. 1, pp. 190–204, 2009. [81](#)
- [72] V. Tarokh, C.-B. Chae, I. Hwang, and R. W. Heath Jr, "Interference aware-coordinated beamforming system in a two-cell environment," 2009. [81](#)
- [73] D. Gesbert, S. Hanly, H. Huang, S. Shamai Shitz, O. Simeone, and W. Yu, "Multi-cell MIMO cooperative networks: A new look at interference," *IEEE Journal on Selected Areas in Communications*, vol. 28, no. 9, pp. 1380–1408, 2010. [81](#), [104](#)
- [74] V. H. MacDonald, "The cellular concept," *Bell System Technical Journal*, vol. 58, no. 1, pp. 15–41, 1979. [82](#)

- [75] T. S. Rappaport and Others, *Wireless communications: principles and practice*. Prentice Hall PTR New Jersey, 1996, vol. 2. 82
- [76] A. Goldsmith, *Wireless communications*. Cambridge university press, 2005. 82
- [77] M. Haenggi and R. K. Ganti, *Interference in large wireless networks*. Now Publishers Inc, 2009, vol. 3, no. 2. 82
- [78] M. Haenggi, J. G. Andrews, F. Baccelli, O. Dousse, and M. Franceschetti, “Stochastic geometry and random graphs for the analysis and design of wireless networks,” *IEEE Journal on Selected Areas in Communications*, vol. 27, no. 7, pp. 1029–1046, 2009. 82
- [79] F. Baccelli and B. Blaszczyszyn, “Stochastic Geometry and Wireless Networks: Volume I Theory,” *Foundations and Trends in Networking*, vol. 3, no. 3-4, pp. 249–449, 2010. 82
- [80] ———, “Stochastic Geometry and Wireless Networks: Volume II Applications,” *Foundations and Trends in Networking*, vol. 4, no. 1-2, pp. 1–312, 2010. 82
- [81] F. Baccelli and S. Zuyev, “Stochastic Geometry Models of Mobile Communication Networks,” in *Frontiers in queueing: models and applications in science and engineering*. Citeseer, 1996. 82
- [82] T. X. Brown, “Cellular performance bounds via shotgun cellular systems,” *IEEE Journal on Selected Areas in Communications*, vol. 18, no. 11, pp. 2443–2455, 2000. 82
- [83] F. Baccelli, P. Miihlethaler, and B. Blaszczyszyn, “Stochastic analysis of spatial and opportunistic Aloha,” *IEEE Journal on Selected Areas in Communications*, vol. 27, no. 7, pp. 1105–1119, 2009. 83
- [84] P. Madhusudhanan, J. G. Restrepo, Y. Liu, and T. X. Brown, “Carrier to interference ratio analysis for the shotgun cellular system,” in *IEEE Global Telecommunications Conference, 2009. GLOBECOM.*, 2009, pp. 1–6. 83

- [85] J. Andrews, F. Baccelli, and R. Ganti, “A tractable approach to coverage and rate in cellular networks,” *IEEE Transactions on Communications*, no. 99, pp. 1–13, 2010. 83
- [86] C.-H. Lee, C.-Y. Shih, and Y.-S. Chen, “Stochastic geometry based models for modeling cellular networks in urban areas,” *Wireless Networks*, pp. 1–10, 2012. 83
- [87] L. Decreusefond, P. Martins, and T.-T. Vu, “An analytical model for evaluating outage and handover probability of cellular wireless networks,” in *Wireless Personal Multimedia Communications (WPMC), 2012 15th International Symposium on*, 2012, pp. 643–647. 83
- [88] H. S. Dhillon, R. K. Ganti, F. Baccelli, and J. G. Andrews, “Coverage and ergodic rate in K-tier downlink heterogeneous cellular networks,” in *49th Annual Allerton Conference on Communication, Control, and Computing (Allerton), 2011*, 2011, pp. 1627–1632. 83
- [89] P. Madhusudhanan, J. G. Restrepo, Y. Liu, T. X. Brown, and K. R. Baker, “Multi-tier network performance analysis using a shotgun cellular system,” in *IEEE Global Telecommunications Conference (GLOBECOM 2011)*, 2011, pp. 1–6. 83
- [90] H. Wang and M. C. Reed, “A novel tractable framework to analyse heterogeneous cellular networks,” in *IEEE GLOBECOM Workshops (GC Wkshps), 2011*, 2011, pp. 287–292. 83
- [91] ———, “Tractable model for heterogeneous cellular networks with directional antennas,” in *Australian Communications Theory Workshop (AusCTW), 2012*, 2012, pp. 61–65. 83
- [92] T. D. Novlan, H. S. Dhillon, and J. G. Andrews, “Analytical modeling of uplink cellular networks,” *Wireless Communications, IEEE Transactions on*, vol. PP, no. 99, pp. 1–11, 2013. 83

- [93] H. S. Dhillon, R. K. Ganti, F. Baccelli, and J. G. Andrews, “Modeling and analysis of K-tier downlink heterogeneous cellular networks,” *IEEE Journal on Selected Areas in Communications*, vol. 30, no. 3, pp. 550–560, 2012. [83](#)
- [94] S. Mukherjee, “Distribution of downlink SINR in heterogeneous cellular networks,” *IEEE Journal on Selected Areas in Communications*, vol. 30, no. 3, pp. 575–585, 2012. [83](#)
- [95] W. C. Cheung, T. Q. S. Quek, and M. Kountouris, “Throughput Optimization, Spectrum Allocation, and Access Control in Two-Tier Femtocell Networks,” *IEEE Journal on Selected Areas in Communications*, vol. 30, no. 3, p. 1, 2012. [83](#), [104](#)
- [96] S. M. Yu and S.-L. Kim, “Downlink capacity and base station density in cellular networks,” *arXiv preprint arXiv:1109.2992*, 2011. [83](#)
- [97] H. S. Dhillon, R. K. Ganti, and J. G. Andrews, “Load-aware modeling and analysis of heterogeneous cellular networks,” *Wireless Communications, IEEE Transactions on*, vol. 12, no. 4, pp. 1666–1677, 2013. [83](#)
- [98] S. Akoum and R. W. Heath, “Multi-cell coordination: A stochastic geometry approach,” in *IEEE 13th International Workshop on Signal Processing Advances in Wireless Communications (SPAWC), 2012*, 2012, pp. 16–20. [83](#)
- [99] D. Cao, S. Zhou, and Z. Niu, “Optimal base station density for energy-efficient heterogeneous cellular networks,” in *IEEE International Conference on Communications (ICC), 2012*, 2012, pp. 4379–4383. [83](#)
- [100] P. Xia, H.-S. Jo, and J. G. Andrews, “Fundamentals of inter-cell overhead signaling in heterogeneous cellular networks,” *IEEE Journal of Selected Topics in Signal Processing*, vol. 6, no. 3, pp. 257–269, 2012. [83](#)
- [101] S. Lee and K. Huang, “Coverage and economy of cellular networks with many base stations,” *IEEE Communications Letters*, vol. 16, no. 7, pp. 1038–1040, 2012. [83](#)

- [102] T. Bai, R. Vaze, and R. W. Heath, "Using random shape theory to model blockage in random cellular networks," in *International Conference on Signal Processing and Communications (SPCOM), 2012*, 2012, pp. 1–5. [83](#)
- [103] H. Jo, Y. Sang, P. Xia, and J. Andrews, "Heterogeneous cellular networks with flexible cell association: A comprehensive downlink SINR analysis," *IEEE Transactions on Wireless Communications*, vol. 11, no. 10, pp. 3484–3495, 2012. [83](#)
- [104] S. Akoum and R. W. Heath, "Interference Coordination: Random Clustering and Adaptive Limited Feedback," *IEEE Transactions on Signal Processing*, vol. 61, no. 7, pp. 1822–1834, 2013. [83](#)
- [105] P. Madhusudhanan, J. G. Restrepo, Y. Liu, and T. X. Brown, "Downlink coverage analysis in a heterogeneous cellular network," in *IEEE Global Communications Conference (GLOBECOM), 2012*, 2012, pp. 4170–4175. [83](#)
- [106] E. S. Sousa, "Performance of a spread spectrum packet radio network link in a Poisson field of interferers," *IEEE Transactions on Information Theory*, vol. 38, no. 6, pp. 1743–1754, 1992. [83](#)
- [107] J. Ilow, D. Hatzinakos, and A. N. Venetsanopoulos, "Performance of FH SS radio networks with interference modeled as a mixture of Gaussian and alpha-stable noise," *IEEE Transactions on Communications*, vol. 46, no. 4, pp. 509–520, 1998. [83](#)
- [108] J. Ilow and D. Hatzinakos, "Analytic alpha-stable noise modeling in a Poisson field of interferers or scatterers," *IEEE Transactions on Signal Processing*, vol. 46, no. 6, pp. 1601–1611, 1998. [83](#)
- [109] K. F. McDonald and R. S. Blum, "A statistical and physical mechanisms-based interference and noise model for array observations," *IEEE Transactions on Signal Processing*, vol. 48, no. 7, pp. 2044–2056, 2000. [83](#)

- [110] X. Yang and A. P. Petropulu, “Co-channel interference modeling and analysis in a Poisson field of interferers in wireless communications,” *IEEE Transactions on Signal Processing*, vol. 51, no. 1, pp. 64–76, 2003. [83](#)
- [111] Y. Han and K. C. Teh, “Performance study of asynchronous FFH/MFSK communications using various diversity combining techniques with MAI modeled as alpha-stable process,” *IEEE Transactions on Wireless Communications*, vol. 6, no. 5, pp. 1615–1618, 2007. [83](#)
- [112] M. Z. Win, P. C. Pinto, and L. A. Shepp, “A mathematical theory of network interference and its applications,” *Proceedings of the IEEE*, vol. 97, no. 2, pp. 205–230, 2009. [83](#)
- [113] E. Salbaroli and A. Zanella, “Interference analysis in a Poisson field of nodes of finite area,” *IEEE Transactions on Vehicular Technology*, vol. 58, no. 4, pp. 1776–1783, 2009. [83](#)
- [114] Y. M. Shobowale and K. A. Hamdi, “A unified model for interference analysis in unlicensed frequency bands,” *IEEE Transactions on Wireless Communications*, vol. 8, no. 8, pp. 4004–4013, 2009. [83](#)
- [115] P. C. Pinto and M. Z. Win, “Communication in a Poisson field of interferers—part I: interference distribution and error probability,” *IEEE Transactions on Wireless Communications*, vol. 9, no. 7, pp. 2176–2186, 2010. [83](#)
- [116] ———, “Communication in a Poisson field of interferers—Part II: Channel capacity and interference spectrum,” *IEEE Transactions on Wireless Communications*, vol. 9, no. 7, pp. 2187–2195, 2010. [83](#)
- [117] O. B. S. Ali, C. Cardinal, and F. Gagnon, “Performance of optimum combining in a Poisson field of interferers and Rayleigh fading channels,” *IEEE Transactions on Wireless Communications*, vol. 9, no. 8, pp. 2461–2467, 2010. [83](#)
- [118] P. Cardieri, “Modeling interference in wireless ad hoc networks,” *IEEE Communications Surveys & Tutorials*, vol. 12, no. 4, pp. 551–572, 2010. [83](#)

- [119] K. Gulati, B. L. Evans, J. G. Andrews, and K. R. Tinsley, "Statistics of co-channel interference in a field of Poisson and Poisson-Poisson clustered interferers," *IEEE Transactions on Signal Processing*, vol. 58, no. 12, pp. 6207–6222, 2010. [83](#)
- [120] C. Merola, A. Guidotti, M. Di Renzo, F. Santucci, and G. E. Corazza, "Average Symbol Error Probability in the presence of network interference and noise," in *IEEE International Conference on Communications (ICC), 2012*, 2012, pp. 2585–2590. [83](#)
- [121] A. Chopra and B. L. Evans, "Joint Statistics of Radio Frequency Interference in Multiantenna Receivers," *IEEE Transactions on Signal Processing*, vol. 60, no. 7, pp. 3588–3603, 2012. [83](#)
- [122] P. Mogensen, W. Na, I. Z. Kovacs, F. Frederiksen, A. Pokhariyal, K. I. Pedersen, T. Kolding, K. Hugl, and M. Kuusela, "LTE capacity compared to the shannon bound," in *IEEE 65th Vehicular Technology Conference, 2007. VTC2007-Spring.*, 2007, pp. 1234–1238. [88](#)
- [123] D. Stoyan, W. S. Kendall, J. Mecke, and L. Ruschendorf, *Stochastic geometry and its applications*. Wiley New York, 1987, vol. 2. [91](#)
- [124] H. Claussen, L. T. W. Ho, and L. G. Samuel, "An overview of the femtocell concept," *Bell Labs Technical Journal*, vol. 13, no. 1, pp. 221–245, 2008. [104](#)
- [125] D. Lopez-Perez, I. Guvenc, G. De La Roche, M. Kountouris, T. Q. S. Quek, and J. Zhang, "Enhanced intercell interference coordination challenges in heterogeneous networks," *IEEE Wireless Communications*, vol. 18, no. 3, pp. 22–30, 2011. [104](#)
- [126] G. H. H. Sung, K. W. Sowerby, M. J. Neve, and A. G. Williamson, "A frequency-selective wall for interference reduction in wireless indoor environments," *Antennas and Propagation Magazine, IEEE*, vol. 48, no. 5, pp. 29–37, 2006. [104](#)



- [127] G. I. Kiani, A. R. Weily, and K. P. Esselle, "A novel absorb/transmit FSS for secure indoor wireless networks with reduced multipath fading," *IEEE Microwave and Wireless Components Letters*, vol. 16, no. 6, pp. 378–380, 2006. [104](#)
- [128] F. Pantisano, K. Ghaboosi, M. Bennis, and M. Latva-Aho, "Interference avoidance via resource scheduling in TDD underlay femtocells," in *IEEE 21st International Symposium on Personal, Indoor and Mobile Radio Communications Workshops (PIMRC Workshops)*, 2010, pp. 175–179. [104](#)
- [129] I. Guvenc, M. R. Jeong, M. E. Sahin, H. Xu, and F. Watanabe, "Interference avoidance in 3GPP femtocell networks using resource partitioning and sensing," in *IEEE 21st International Symposium on Personal, Indoor and Mobile Radio Communications Workshops (PIMRC Workshops)*, 2010, pp. 163–168. [105](#)
- [130] S. Oh, H. Kim, B. Ryu, and N. Park, "Inbound Mobility Management on LTE-Advanced Femtocell Topology Using X2 Interface," in *Proceedings of 20th International Conference on Computer Communications and Networks (ICCCN), 2011*, 2011, pp. 1–5. [105](#)
- [131] Y. Jeong, T. Q. S. Quek, and H. Shin, "Beamforming optimization for multiuser two-tier networks," *Journal of Communications and Networks*, vol. 13, no. 4, p. 327, 2011. [105](#)
- [132] S. Akoum, M. Kountouris, and R. W. Heath, "On imperfect CSI for the downlink of a two-tier network," in *IEEE International Symposium on Information Theory Proceedings (ISIT)*, 2011, pp. 553–557. [105](#)
- [133] Y. Jeong, H. Shin, and M. Z. Win, "Interference rejection combining in two-tier femtocell networks," in *IEEE 22nd International Symposium on Personal Indoor and Mobile Radio Communications (PIMRC)*, 2011, pp. 137–141. [105](#)
- [134] C. W. Tan, S. Friedland, and S. H. Low, "Spectrum management in multiuser cognitive wireless networks: Optimality and algorithm," *IEEE Jour-*

- nal on Selected Areas in Communications*, vol. 29, no. 2, pp. 421–430, 2011. 105
- [135] D. T. Ngo, L. B. Le, and T. Le-Ngoc, “Distributed pareto-optimal power control in femtocell networks,” in *IEEE 22nd International Symposium on Personal Indoor and Mobile Radio Communications (PIMRC)*, 2011, pp. 222–226. 105
- [136] S. M. Cheng, S. Y. Lien, F. S. Chu, and K. C. Chen, “On exploiting cognitive radio to mitigate interference in macro/femto heterogeneous networks,” *IEEE Wireless Communications*, vol. 18, no. 3, pp. 40–47, 2011. 105
- [137] A. Adhikary, V. Ntranos, and G. Caire, “Cognitive femtocells: Breaking the spatial reuse barrier of cellular systems,” in *Information Theory and Applications Workshop (ITA), 2011*, 2011, pp. 1–10. 105
- [138] I. Guvenc, M. R. Jeong, F. Watanabe, and H. Inamura, “A hybrid frequency assignment for femtocells and coverage area analysis for co-channel operation,” *IEEE Communications Letters*, vol. 12, no. 12, pp. 880–882, 2008. 105
- [139] P. Xia, V. Chandrasekhar, and J. G. Andrews, “Open vs. closed access femtocells in the uplink,” *IEEE Transactions on Wireless Communications*, vol. 9, no. 12, pp. 3798–3809, 2010. 105
- [140] C. H. Ko and H. Y. Wei, “On-Demand Resource Sharing Mechanism Design in Two-Tier OFDMA Femtocell Networks,” *IEEE Transactions on Vehicular Technology*, no. 99, p. 1, 2011. 105
- [141] V. Chandrasekhar and J. Andrews, “Spectrum allocation in tiered cellular networks,” *IEEE Transactions on Communications*, vol. 57, no. 10, pp. 3059–3068, 2009. 105
- [142] R. Madan, J. Borran, A. Sampath, N. Bhushan, A. Khandekar, and T. Ji, “Cell association and interference coordination in heterogeneous LTE-A cellular networks,” *IEEE Journal on Selected Areas in Communications*, vol. 28, no. 9, pp. 1479–1489, 2010. 105

- 
- [143] S. Akoum, M. Zwingelstein-Colin, R. W. Heath, and M. Debbah, “Cognitive cooperation for the downlink of frequency reuse small cells,” *EURASIP Journal on Advances in Signal Processing*, vol. 2011, p. 7, 2011. [105](#)
- [144] J. H. Yun and K. G. Shin, “Adaptive Interference Management of OFDMA Femtocells for Co-Channel Deployment,” *IEEE Journal on Selected Areas in Communications*, vol. 29, no. 6, pp. 1225–1241, 2011. [105](#)
- [145] A. K. Dinnis and J. S. Thompson, “The effects of including wraparound when simulating cellular wireless systems with relaying,” in *IEEE 65th Vehicular Technology Conference, 2007. VTC2007-Spring*, 2007, pp. 914–918. [106](#), [107](#)
- [146] M. Kobayashi, S. Haruyama, R. Kohno, and M. Nakagawa, “Optimal access point placement in simultaneous broadcast system using OFDM for indoor wireless LAN,” in *The 11th IEEE International Symposium on Personal, Indoor and Mobile Radio Communications (PIMRC)*, vol. 1, 2000, pp. 200–204. [108](#)